MASTER THESIS IN QUATERNARY GEOLOGY AND PALEOCLIMATE

"Investigations of abrupt climate change offshore east Greenland continental margin during Marine Isotope Stages 3 and 5"

By

Ida Synnøve Folkestad Olsen

Department of Earth Science
University of Bergen

June 2016

Abstract

Paleoclimatic records obtained from western Nordic Seas core GS15-198-38CC (70°N, 17°W) exhibit fluctuating climatic patterns. Here, foraminifera isotope records used to reconstruct sea surface water mass properties indicated that variability changes during the last ~130 kyr have been dominated by forcing at precession (21 kyr) and millennial timescales. Observed shifts in $\delta^{18}O$ records, abundance ice-rafted detritus and planktonic foraminifers display a good agreement to Greenland atmospheric temperatures changes, indicating a coupling between ice sheet dynamics and sea surface processes east of the Greenland continental margin.

The most frequent abrupt stadial/interstadial changes retained from the marine sediments are known as Dansgaard–Oeschger (D-O) cycles, and appear every 1-2 kyr. These cycles are characterized by abrupt short-lived increase in temperatures (10 ± 5°C) followed by a gradual cooling preceding the next rapid event. A second millennial scale feature detected in the sediments record is cooling events culminating in significant iceberg discharges analogous to Heinrich events.
Mechanisms triggering abrupt changes display great uncertainties, but leading hypothesis is attributed to modifications in the Atlantic Meridional Overturning Circulation (AMOC) and deep-water formation initiated by freshwater input.

Finally, contrasting climatic variabilities between Marine Isotope Stages (MIS) 5 and 3 is apparent in the different proxy records. MIS 3 is dominated by rapid oscillations, indicating that climatic changes were arising at a high pace during this period. In contrary, MIS 5 exhibit longer, less frequent oscillations suggesting more stable climatic conditions, and hence also a difference in forcing mechanisms.

Acknowledgments

A sincere thank-you to my supervisor Eystein Jansen and co-supervisor Ulysses S. Ninnemann, for help and guidance throughout this process. I would also like to express my appreciation towards UIB geoscience employees, especially Eivind W.N Støren and Eirik V. Galaasen for always leaving the door open, and helping out with minor and major issues along the way. Also, a special thank you to Rune Søraas for running of isotope samples in the GMS laboratory.

I am very grateful for being given the opportunity to join the ice2ice summer cruise 2015. Little did I know that these four weeks in the Greenland Sea would nourish so many great memories both scientifically and socially. To my fellow members of team nightshift; Bjørg, Margit, Eva, Amandine, Mads, Ashley, Jørund and Dag Inge, thank you for all the laughter, donkey nights and good times. To all the scientists and crew, thank you for sharing your experience and knowledge with me. For that, I am forever grateful.

Last but not least, I want to thank my family and friends for chants and support during this process. A special thank you to Mats for being extremely patient and understanding, and to my fellow student Anna for support and long nights at Realfagsbygget. It would not have been the same without you.

We made it!

Bergen, May 2016

Ida Synnøve Folkestad Olsen

Contents

1. Background

1.1 Project

This thesis is part of the ice2ice project which studies Arctic sea ice and Greenland ice sheet sensitivity. The ice2ice project is funded by the European Research Council (ERC) and started in August 2014 with a five-year duration. The project is an international collaboration between 4 institutions; University of Bergen, Uni Research Climate, both part of the Bjerknes Center for Climate Research (BCCR). Niels Bohr Institute (NBI) of Copenhagen University, and Danish Metrological Institute (DMI).
The ice2ice project set out to investigate and elaborate on the mechanisms of abrupt climate changes observed in Greenland during the last ice age, seeking answers to important questions as: What if sea ice would abruptly disappear? Which implications would this have on the Greenland ice sheet and surrounding seas?

The broader objectives of the project are to utilize both marine sediment cores from the ocean off the east coast of Greenland, a new ice core drilled on the Renland ice cap in Scoresby Sund on Greenland`s East coast, as well as other Greenland ice cores. Ice core and ocean climate proxy records will describe in greater detail the dynamics of the abrupt events, and its relation to the sudden demise of sea ice cover. Another objective is to explain if the observed rapid diminution of the Arctic sea ice cover may lead to abrupt climate changes in the future, as well as determine the impact of such changes on the Greenland ice sheet (GIS). For more documentation see: https://ice2ice.b.uib.no/overview/ice2ice-objectives/

New datasets, both in the Nordic Seas and Greenland Ice sheet, aim to provide greater insight to these abrupt events. This master thesis does not constitute a direct contribution to the main goals of the project, but is merely a presentation of newly retrieved and processed data, which may throw light upon the degree of rapid changes affecting the areas off Greenland. This will provide an initial overview to guide further high-resolution investigations in the area.

1.2 Aim of this study

The main purpose of this study is to investigate the suitability of sediments offshore east Greenland, to document the regional extent and nature of abrupt climate change events in this region during the last glacial. A newly retrieved sediment core from the Western Nordic Seas, spanning the last ~160 000 years are presented. Emphasis of the study is aimed at detecting variabilities during Marine Isotope Stages 3 and 5, and hence providing an initial overview of climatic signals obtained in the sediments off Greenland during these periods. This overview is made with the purpose of setting the premises for future high-resolution studies in the area. The main objectives of this study are summarized as followed:

1) Establish an oxygen isotope stratigraphy based on the planktonic foraminifer *N. pachyderma* (sin) for the Marine Isotope Stages 6 to present.

2) Investigate how the offshore record aligns with the variability of the Greenland Ice Sheet in the last glacial, through comparisons of low resolution planktonic $\delta^{18}O$ with oxygen isotopes obtained from the NGRIP ice core.

3) Correlate the marine and terrestrial signals by the use of magnetic susceptibility measurements, and XRF analyses of elements such as Calcium, Iron and Titanium.

4) Describe the variabilities of surface water physical properties reflected in both planktonic foraminifer $\delta^{18}O$ values, as well as assemblage counts of the species *N. pachyderma* (sin).

2. Introduction

"Ocean circulation in the northern North Atlantic seems to be intimately coupled to the processes of climate change on various timescales, so that climate variability – and the associated mechanisms of change – should be well recorded by sediments from these high latitudes" – Fronval & Jansen (1996).

To achieve an understanding of how the climate will evolve, and anticipate the future challenges, knowledge of past climates is crucial. The highest latitudes in the northern hemisphere represent an area of major climatic importance, in parts, due to deep-water convection in the Nordic seas, and its influence on the global ocean conveyor circulation. Northern latitudes are also important due to its proximity to past and present continental ice sheets, and their dynamics. It is well documented that the climate system of the northern hemisphere has experienced large and abrupt events over the last hundred thousand years (last ice age). These appear on different timescale, ranging from decadal to multi-millennial duration. Common to all of these events is generally scarse understanding of its dynamics. This section aims to provide a brief introduction to the phenomena's and drivers of the climate variability observed in the Nordic Seas /North Atlantic.

2. 1 Drivers and phenomena`s of North Atlantic/Nordic Seas climate variability

2.1.1 Milankovitch Cycles

Glacials have been known to arise and persist in a combination and interaction of cycles of 23 000 yr, 41 000 yr and 100 000 years (Imbrie et al., 1993), denoted as Milankovitch cycles. The first scientist to stress the influence of variations in solar insolation on high latitudes, was Murphy (1869) who suggested that favorable conditions related to onset of glaciations being long cold summers, and short mild winter. This idea was later recognized by other scientists, among them Milankovitch. Milankovitch elucidated on the theory, and ascribed the glacial variations to astronomical phenomena, such as variations in the orbital elements and consequent insolation intensity (Berger, 1988). From this, the Milankovitch or orbital theory of glaciation was developed, based on three astronomical states; eccentricity, obliquity and precession, see figure 1.3.1.

The cycles of the shortest duration, 23 000 yr and 41 000 yr have been attributed to insolation feedbacks due to the obliquity and precession cycles (Imbrie et al., 1993).
However, insolation signal for the 100 000- yr cycle is not sufficiently significant (too small), and therefor dependent on a larger scale climatic inertia. Fundamental for this initiation are ice sheets large enough to make an impact on the global climate and with a feedback mechanism causing oscillations on a larger scale than 41 000 yr (Imbrie et al., 1993).

As the earth travels around the sun, this motion may occur either in a circular-, or elliptical orbit. During this rotation the earth will at some point be located near the sun, referred to as the "perihelion", or furthest from the sun, at "aphelion". If the earth is rotating in a circular orbit, the incoming solar radiation during perihelion and aphelion will be the same. Conversely, in the state of maximum eccentricity, the incoming solar radiation during perihelion and aphelion may vary as much as 30%. This is known as the orbital *eccentricity* and explains the earth's alternation between a circular orbit and a highly eccentric orbit. The length of this cycle is 95 800 years.

The second astronomical state is the *obliquity*. This is also known as inclination of the earth's axis, and it varies in the range of 21,39-24,36˚, on a time scale of 41. 000 years. The more extreme the tilt, the longer the duration of winter darkness persist in the northern most regions, and the summer season experiences midnight sun conditions further towards the equator and a higher solar angle. Higher latitudes are more sensitive to obliquity changes as incoming solar radiation are more affected in these areas.

The timing of aphelion and perihelion varies due to instability of the earth's axis of rotation as it travels around the sun. The earth's axis rotates in a conical matter, over a period of 21 700 years around a line perpendicular to the orbital plane. This dynamic is known as the *precession* of the equinoxes**.**

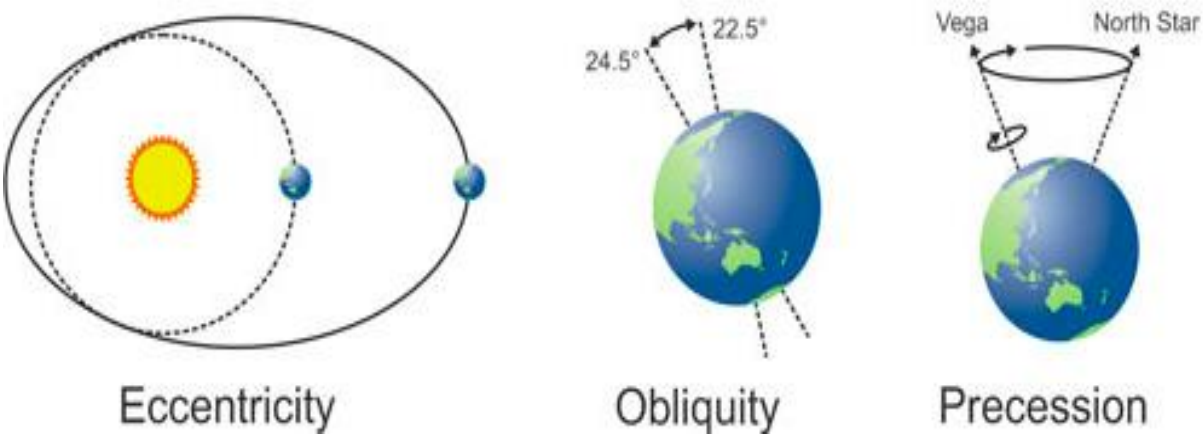

Figure 1.3.1. Simplified sketch of the three astronomical features; eccentricity, obliquity and precession. The eccentricity state refers to variations in energy received from the sun during the different orbits. Obliquity defines the tilt of the axis, controlling the solar energy flux at the poles. Precession refers to the orientation of the earth's axis. Figure derived from http://extremeearth.net/climate-change/causes/.

2.1.2 Dansgaard – Oeschger (D-O) Cycles and Heinrich events

D-O cycles are named after the scientist who first recognized the phenomenon in Greenland ice cores (Dansgaard et al., 1993) and Hans Oeschger the Swiss pioneer in the ice core and carbon cycle research. D-O cycles are an example of millennial scale oscillations observed during the last glacial. The main features of these oscillations are events of abrupt warming (10 ± 5°C) in Greenland followed by a gradual cooling period, lasting for 1-2 kyr. The cooling period terminate in a rapid shift back to stadial conditions (Dokken et al., 2013). The driving mechanism of these sudden climatic changes are still debated, but it has become more recognized that the mechanism is related to modification of the Atlantic Meridional Overturning Circulation (AMOC) likely caused by freshwater input and associated sea ice variations. The causal agent for the D-O cycle to shift into interstadial warming, are attributed to abrupt reduction in the extent of sea ice in the North Atlantic (Dokken et al. 2013).

Recent coupled Earth System Model investigations of underlying mechanisms of abrupt events stresses an intermediate height of Northern Hemisphere ice sheets as a possible prerequisite for altering the ocean-atmosphere system and cause D-O like events (see Zhang et al., 2014 for an overview).

Another prominent millennial scale feature detected in proxy records from the last glacial, are Heinrich events. These events are associated with short-lived massive discharges of icebergs (Bond and Lotti, 1995) transporting detritus to the open ocean, where it consequently accumulates in distinct layers. Ice rafting events are also associated with decrease in sea surface temperature and salinity, as well as lower concentration of planktonic foraminifers.

The timing of the events is repeated with 5-10 kyr intervals, indicating low consistency with Milankovitch orbital periodicities. The most recognized cause of these events concerns instability of the Laurentide ice sheet (Bond et al., 1992). In this relation MacAyeal (1993) proposed unforced "Bing-purge" oscillations of the ice sheet as a probable mechanism. Attributing instability variations to the bedrock interaction with ice sheet dynamics. The "bing" phase of the Heinrich event is dominated by stable ice sheet growth on frozen underlain sediments. As the sediments start to thaw, the connecting surface becomes slippery, causing movement of the ice sheet. These motions are seen as comprehensive discharge of icebergs into the North Atlantic Ocean, and represent the "purge" phase of the event. Subsequent fresh water input due to these events has been proven to be extensive enough to shut down or markedly reduce the North Atlantic Deep Water (NADW) formation (e.g Broecker et al., 1990) and therefor impact the climate on a global scale.

2.1.3 Atlantic Multidecadal Oscillation (AMO)

The Atlantic Multidecadal Oscillation (AMO) is a mode of natural variability in the North Atlantic Ocean. Characterized by fluctuating changes in sea-surface temperatures (SST) and sea level pressure (Grossmann & Klotzbach, 2009), spanning approximately 60-90 years. Whether the mechanisms of the AMO appear as repeated periodic driver of the climate, or a short – term feature (Knudsen et al., 2011) is still unclear. These uncertainties arise partly from lack of observational evidence, as the instrumental data only extends to the 19th century. A positive phase of the AMO portray as SST anomalies, with generally warmer surface waters of the North Atlantic (Enfield et al., 2001). Possible mechanisms driving the different modes of the oscillations are air-sea- heat flux changes, modification of wind patterns across the Atlantic, as well as feedbacks between SST and winds. The third factor of importance involve the North Atlantic salinity budget (Grossmann &Klotzbach, 2009). In general, the

density of North Atlantic Deep Water (NADW) is highly sensitive to changes in salinity, and the smallest variation may affect the properties of this water mass, consequently altering the strength of the thermohaline circulation (Bjerknes, 1964 in Grossmann & Klotzbach, 2009).

2.1.4 North Atlantic Oscillation (NAO)

The North Atlantic Oscillation (NAO) is a second mode of interannual/decadal climate variability, first cited by Walker (1924). The definition of the NAO is referred to as the sea level pressure (SLP) difference between the Icelandic Low and Azores High (Marshall et al., 2001). Positive NAO index permit stronger-than-usual westerly winds, promoting transport of warm waters into the eastern part of the Atlantic basin, and resulting in higher-than-normal temperatures in Europe (Rogers 1985). Similarly, during abating NAO index trends, lower winter temperatures have been recorded in Europe as a direct consequence (Van Loon and Williams, 1976), see figure 2.1.4.

The NAO undergoes different phases, modulating the strength, direction and intensity of the resulting storm tracks (Rogers, 1990). The highest amplitude and distribution according to Wallace and Gutzler (1981) occurs during wintertime (December-March).

The impact of the NAO extends far, reaching from North America to Siberia on a longitudinal scale, and crossing the whole of the northern hemisphere from the Arctic Ocean to the equator. The North Atlantic Ocean is significantly affected by the changing pressure gradients from the NAO. Pattern of sea surface temperature (SST) variability in the Atlantic Ocean is displayed as a “tripole”. This tripole consists of warming in mid-latitudes, whilst colder conditions occupy the subpolar regions, as well as between 30ºN and the equator. This pattern is promoted by air-sea fluxes derived from the positive NAO index during winter. Wintertime SST in the eastern America, Arctic and even the Mediterranean are correlated with NAO variability (Marshall et al., 2001).

As the NAO affects the circulation of the North Atlantic basin, the accumulation of moisture in the atmosphere and consequently transport of this moisture is reflected in variations of regional wintertime precipitation (Rogers and Loon, 1979). High NAO winter index: drier

than normal conditions over central and southern Europe and northern Mediterranean. Simultaneously, wetter than normal conditions appear over Island and Scandinavia.

Deser et al. (2000) point out the relation between extent of interannual Arctic sea ice variability and atmospheric forcing. Indicating that wintertime NAO index will drive arctic sea ice into the North Atlantic sector. They further conclude that a NAO low index will drive the ice extent of the Labrador Sea to migrate south, whilst the Greenland Sea ice retrieve north of its boundary.

According to Nakamura (1996), the Atlantic display a correlation to the NAO index and low frequency fluctuations within a season. During a positive mode the intra-seasonal variability near Greenland and Labrador Sea is considerably weaker, whilst seasonal variability over Europe are strong. Conversely, negative NAO mode resembles higher seasonal variability over Greenland and Labrador Sea and weaker over Europe.

Similar to the AMO, the imprint of the NAO variability to the North Atlantic sediments is difficult to assess on timescales longer than decades, due to records extending only 500-600 years back. However, multiple proxies indicate that periodic episodes of stable conditions of the NAO occur on decadal and centennial timescales (Rousse et al., 2006).

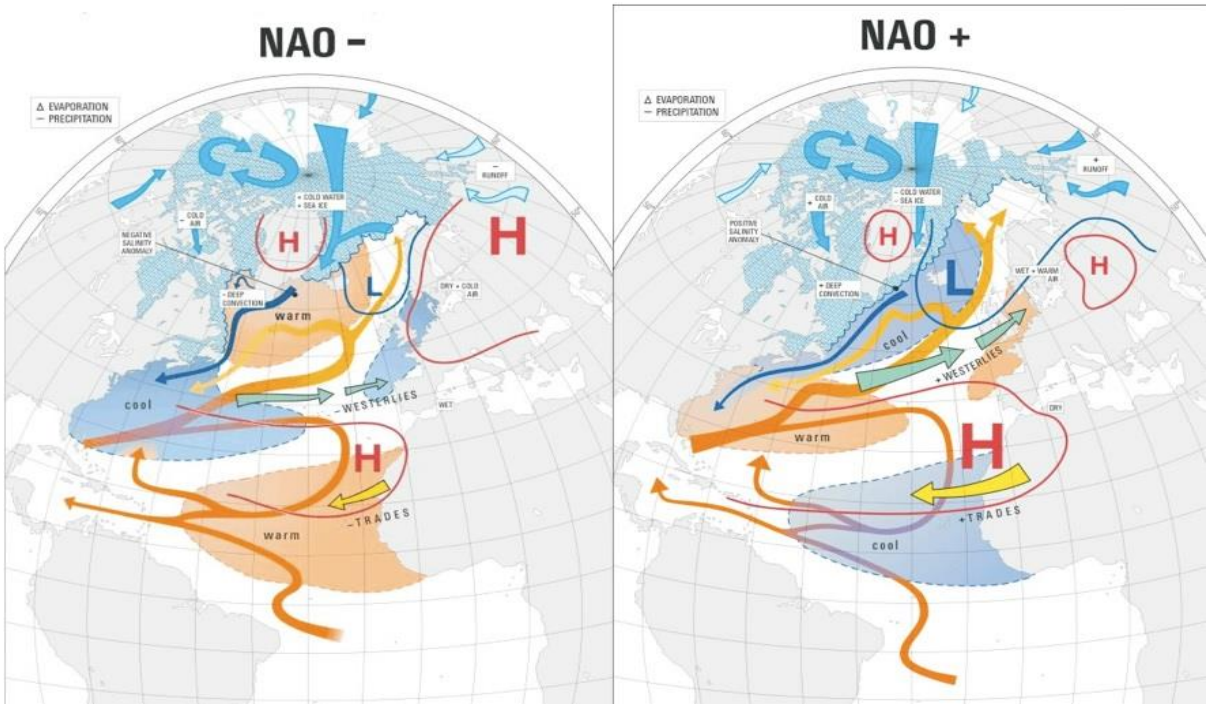

Figure 2.1.4. Simplified sketch representing the positive and negative modes of the North Atlantic Oscillation (NAO). Positive modes display features including strong low atmospheric pressures over Iceland, warm weathers over Europe and more sea ice in the Canadian basin. A negative NAO mode drives a weak low over Iceland, cold and dry conditions over Scandinavia and warmer SST`s in the North Atlantic. Figure derived from http://ossfoundation.us/projects/environment/global-warming/north-atlantic-oscillation-nao

2.1.5 Thermohaline Circulation (THC)

Circulation of deep-water masses is dependent on the changing physical properties of the surface waters, such as salinity and temperature, which make up the engine of the thermohaline circulation. The density of the ocean may vary as a result of heat flux, precipitation or runoff into the surface waters. Warm surface waters flow into the North Atlantic where it undergoes heat loss to the atmosphere, due to colder surroundings. Surface waters may also experience increase in evaporation, leaving the remaining water masses enriched in salt. Both these processes promote denser water masses. As the dense waters sink deeper into the water column they ultimately reach neutral buoyancy with the surrounding waters. The newly formed deep-water, as in the North Atlantic, termed as North Atlantic Deep Water (NADW) flows southward, carrying saline waters to the south Atlantic (Bradley, 2014). The “conveyor belt” effect of the THC is maintained as dense water sink and flow

towards the tropics by compensating northward inflow of surface waters into the North Atlantic (Fig. 2.1.5). Mechanisms that are known to inhibit the deep-water production in the North Atlantic, and hence also cause limitations to the thermohaline circulation are supply of fresh water (Bradley, 2014). Melting of continental ice sheets result in formation of a layer of low salinity water, reducing or potentially initiating shutdown of deep-water formation, thus affecting the global ocean circulation and climate.

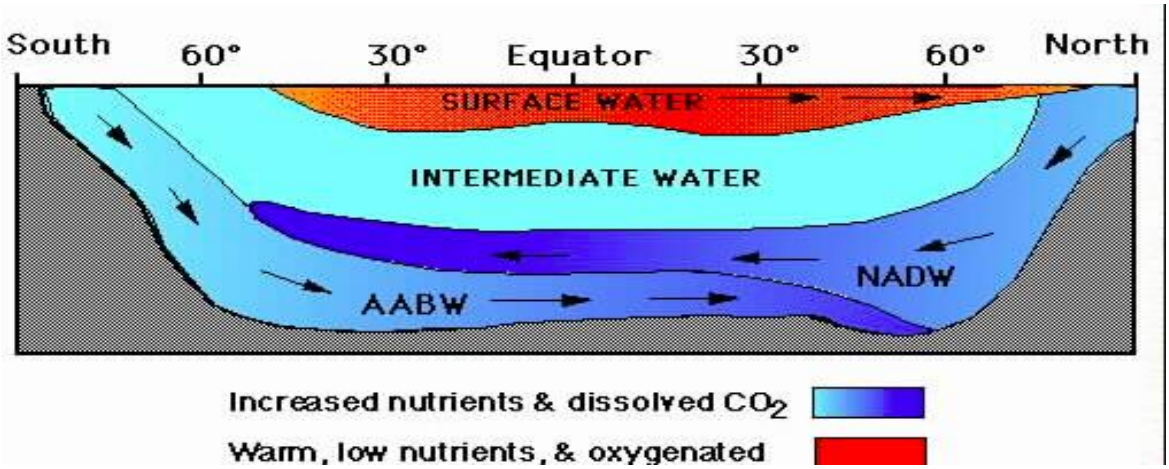

Figure 2.1.5. Formation of North Atlantic Deep Water (NADW). Warm surface waters experience heat loss to the atmosphere at high latitudes, become denser and sink to intermediate-deep water depths. Oxygenated and nutrient rich deep-waters flow southward.

2.1.6 Atlantic Meridional Overturning Circulation (AMOC)

The Atlantic Meridional Overturning Circulation (AMOC) is often mistaken for the thermohaline circulation (THC). The two are intimately associated with each other as part of the global ocean circulation "conveyor belt". As THC is strictly driven by density, the AMOC is also affected by winds and atmospheric pressure variations related to the NAO. The AMOC is a global major current system, transporting heat from low latitudes (tropics) to higher latitudes in both hemispheres in the Atlantic. The AMOC is driven primarily by upwelling and downwelling of water masses; hence it will inhabit contribution from the THC in the cycle. Wind forcing of the surface waters is another driving factor. The AMOC transports warm nutrient poor waters from the equator poleward. As heat (and other components, such as carbon) is lost to the atmosphere through air-sea interference, the water is converted into cold North Atlantic Deep Water (NADW), through the THC dynamics (Figure 2.1.6). This poleward transport and formation of water masses are strongly

dependent on the NAO, as it serves as a controlling factor of sea ice/fresh water and air-sea fluxes (Coachmann & Aagaard, 1988).

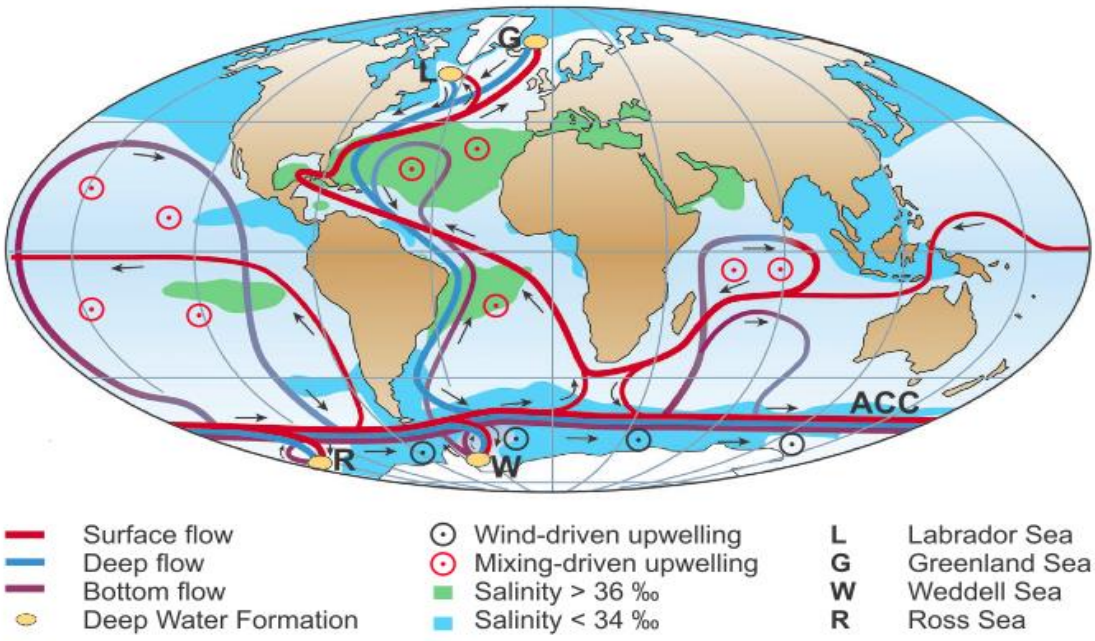

Figure 1.3.6. Overview of the global ocean circulation associated with the Atlantic Meridional Overturning Circulation (AMOC), derived from Rahmstorf (2000). This sketch provides a simplified understanding of the THC dynamics, taking into account the surface flow, deep water flow, sites of deep water formation as well as upwelling regions.

3. Study area

3.1 Geographical setting

The site of core GS15-198-38CC is situated in the Greenland Sea. The Greenland Sea is part of the Nordic seas, including Iceland-, Norwegian-, and Barents Sea. In the north, the Fram Strait connects the Nordic seas to the Arctic Ocean. Whereas the southern boundaries to the North Atlantic follows the Denmark Strait west of Iceland, and the Iceland-Faeroe, Iceland-Shetland Channel in the east (Nam, 1995).

In general, the bathymetry of an area constitutes a crucial factor in the dynamics of the water mass circulation. The seafloor topography may exhibit constraints or limitations to the circulation, and thus effect the interaction and mixing of water masses with nearby oceanic regions (Hopkins, 1991). The major features of the Nordic Sea bathymetry comprise three basins separated by the Mohns mid oceanic-ridge system. The basin of special interest of this thesis is the Greenland basin, which is defined by Fram strait in the north, the Greenland continental shelf to the west and Mohns ridge to the south and east, see figure 3.1 (Hopkins, 1991).

Important water mass exchanges to the Nordic Seas occur through six boundaries, whereas the two northernmost boundaries ensure flow exchange with polar waters. The geomorphology of the two passageways display differences reflected in boundary conditions. The Fram Strait represents an oceanic boundary, where water masses may flow unrestrictedly, whereas Barents Sea inflow to polar areas occurs in shallower continental shelf seas (Hopkins, 1991). Exchange with the Atlantic Ocean occurs mainly over the continental Greenland- Scotland ridge, through the Denmark Strait west of Iceland. East of Iceland, Faroese Channel and Shetland – Færoe Ridge, and North Sea entrance constitute the connection between Nordic Seas and Atlantic Ocean. The bathymetry of the boundary between the Nordic Seas and Atlantic Ocean is as opposed to the Fram Strait much shallower in depth, contributing to restrictions in the circulation dynamics.

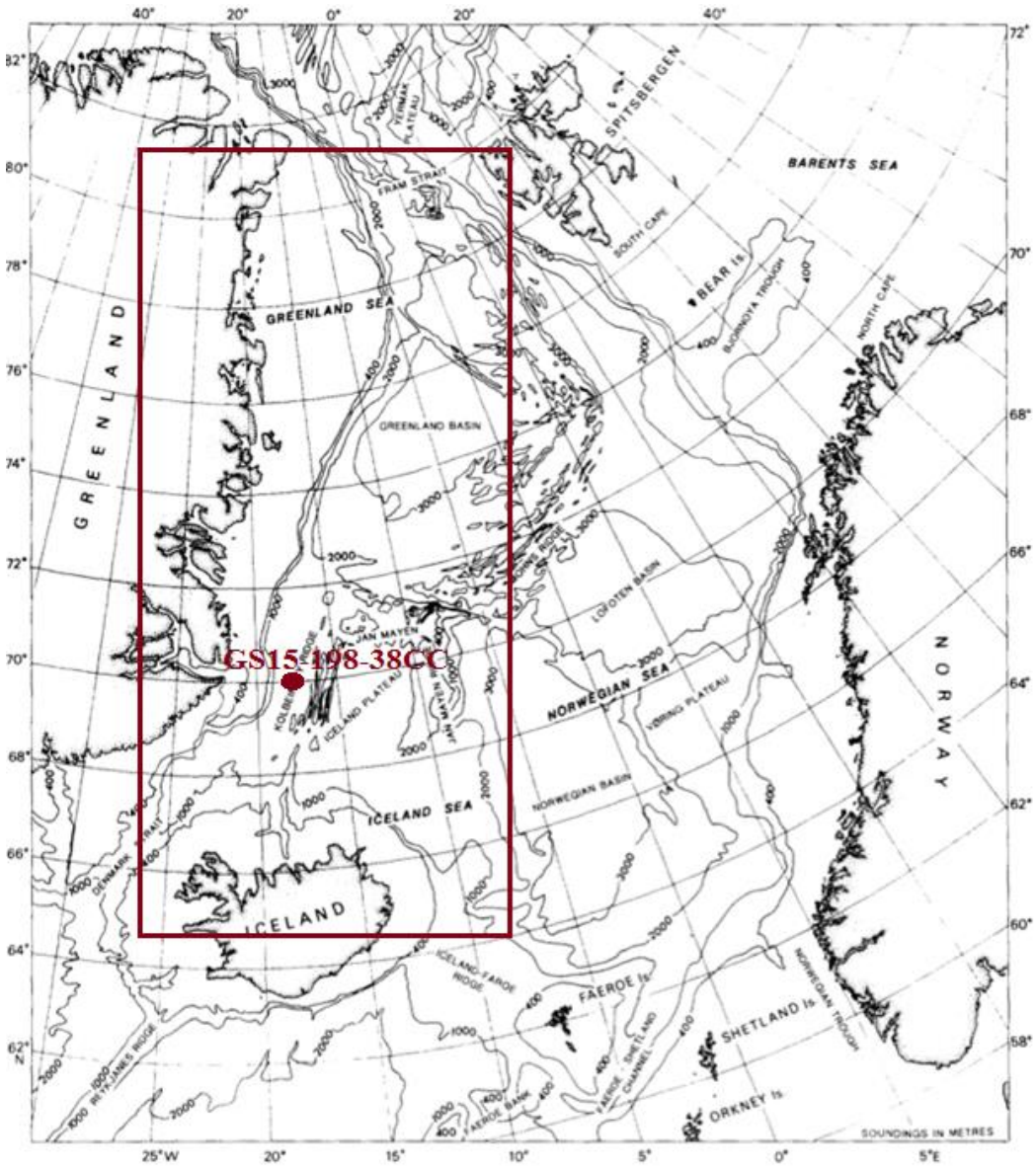

Figure 3.1. Bathymetric features of the Nordic Seas derived from Hopkins (1991). Red square indicates the Greenland basin, whilst red dot is the approximate location of the core site.

3.2 Oceanographic setting

The oceanic area of special interest for this thesis is the Nordic Seas. This Sea acts as a connective basin between the ice-covered polar waters in the north, and warmer North Atlantic waters in the south. In addition, it constitutes an important role in relation to deep water formation of the Northern Hemisphere (Hopkins, 1991).

Water masses are differentiated both vertically and horizontally on the basis of density. This parameter reflects the salinity and temperature of the ocean, and may act as a unique tracer. Subdivision of the waters is classified as surface, - intermediate-, and deep waters. Water masses dominating the Nordic Seas originates from two main sources; Cold, low salinity Polar Water (PW) derived from the Polar Sea, or warm, high salinity North Atlantic Water (NwAtW) from the North Atlantic (Hopkins, 1991)

North Atlantic water masses enter through the Faroese Channel and travels further north towards Spitsbergen. Due to the Nordic Seas bathymetry, NwAtW is dynamically constrained to the eastern part of the basin. Lateral extent of NwAtW is normally greater in winter than in summer, but the existence of a seasonal pattern of NwAtW volume is still debated. As it enters the Nordic Seas in the south it possesses high levels of heat, and is too buoyant to mix with the surrounding water masses. Transport to the north results in heat loss, just enough to reduce the buoyancy, and induce mixing. This dynamic results in increasing density down the water column, known as “precondition phase”. Precondition phase is an important feature requisite for deep-water production, and hence also the thermohaline dynamics of the Nordic Seas (Hopkins, 1991).

Another Surface water mass of significance is the Greenland Polar Water (GPW). GPW enters the Nordic Seas through the Fram Strait, and acts as a boundary current, flowing down the continental margin of eastern Greenland. As the NwAtW is constrained to the east part of the sea, equally are the GPW dynamically limited to the western part. Underneath the Greenland Polar water is the presence of a strong halocline, originating from polar waters, and maintained by fresh water supply through melting of ice bergs. During increased summer melting a resulting sharper halocline becomes evident. Following deepening of the thermocline occur during winter convective mixing of the water masses (Hopkins, 1991).

The third surface water mass of special interest is the Arctic surface water (ArSW)**.** It is of local origin and occupies the area between the GPW and NwAtW, and is essentially made up of a mixture of boundary waters (Hopkins, 1991). Blending occurs as parts of the Atlantic waters flow slightly west towards Jan Mayen, simultaneously as the East Greenland Current branch eastward into the Iceland Sea. Resulting in waters with complex properties, and the Iceland Gyre (Johannessen et al., 1994). In addition, artic waters play a key role in formation of North Atlantic Deep Water (Aagaard et al., 1995). The ArSW display the most prominent seasonal variability. During winter and autumn, a collapse of the thermal stratification takes place as a result of heat loss to the atmosphere, leading to a merge with the underlying upper intermediate waters. This stratification is reestablished during spring and summer.

Intermediate water masses comprise an intermediate stage in the transition from surface waters to deep water. These water masses occupy the intermediate depth of the water column. Formation occurs during winter as heat loss and potentially sea ice formation induces a decrease in temperature and increase in salinity, and hence heavier and denser waters. Four types of intermediate waters are present in the Greenland Sea:(1) Return Atlantic Intermediate Water (rAtIW), (2) Jan Mayen Intermediate Waters (JMAtIW), (3) Greenland Atlantic Intermediate Water (GAtIW) and (4) Greenland Arctic Intermediate Water. For a more extensive review of these water masses see Hopkins (1991).

Thirdly, the most important water mass, controlling the overall thermohaline circulation of the basin is the deep-water masses. The formation process of deep-waters may differ greatly resulting in water mass properties in opposite ends of the scale. This is evident in the Canadian and Greenland basins (Hopkins, 1991). Canadian Deep Water (CDW) consists of the saltiest and warmest waters, whilst Greenland Deep Water (GDW) is the freshest and coldest. According to Carmack (1973) Greenland deep-water formation occurs through subsurface cooling of GAtIW. As warm, and salty GAtIW approximate the Greenland gyre center, heat is lost quicker than salt to the GArSW, through a double diffusive mechanism. Heat from the intermediate water masses is further transported to the atmosphere through the surface layer. As a result, the surface layer experience warming from below, and cooling at the ocean-atmosphere interface. During this process the buoyancy is alternated, driving GAtIW to resemble the water properties of GDW.

The current of special relevance for this thesis is the East Greenland Current (EGC). This current transport cold, fresh waters southward from the Fram Strait, through the Greenland Sea and into the Denmark Strait. The upper fraction of the current conveys GPW southward (Hopkins, 1991). On this southward path GPW has an eastward input to The Jan Mayen current (JMP) and Icelandic Current. Because of its proximity to the Greenland continental shelf, the boundary flow is geostropically constrained to remain along the margin. Due to Ekman transport, a westward motion of mass flux sustains the barotropic high along Greenland, driving the EGC southward (Hopkins, 1991).

3.2 Climatic setting

The climatic setting of a region is a result of complex dynamics between meteorological phenomena, such as atmospheric pressure and wind patterns, as well as interaction between the atmosphere and the surface ocean. These dynamics serves as a modulator for both local and regional climatic variations. In this relation a commonly discussed inhibitor of atmosphere-ocean dynamics is the presence of an ice cover, and its implications on the physical properties of the ocean (Hopkins, 1991).

The climatic pattern of the Nordic Seas is "split" into two sectors at 70° latitudes by the polar easterlies and the mid latitude westerlies. It is in this area, the Arctic front reaching from Iceland northeast to Bear Island; separates the Norwegian Sea from the Greenland and Iceland seas (Hopkins, 1991). The Arctic front is defined by two surface waters masses. The cold arctic waters to the west and warm Atlantic waters in the east. Another front, denoted as the Polar front separates the low salinity polar waters from the arctic surface masses.

In the northern hemisphere the atmospheric surface pressure field appears as features of low- and high-pressures. Located at 60º latitude low-pressure cells; Icelandic (North Atlantic) and Aleutian (North pacific), are prominent. At the latitude of 70º there are two high-pressure cells, the Siberian and McKenzie. Out of all the pressure cells, the Icelandic Low lead the primary influences to the Nordic Seas region (Hopkins, 1991).

The Icelandic low is at its most intensive and extensive during winter as the pressure gradient strengthens across the Nordic Seas. Due to sea surface convergence underneath the Icelandic low, this strengthening feature is enhanced and elongated northeast into the basin. At its most

intensive the Icelandic Low produce winds of cyclonic storm strength dictating the wind pattern of the southeast region of the Nordic Seas.

During March, a decrease in the Icelandic Low intensity is prominent as the Polar High starts to build up. As a consequence, the easterlies extend to the south. Icelandic Low constitutes its weakest form in July due to minimal pressure gradient configuration. The same accounts for the Polar High situated over Bear Island. As the high-pressure cell shifts towards Canadian Basin during fall, the weak wind field increases as a result of development of greater pressure gradients over the Nordic Seas. Once more the northeasterly winds flow over Greenland seas.

Most of the ice-cover present in the Nordic Seas is in the form of pack ice, icebergs, ice islands and land fast ice. Highest distribution of ice bergs is found in the southernmost part of the Greenland coast, often in connection to fjord systems (Scoresby Sund in particular) where conditions for escape into open waters are more favorable compared to north of Greenland. Due to steep bathymetry along the east Greenland coast, most land fast ice detaches north of Greenland and enters the EGC through the Fram Strait (Hopkins, 1991). The boundary between pack ice and open waters are called the marginal ice zone (MIZ), a region where ice growth and decay are prominent (Hopkins, 1991).

The highest percentage of icebergs in the eastern margin of Greenland originates as outlet glaciers entering the Scoresby Sund fjord (Dowdeswell et al., 1993). Icebergs situated at the mouth of the fjord incorporate into the EGC and flow southward (Wadhams, 1981).
There is a greater year-to-year variability compared to seasonal trends, due to self-regulation within an annual cycle. As the production rate of ice increases during winter, the amount of ice accessible for melting raise correspondingly. Also, the presence of ice cover inhibits the heat loss of the surface waters, resulting in accumulation of heat below, and colder air temperatures above the ice-cover. Potentially inflicting changing wind patterns and sea ice distribution. Skov (1967) elaborated on the idea of possible connections between yearly sea ice variability and the dynamics of the currents. Seeing that warm and saline North Atlantic waters entering the Nordic Seas may inhibit the extension of the EGC and therefor subsequently slow down the rate of incoming ice-producing waters from the Arctic. This is a statement in line with warm saline waters preventing formation of ice, whilst colder less saline waters facilitate growth

4. Materials and Methods

This chapter provides an overview of the procedures carried out during the cruise, and information about the following laboratory work. In addition, a brief introduction to the background of the various methods and its application to paleoclimatic studies is presented.

4.1 Shipboard Analyses

Marine core GS15-198-38CC (hereinafter, core 38CC) was recovered during the 2015 cruise of R/V G. O Sars in the Greenland Sea, as part of the ERC-Synergy granted ice2ice-project (chapter 1.1). Core 38CC (70`07.521N, 17`32.812W) was retrieved at a water depth of 1609 m, located on the continental slope east of Scoresby Sund, Greenland (see figure 4.1). The core site is situated below the path of southbound East Greenland current and Denmark Strait Overflow Water (DSOW).

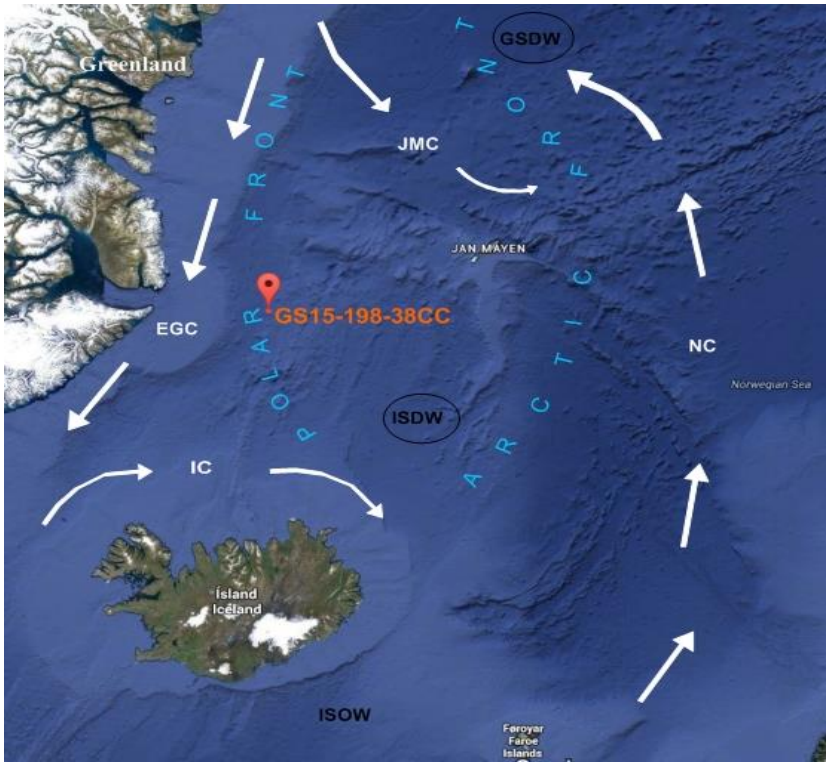

Figure 4.1. Overview of the main surface circulation in approximation to the core site (orange), modified after Nam et al. (1995). IC= Iceland Current, EGC= East Greenland Current. NC= Norwegian Current. JMC= Jan Mayen Current. Oceanic fronts are highlighted in blue capital letters, modified after Johannessen et al. (1994). Deep-water masses are modified after Pirrung et al. (2002). Black circle indicates site of deep-water formation. GSDW= Greenland Sea Deep Water, ISDW=

Iceland Sea deep water, ISOW = Iceland Scotland overflow water. DSOW= Denmark Strait Overflow Water.

4.1.1 Coring device

For the recovery of core 38CC, the Calypso piston core system was used (Figure 4.1.1). The customized G.O Sars version of this corer is capable of retrieving sediments up to 22 m, at maximum depths of 6000 meters.

The Calypso corer is leveled down the water column, up until one meter above the sea floor, where it is stabilized to minimize the horizontal movements. This action is taken to increase the probability of perpendicular penetration of the sea floor sediments. Once optimal conditions are obtained, the Calypso corer is released from the main cable. During this procedure an internal wire connected to a piston at the bottom of the corer, help neutralize the pressure at impact. This wire also connects the corer to the main cable, permitting recovery of the sediments (for further reference, http://www.kleyfrance.fr/product_06.htm)

Figure 4.1.1. Picture of the calypso corer used on board F/F G. O Sars, taken during the Ice2ice cruise (Photo: Ida Synnøve Folkestad Olsen).

Immediately after recovery, the core was split into two halves, working-, and archive half. Both surfaces were cleaned, before further constructing u-channels from the archive half. The purpose of making u-channels was to simplify the process of x-ray fluorescence scanning, once ashore. The remains of the archive half were stored and kept as a possible future reference. Several analyses were conducted on the working half, including logging of visual characteristics, photographs and color scanning. Measurement of low field magnetic susceptibility (MS) was also conducted with a handheld Bartington MS2 device.

4.1.2 Visual core description

During the Ice2ice cruise a visual description of the core sediments was made. In general, the sediments did not display any major features and were dominated by alternations of silty clays of varying color. A brief summary of the visual description is presented below.
The interval 0-106 cm is dominated by light milky brown colored silty clays with darker brown staining bands. At 106-112.5 cm a clear increase of grey color is obvious. The following sediment is clay of a grayer color, and a feature of reddish tint/rusty streak at 156 cm. The interval 196-326 cm is made up of silty clays with colors ranging from beige to blackish gray. The following 326-336 cm has a more olive gray brown color; with a sharp transition to slightly coarser material in layers at 332 cm. 332-398 cm is milky brown with darker brown splotches at 386-387 cm. The interval 387-605 has a higher frequency of streaks, which are black and dark brown in color. The sedimentology of this interval is still silty clays of varying color. At 605-635.5 cm the color has a more yellow character, and a large stone is prominent at 610-613 cm. The last 635.5-900 cm varies between brownish and greenish silty clays with occasional black stains at 638cm and 770-773 cm.

4.1.3. Color scanning & Photos of the core

After the surfaces were thoroughly cleaned, the sections were placed under a stand and photographed with an SLR camera. Thin slices of cling foil were used to prevent the measuring equipment to touch (and contaminate) the sediments. Any air bubbles trapped between the foil and sediments were removed accordingly, to minimize interference of the measurements. The color scanning was performed with a handheld spectrophotometer, measuring every centimeter (Figure 4.1.3). From the color scanning data one can extract information about the color range and lightness of the sediments, providing information about the sediment composition.

Figure 4-1-3. Picture taken during the ice2ice cruise showing color scanning of sediment with the use of a spectrophotometer (Photo: Ida Synnøve Folkestad Olsen)

.

4.2 Shore based Laboratory methods

Initial processing of the core sediments was performed mainly in the sediment laboratory of the University of Bergen. This implies XRF-scanning and washing of samples. Preparations and running of samples for stabile isotope measurements were conducted in the Geological Spectrometry (GMS) laboratory of the Department of Earth Sciences and the Bjerknes Center of Climate Research (BCCR), Bergen.

4.2.1 Sampling and washing

Core 38CC was sampled every 5 cm, starting from 0-0,5, 5-5,5 and so on. The uppermost 9 meters of the calypso core was sampled, which is the focus area of this thesis. Every 10 cm a 1 cm slice was taken, whilst every 5cm only 0,5cm was collected. This inconsistency is due to a reconsideration of producing higher resolution records than first outlined. When sampling the sections, a thin slice of sediment closest to the plastic tube was left out, to prevent contamination of the sediments.

All samples were weighed before and after the drying process, to obtain wet-, and dry weight of the sediment. During the drying process (at 50°C), each sample was mixed with distillated water and placed on a shaking machine for approximately 24 hours to disperse the sediments. Suspended sediments were further sieved into fractions of >0,5 mm, >0,150 mm and >0,0063mm. The fine fraction (<0,0063mm) was collected in a container to settle, and was later bagged.

4.2.2 X-ray fluorescence (XRF)

Variations in a sediment core imply changes in depositional environment, possible contamination, diagenetic transformation etc. It is essential to obtain precise analyses of sediments to acknowledge these changes. The x-ray fluorescence method provides high-resolution data of the geochemical elements present, invaluable for the initial analytical process of a core (Croudace et al., 2006).

The ITRAX- X-ray fluorescence scanning system used for analyses of core 38CC is a fully automated multifunctional scanner. It ensures radiographic, optical as well as elemental variations in a split-core, with no destruction of the sediment. This is performed with the use of an intense micro-X-ray beam irradiating the samples. The ITRAX has the capacity of scanning core sections up to 1,8 meters with a resolution of 200 µm (Croudace et al., 2006). It is also known to be less time consuming, in terms of the preparation process as well as the actual analysis, compared to traditional methods of detecting geochemical elements.

The application of XRF scanning in marine science has been largely related to determination of climatically driven modifications in the composition of core sediments, often associated to glacial – interglacial cycles (Lebreiro et al., 2009). It is useful for attaining high-resolution data of elemental fluctuations. Sedimentological features, such as ash layers, turbidities and ice rafted debris are also more recognizable with the use of XRF. A fourth application might be examination of element ratios compared to magnetic susceptibility to yield information about authigenic and diagenetic processes (Rothwell, 2015).

Elements emphasized in this thesis are Calcium (Ca), Iron (Fe) and Titanium (Ti), all of which are correlated with glacial cycles and abrupt climatic changes (Hepp et al., 2006). In

general Fe and Ti are considered as a proxy for terrigenous input (Vidal et al., 2002), peaking in values during events of iceberg rafting (Hepp et al., 2006).
Calcium values found in the marine sediment cores can potentially be of detrital origin, but the dominant contribution in the Greenland Sea is, due to the low occurrence of carbonates in the continental surroundings, normally from biogenic sources. This element is therefore a recognized proxy for $CaCO_3$ production in the ocean (Rothwell, 2015). The general fluctuation pattern of Ca, display increasing values during interglacials, and subsequently decreasing values during cold glacial conditions, where sea ice cover and low temperatures reduce carbonate productivity in the upper ocean (Arz et al., 2003). Calcium may also serve as a proxy for bottom water corrosiveness, as low values of Ca can be correlated with carbonate dissolution. This may in turn be related to oceanic water mass changes (Arz et al., 2001a). In general, glacial-interglacial transitions result in significant anti-correlated changes in Ca, Fe and Ti.

4.2.3 Magnetic Susceptibility (MS)

As mentioned in section 4.1.1, low-field magnetic susceptibility was measured during the cruise with a handheld Bartington MS2 system. The core was wrapped in cling foil to prevent contact between the MS detector and the sediment. Every 1/2-centimeter was measured, and the device was properly zeroed before use.

Magnetic susceptibility is widely used for environmental research due to magnetic mineralogical approach being so applicable and simple to use. Advantages to this analytical technique are the measurements being quick and non-destructive. The fact that measurements can be made on any type of material, as well as complement many other forms of analytical techniques (Dearing, 1994).

Magnetic susceptibility is the measure of how attracted a material is relative to an external forcing, in this case, the magnetic field. This attraction is considered to be the magnetic behavior of a material, and it is this effect that is desirable to measure.
Magnetism is created by electron spin around the atoms nucleus and its own axis. Alignment of the electron motions constitutes the magnetic energy of an atom. Configuration and

interaction between all the electrons in the atoms determine the magnetic behavior of the material (Dearing, 1994).

Magnetic behavior can be subdivided into five categories; Ferromagnetism, ferri-, canted antiferro-, para-, and diamagnetism. Ferromagnetism term is used to describe the most magnetic substances, like Fe. The magnetic moment in these substances is ordered and aligned in the same direction leading to high magnetic susceptibility. Ferrimagnetism also display high magnetic susceptibility, and includes magnetite and Fe-bearing minerals. These types of minerals are present in both rocks and soils, and are therefore the most common magnetic behavior of natural materials.
The third group of magnetic behavior is the canted antiferromagnetism. This group of iron minerals is common in many rocks and soils, and displays a lower magnetic susceptibility because of opposing magnetic moments in the alignment (Dearing, 1994).

Examples of minerals in the fourth group are biotite and pyrite. In the presence of a magnetic field, the magnetic moments of Fe or Mn in these minerals are aligned and display week susceptibility. The last group, diamagnetism, includes minerals that do not contain any iron, such as quartz and calcium carbonate, and even organic substances. Diamagnetic materials are known to produce weak or negative values of magnetic susceptibility (Dearing, 1994).

Measured magnetic properties of sediments may provide information about source region and past changes in transport of the material, hence the dynamics of deep-water currents (Rousse et al., 2006). The magnetic content is in turn dependent on the biological productivity. When biological productivity increases, dilution of the magnetic minerals will occur, leading to a decrease of the magnetic elements and a lower MS value (SI). Higher values of MS indicate glacial periods, characterized by lower productivity of biogenic carbonate, and generally higher input of ice rafted detritus, than during interglacials (Robinson, 1986a). This is, however, dependent on the type of detritus, whether it is derived from rocks with low or high abundances of magnetizeable minerals.
The glacial-interglacial changes detected in magnetic susceptibility (MS) are driven primarily by the dilution and productivity of carbonate, and low susceptibility terrestrially derived minerals and their effect on the concentration of magnetic minerals in the bulk sediment (Robinson et al., 1995).

Often magnetic susceptibility is used as a correlation tool since cores over wider regions may display the same magnetic susceptibility record.

4.2.4 Isotope Ratio Mass Spectrometer (IRMS)

Stabile isotope measurements were conducted by the use of Finnegan MAT 253 mass spectrometer. For this analysis, planktonic foraminifera, *Neogloboquadrina pachyderma senestre* (hereinafter *N. pachyderma* sin.) was picked from the >150 μm fraction. In general, the samples were dominated by this species, with few other planktonic or benthic foraminifers present. Foraminifers was transferred into a glass vial one by one and carefully weighed to obtain the optimal weight of 40-60 μm. Because the foraminifera were picked from a size specific fraction, the same amount of species (approximately 10) was needed for each sample. Control weight was performed every 5 sample.

The tests in glass vails were further broken into pieces with the use of a glass rod. Drops of methanol were added, and the sample was placed in an ultrasonic bath for approximately 10 seconds. In cases where the sample did not seem adequately clean, a second run of ultrasonic bath was performed. The contaminated methanol was removed with a syringe carefully to make sure all sample components remained in the veil. The sample was put in a drying cabinet to evaporate the remnant of fluids.

The analysis of both oxygen and carbon isotopes of carbonate shells is executed by measures of the mass ratios of carbon dioxide (CO_2) in a sample. This is obtained by reacting carbonate with phosphoric acid, with reference to a standard, comprised of CO_2 of a known isotopic composition. See Equ. 4.1. (Rohling & Cooke, 1999).

$$CaCO_3 + H_3PO_4 = CaHPO_4 + CO_2 + H_2O$$ **Equation 4.1 (Rohling & Cooke, 1999)**

The carbonates are measured against the Vienna Pee Dee Belemnite (VPDB), which is correlated/related to the Vienna Standard Mean Ocean Water (VSMOW) according to the equation below (Equ. 4.2).

$$\delta\,^{18}O_{VSMOW} = 1.03092\,\delta\,^{18}O_{VPDB} + 30.92$$ **Equation 4.2 (Rohling, 2013)**

Results from isotopic measurements of ^{18}O and ^{13}C are calibrated to the National Institute of standard and Technology NPS 19 standard and given according to the PeeDee Belemnite (PDB) scale.

4.3 Planktonic foraminifers

Planktonic foraminifera are a single-celled zooplankton primarily living in the uppermost 10-100 meters of the euphotic near-surface waters. Below this depth the abundance display an exponential decline (Bé, 1977) due to lack of nutrients and prey. Other controllers of the planktonic depth habitats are factors such as salinity, temperature and dissolved oxygen (Barun, 1999).

Foraminifer's shells (tests) are composed of calcium carbonate ($CaCO_3$), either from secreted calcite, aragonite or incorporated surrounding particles. The tests are constructed of a number of chambers added sequentially during growth (Mortyn and Boti, 2007). It is the amount and orientation of these tests that classifies the type of planktonic species. Size normally ranges from 100 microns to 1mm. The minority of foraminifera are planktonic, approximately 1%, making up 40-50 species. The remaining 99% of the species are benthic (Dowsett, 2007).

The relative abundance of foraminifera is lower in high salinity environment, with weak circulation central basin waters like the North Atlantic. On the contrary, high relative abundances tend to thrive in major current gyres, boundary currents, divergent and upwelling zones, as well as frontal systems (Barun, 1999). Their species geographic distribution is vast, and they inhabit very different oceanic regimes, from high latitude polar waters, to more tropical/subtropical environments (Mortyn & Boti, 2007). Planktonic foraminifera experience seasonal, diurnal and ontogenetic variations during their life cycle, making exact depth determination of a species problematic (Bé, 1977).

The planktonic species of special relevance for this study is the *N. pachyderma* (sin), also commonly referred to as "NPS", see Fig. 4.3. This particular species inhabits polar waters, where it is the most dominant type of planktonic foraminifers, but also thrives in sub polar regions (Dowsett, 2007).

Foraminifera are widely studied for global environmental changes due to the preservative abilities of the tests, serving as "recorders" of chemical and physical properties of the ocean through times. Due to its habitat in the surface ocean, planktonic foraminifera are used as an indicator of the surface waters role in climate changes. High abundances and prevalence spanning far back in time allows for paleoceanographic studies on glacial-interglacial time scales (Mortyn & Boti, 2007).

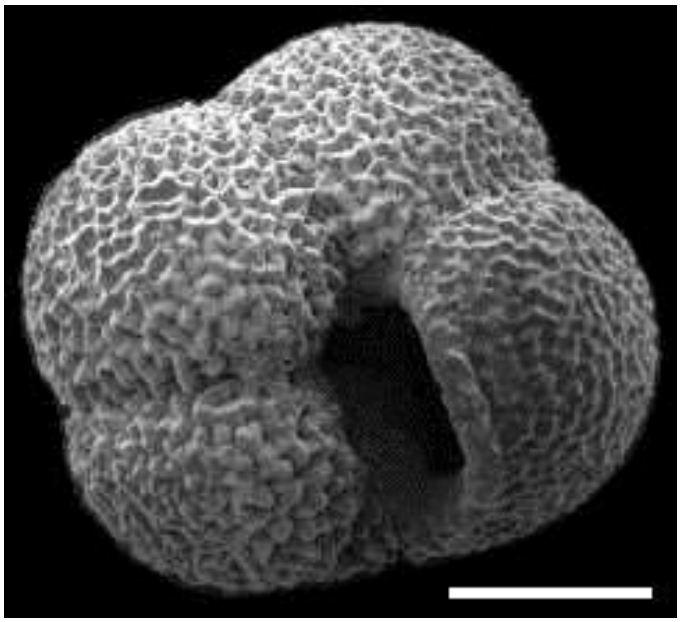

Figure 4.3. Image of the planktonic foraminifera species *N. pachyderma* (sin), constrained from website http://acces.enslyon.fr/acces/terre/paleo/systemclim/gulfstream/pages_gulfstream/dosstech/techpaleoclim/sst/sst.

4.4 Stable Isotopes

Interpretation of stabile isotopic record conducted from deep-sea cores has been a widely used proxy for investigations of climatic cycles, much because of pioneering work conducted by C. Emiliani during the mid 50`s. It is now a well-established stratigraphic and chronological tool for the Quaternary. The following section provides a brief introduction to the main aspects of stable isotope geochemistry, basically summarized by Rohling and Cooke (1999) and references therein.

Elements consisting of multiple versions, separated by differences in atomic masses, are known as isotopes. Two examples being oxygen and carbon. Each atom nucleus consists of both protons and neutrons, and it is the combined amount of these that make up the atomic mass. As the number of protons is set, the difference in neutrons is reflected in the isotope-mass of an element. This mass difference imposes small differences in the isotopes physicochemical properties, and is reflected in the strength of the bonds between the molecules. In a general, the light isotopes bonds are weaker more reactive than the heavy ones (Rohling & Cooke, 1999).

For the isotopes of least abundance, minor isotopes, the absolute abundance cannot be determined accurately, but by comparing the result with a known external standard, the quantitative relationship, known as differences in isotope ratios (delta values) can be determined (Equ.4.4a).

$$\delta_{sample} = ((R_{sample} - R_{std})/ R_{std}) * 1000$$ **Equation 4.4a (Rohling & Cooke, 1999)**

Positive d values are equivalent to enrichment in the heavy isotopes (^{18}O) relative to a standard known as Vienna Standard Mean Ocean Water (VSMOW) or PDB. Conversely, negative d values indicate a depletion of the same heavy isotopes.

When isotopes are “transferred” from one face (substance) to another, a fractionation process occurs, this is referred to as the “equilibrium isotope fractionation”, stated in the equation 4.4b, where the fractionation factor are**:**

$\Delta_{A-B} = R_A - R_B$ **Equation 4.4b (Rohling & Cooke, 1999)**

R_A, represent the heavy isotope of an element, and R_B the light isotope of the same element (e.g. $^{18}O/^{16}O$).
The fractionation is largely due to kinetic effects, such as isotopes having different reaction rate which in turn result in deviation from the equilibrium, or molecular diffusion within the boundary layer between the water-air interface (Barun, 1999) or in biological processes.

The process of isotopes being divided into substances of different isotopic composition is termed `fractionation`. The fractionation factor (alfa), quantifies isotopic fractionation between substances A and B in the equation below. R_A and R_B are the heavy/light ration between two isotopes e.g $^{18}O/^{16}O$ in chemical compounds A and B, see equation 4.4.c (Rohling & Cooke, 1999).

$Alfa = R_A / R_B$ **Equation 4.4.c (Rohling & Cooke, 1999)**

Controlling factors of the fractionation process are isotope exchange reactions, which are temperature dependent. Kinetic effects associated with diffusion cause deviation from the equilibrium process because of different reaction rates of the isotopic species (Rohling & Cooke, 1999).

4.4.1 Oxygen isotopes

Oxygen appears in nature in the form of three isotopes, ^{16}O, ^{17}O and ^{18}O. These can be found in relative proportions of 99,76%, 0,04% and 0,2% respectively (Bradley, 2014). The following section will focus on the ratio and alternations between the heavy and light oxygen isotopes in seawater and foraminifera carbonate.

The $^{18}O/^{16}O$ ratio, referred to as $\delta^{18}O$ of seawater are constantly alternating due to its close linkage to the hydrological cycle. The hydrological cycle consists of factors as evaporation, precipitation, runoff from iceberg melting and storage of freshwater in ice sheets, see figure 4.4.1a. Especially storage of large quantities of freshwater, severely depleted in ^{18}O, over longer periods than the ventilation time of the ocean, leads to a delay in the hydrological cycle and signal between isotope and ocean circulation.

The distribution of $\delta^{18}O$ in seawater is also very dependent on the ocean circulation and mixing, as well as the surrounding environment (Barun, 1999).

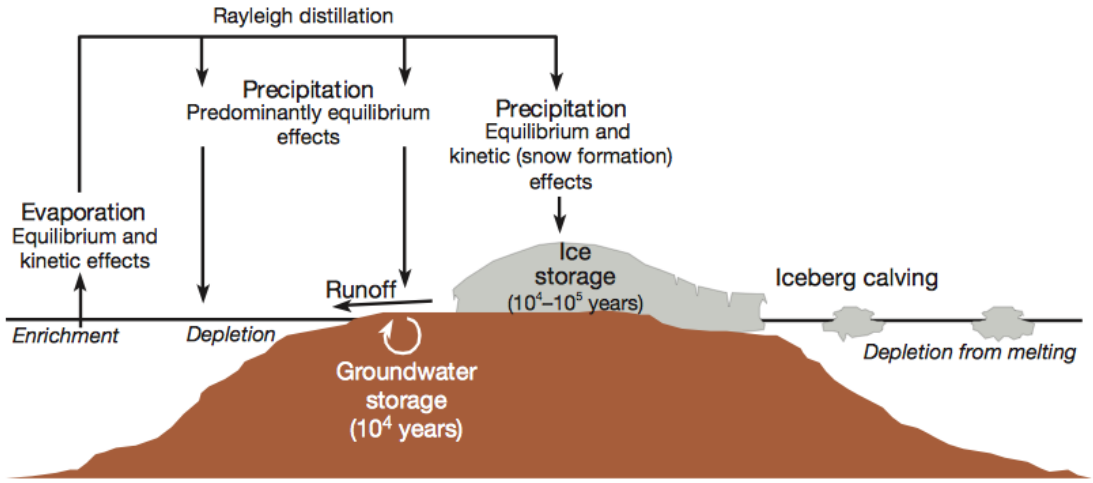

Figure 4.4.1a. An overview of the hydrological cycle and its implications on the oxygen isotope ratios (Rohling and Cooke, 1999).

The exchange of oxygen isotopes occurs in the air-sea interface and is modified in the following equation:

$H_2{}^{16}O_{liquid} + H_2{}^{18}O_{vapor} \leftrightarrow H_2{}^{18}O_{liquid} + H_2{}^{16}O_{vapor}$ **Equ. 4.4.1.a (Rohling & Cooke, 1999)**

As water is evaporated from the surface waters, the light isotopes are preferably incorporated in the vapor phase, leaving the remaining water masses/vapor depleted/enriched in $\delta^{16}O$. The amount of ^{16}O uptake in the vapor phase is dependent on factors like humidity (Barun, 1999).

In proximity to the source region, the first precipitation has an isotopic composition similar to the water masses it was evaporated from. As the proximity to the source region decreases, the depletion of $\delta^{18}O$ will increase (Rohling & Cooke, 1999).

During condensation the heavier isotope is preferentially removed, the remaining vapor will be subsequently more depleted in $\delta^{18}O$ (Rohling and Cooke, 1999). The atmospheric vapor is transported towards higher latitudes and a quasi-linear relation between $\delta^{18}O$ and

temperature, results in even more depleted precipitation in colder regions than in lower latitudes.

The more or less depleted precipitation will in turn affect its surroundings, and most importantly the surface waters, in terms of adding freshwater either as runoff from rivers or directly into the ocean (Rohling and Cooke, 1999). For an overview of global surface seawater $\delta^{18}O$ values, see figure 4.4.1b.

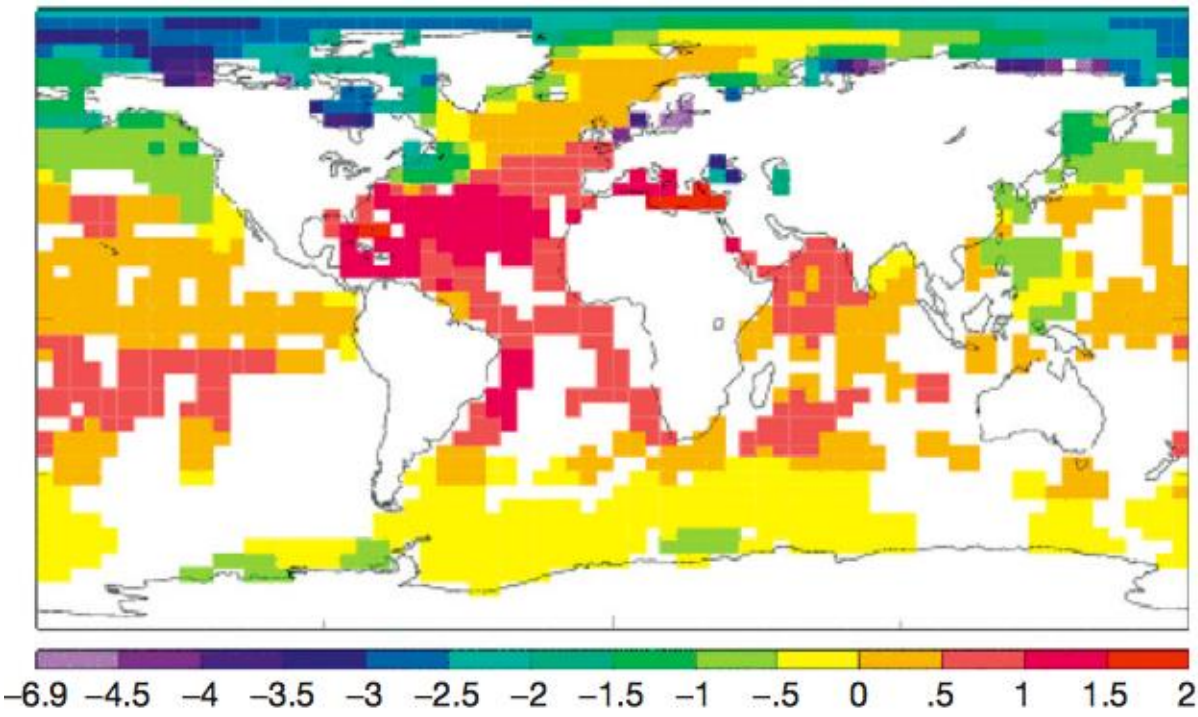

Figure 4.4.1b. An overview of global surface seawater $\delta^{18}O$ integrated over the top 50 meters on a 4 x 5º grid, by Schmidt et al. (1999) in Rohling and Cooke (1999).

Measurement of $\delta^{18}O$ of fossil carbonate is another method of revealing seawater composition of the past. The formation of the oxygen isotope composition of carbonate shells is highly influenced by the "equilibrium fractionation" between the foraminifera and the water. According to Spero et al. (1997) is the $^{18}O/^{16}O$ ratios incorporated in shell carbonates a function of the oxygen isotope ratio in the seawater and the calcification temperature (Equ. 4.4.1.b)

$Ca^{2+} + 2HCO_3^- \leftarrow\rightarrow CaCO_3 + CO_2 + H_2O$ **Equation 4.4.1.b (Rohling & Cooke, 1999)**

An issue concerning the study of carbonate $\delta^{18}O$ is the "vital effects" which are related to the growth rate changes during the life cycle of the organism. Species may change depth habitat during different stages in their life cycle. As a consequence of decreasing temperature with increasing depth, a migration in the water column will influence the fractionation. This is a factor that is normally corrected for by picking in size delimited fractions. According to Rohling (2013) the overall effect of equilibrium fractionation is about 0, 2 ‰ depletion in carbonate $\delta^{18}O$ for every 1° increase in temperature.

4.4.2 Carbon isotopes

Carbon occurs as two stable isotopes, where ^{12}C constitutes 98.89%, and the less abundant ^{13}C make out 1.11% (Rohling & Cooke, 1999). The use of carbon$^{13}C/^{12}C$ ratios is often complementary to oxygen isotope measurements.

The study of carbon isotopes is known to provide information on past oceanographic conditions. Despite being influenced by factors as biological productivity, ventilation rates of the ocean and ecological factors of foraminifera, it can be used for correlation purposes and dating, but more readily as an additional age control (Jansen, 1989).
The $\delta^{13}C$ in planktonic foraminifera reflect the changes in productivity of the uppermost part of the water column (Lowe & Walker), as well as provide an indication of how the ^{12}C flux in surface waters has changed through time (Shackleton & Pisias, 1985). Carbon isotopes of planktonic foraminifera can also provide information about atmospheric variations in CO_2 back in time (Shackleton et al., 1992).

Carbon isotope ratios, expressed as $\delta^{13}C$, are a marker for the fertility of surface waters. Different processes occur in the ocean-atmosphere interface that affection this ratio, such as varying CO_2 exchange with the atmosphere, resupply of carbon from subsurface waters and fractionation. The difference in enrichment of $\delta^{13}C$ in the water column is related to the consumption of carbon during photosynthesis. During this process, ^{12}C is preferentially incorporated in the formation of organic matter, leading to an excess of ^{13}C. Thus, the photic zone of the waters is enriched in ^{13}C compared to the deeper surface waters. However, vertical gradients within the surface waters may drive significant changes in the $\delta^{13}C$ signal. Small changes in thermal stratification may drive the planktonic foraminifera to calcify deeper in the

water column, close to the nutricline (Cermeno et al., 2008), implying mainly changes in depth habitat of the planktonic foraminifera, rather than deep ocean convection and ventilation.
Another factor controlling the distribution and ratio of $\delta^{13}C$ are the temperature dependent fractionation process. Wefer et al. (1999) state that lower temperatures result in greater fractionation, indication potentially higher ^{13}C enrichment in cold surface waters.
Higher values of $\delta^{13}C$, is also related to convection of nutrient rich waters mixed up to the surface, potentially reflecting changes in the deep-water ventilation (Duplessy et al., 1984).

4.5 Assemblage counts of *N. pachyderma* sin and counts of ice-rafted detritus.

To obtain information of the amount and variation of planktonic foraminifera and ice rafted detritus at any given time in the core 38CC, counts of the above were conducted. Emphasis of the counts was constrained to the Marine Isotope Stage 3 (MIS 3) of the core with the purpose of displaying possible Dansgaard-Oeschger events.

For the counting, fraction >150 micron was used. To bring the number of material in a sample down to a desired amount, a micro splitter was used. This splitter divides a sample into two equal halves *(n)*, making a split equal to $1/2^{(n)}$ fraction of the original sample. After splitting the material was transferred onto a picking-tray, where the number of squares was counted until reaching approximately 300 species of *N. pachyderma* (*sin*). The number of other planktonic foraminifera present in the samples was also counted but not further distinguished, see appendix B. The percentages of *N. pachyderma* (*sin*) are calculated relative to the total planktonic foraminifera content.

Absolute and relative abundances were calculated from the counts on the basis of the equations below. For IRD counts, only absolute abundances were constrained. The amount of terrigenous grains was counted, but no further classification of the siliciclastic components was made.

Absolut abundance (ind/g): ind *50/n (squares counted)*splits/ dry weight

***Relative abundance (%)**:* (Total nps in sample * 100)/ (total all planktonic nps in sample).

According to Knudsen et al. (2004) ice-rafted detritus is defined as sediment components released from melting icebergs or sea ice and deposited on the ocean floor. The main quantity of terrigenous debris, independent of grain size is transported to the ocean floors primarily during glacial periods Ruddiman et al. (1989). Estimates from North Atlantic refers to ~40% of the sediments being IRD deposited during Quaternary cold stages (Robinson et al., 1995). The material accumulating in the deeper oceans has a high percentage of biogenic material like remains of siliceous and carbonaceous microorganisms. Accumulation biogenic material is associated with warmer climate and/or interglacial conditions (Lowe and Walker, 1997).

4.6 Sources of error

At different stages in the processing of core 38CC, sources of error may have occurred as listed below.

- Preparations on board the ship, such as splitting, packing, and transport of the cores can potentially lead to disturbance of the sediments.
- During sieving of the sediments in the laboratory, microfossils might be lost in the process due to human error.
- Lack of proper calibration of the scale might lead to offset in the results when extracting the samples.
- During the transfer of dried samples to glass vials, microfossils can get lost. To prevent this, a white sheet of paper was placed on the desk, to detect and potentially recover a spilled sample.
- Picking of wrong foraminifera species for mass spectrometry may occur due to insufficient recognition of the different species.
- When dispersing the sediments on the shaking machine, the presence of ice rafted detritus might potentially crush the foraminifera if the tests are fragile.
- During washing of the sediments, ordinary tap water was used. Hence, the risk of contamination is higher, compared to using distilled water. Such contamination may trigger alternations in the foraminifera test, due to minerals present in the water.

5. Chronology

Making a chronology is much like constructing a timeline. By arranging know events into order of occurrence in time, with the use of a proxy (Lowe & Walker, 1997). The chronology for marine core 38CC is partially based on AMS 14C dating as well as correlation to the benthic oxygen isotope stack LRO4 (Lisiecki and Raymo, 2005). The purpose of establishing a chronology is to allow for comparisons with other proxy based reconstructions on the same time line. This section provides a description of the production of the age model, as well as a brief introduction to the theoretical background of ^{14}C dating and reservoir ages.

5.1 AMS ^{14}C dating and calibration

Radiocarbon dating is a radioisotopic method, and one of the most used dating techniques for the Quaternary time period. The method is applicable for approximately the last 40 000 years. This is due to the short half-life of ^{14}C (-6000 y) and because the risk of contamination during low activity levels are high (Wefer et al., 1999).

There are two stable isotopic forms of carbon, 12C and 13C, the former being the most abundant isotope in nature. Unstable isotopes, such as 14C, more easily undergoes radioactive decay resulting in transition into a new element, also known as the "daughter product". The rate of decay is undeviating, a fact that is key to the method, as it permits establishing half-lives of radioisotopes (Bradley, 2014). The term half-life refers to the amount of time it takes for the radioactive material in a sample to decay to half of its original amount. Gaining knowledge of this parameter makes it possible to assess the time that has elapsed since the deposition of the sample (Bradley, 2014).

Three samples of planktonic foraminifera, *N. pachyderma* (sin) were retrieved from core 38CC and sent to Beta Analytic Inc in Miami Florida for AMS radiocarbon dating. For the results from the dating, see table 5.1. Accelerator mass spectrometry (AMS) is the most common method of radiocarbon dating (Jull, 2007). In comparison to the conventional counting radiocarbon decay method, AMS is 1,000 to 10.000 times more sensitive, seeing that the latter measures the radionuclide directly, while the conventional method wait for each decay event to occur. In this thesis ages are consistently reported as calendar years before present, where present is refers to common Era (CE), denoted as ka BP.

Laboratory number	Core depth (cm)	Conventional radiocarbon age (BP)	Calibrated radiocarbon age (Cal. Yr. BP)	Age range (ka)
Beta - 419048	60-61	15170 +/- 50	**18050**	175
Beta - 419049	180-181	22720 +/- 110	**26920**	660
Beta- 419050	345-346	42150 +/- 560	**46020**	1795

Table 5.1. Result from radiocarbon dating of core GS15-198-38CC. Three dates were obtained.

There are different methods for calibrating a radiocarbon age, either by using probability density curves, or interception. The terms of the latter calibration curves are intercepted by radiocarbon ages with plus/minus one or two standard deviations. That way a calibrated age range can be obtained. A drawback of this approach includes restrictions to the uncertainties of the radiocarbon age, and lack of information about relative probability of calibrated age ranges. A probability density function (PDF) provides information about the distribution shape. By the use of an equation (not further elaborated here), the probability density is altered into calibrated year dependency (cal. yr) (Reimer and Reimer, 2007), with one and two standard deviations, providing 95% or 68% confidence intervals of the probability curve.

For the three dated samples from core GS15-198-38CC, the calibration was performed using 2013 calibration databases (Marine13 database). Measured $^{13}C/^{12}C$ ratios were calculated relative to the PDB-1 standard.

5.2 Reservoir/ventilation ages

Ocean and atmosphere dynamics are closely related to the ventilation of the oceans. The process of incorporating atmospheric carbon dioxide (CO_2) into the surface waters (calcareous organisms) generates an enrichment of ^{14}C activity. Conversely, deep-water upwelling is highly depleted in ^{14}C. Mixing of water masses with different carbon composition makes ^{14}C age (reservoir age) determination from marine organism problematic. For that reason, corrections of reservoir ages are made depending on the climatic setting of the area. The size of the imprint depends on the ocean circulation and limitations to the exchange of CO_2 between ocean and atmosphere, hence interaction between advection and convection of warm and cold waters, respectively (Bradley, 2014).

Differences between surface ocean and atmospheric ages varies due to delays in transmission of newly formed carbon from the atmosphere into the ocean. This delay is referred to as the "reservoir age", and differs strongly throughout the world's oceans.
Factors contributing to a higher reservoir ages may arise from upwelling of old ^{14}C- depleted water, or sea ice coverage. In general, these characteristics coincide with higher latitudes. However, for areas like the North Atlantic, corrections for the apparent age are not as high as for example around Antarctica. This is primarily a function of strong deep-water formation, preventing upwelling of depleted water masses, as well as advection of warmer, enriched ^{14}C waters flowing northward from the tropics (Bradley, 2014).

Reservoir age discrepancy, especially in mid- and low-latitudes, is amplified during periods of weak North Atlantic Deep Water formation (NADW). The presence of sea ice coverage inhibits the ocean-atmosphere interaction for longer periods, simultaneously as deep-water depletion is increasing (Bradley, 2014). The surface reservoir effect in the central North Atlantic today equals to ~ 400 years. Nordic Seas exhibit somewhat lower values, see figure 5.2.

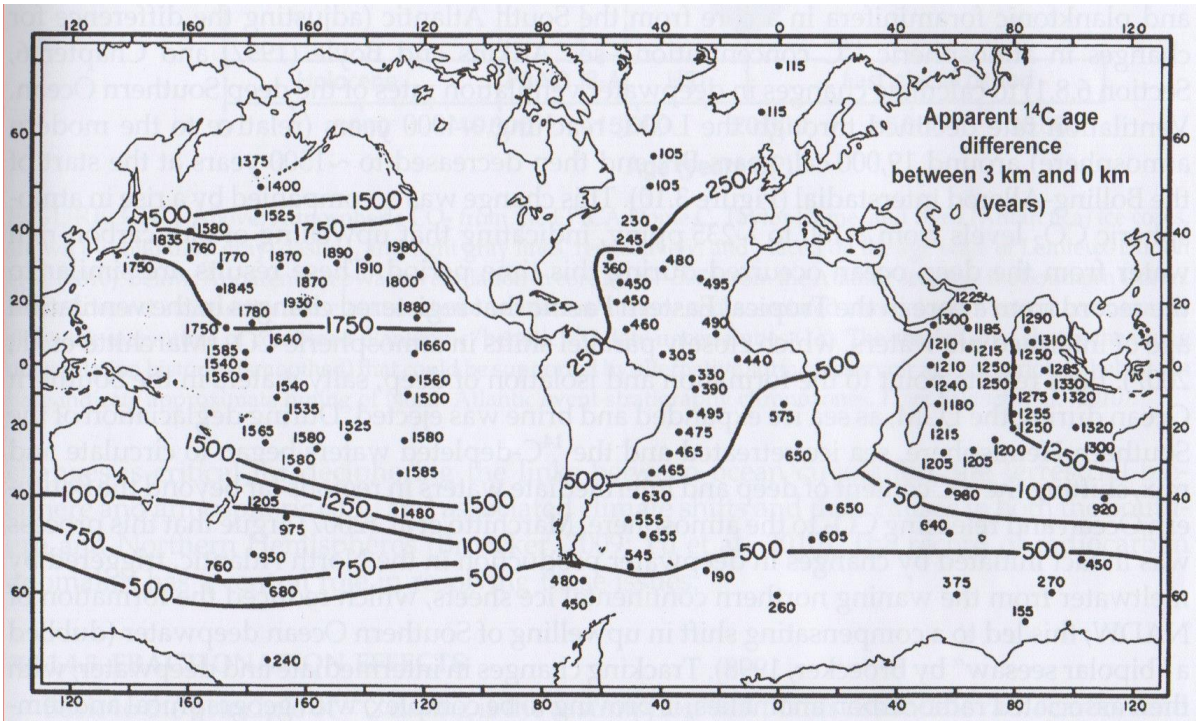

Figure 5.2. A global overview of reservoir ages of surface waters, and extending 3 km down the water column. For the North Atlantic Ocean, increase in reservoir ages is consistent with higher latitudes, except for the Nordic Seas (Broecker et al., 1998).

5.2 Constructed age model

The marine sediments cannot be dated beyond the range of a few radiocarbon half-lives. The time range for the ^{14}C dating is approximately 50 kyr, but a robust ^{14}C calibration curve is only established for the past 26 kyr with the calibration record INTCAL04. Thus, reaching as far back in time as 50 kyr is not reliable with a calibration curve (Reimer & Reimer, 2007). For this reason, an attempt to construct ages based on oxygen isotope measurements, from core 38CC, to extend the timescale further back in time was conducted

When constructing the age model a graphic correlation of ^{18}O isotope values to Lisiecki and Raymo (2005) LR04 "stack" was made. The LRO4 stack contains benthic $d^{18}O$ records from 57 sites well distributed both spatially and at depths, and reflect changes in global ice volume and sea level. Sites included are located in the Atlantic, Pacific and Indian Ocean. Oxygen isotope measurements were derived from two foraminifer species; *Uvigerina peregrina* and *Cibicidoides wuellerstorfi.* The stacking technique purposely excludes sample spacing's greater than 12 kyr, because of poor resolution. Even though records of varying quality have been included, a higher emphasis is placed on sites with greater resolution in the averaging process. The mean standard error of the LRO4 stack is 0,06 ‰, and 2% of the data point have errors greater than 0,1% (Lisiecki and Raymo, 2005). Presented in table 5.2.1 is a correlation of LRO4 ages and corresponding depths (cm) in core 38CC, as well as Marine Isotope Stage (MIS) boundaries defined by Lisiecki and Raymo (2005).

MIS boundary	LRO4 age (ka)	Correlated depth in GS15-198-38CC (cm)
1/2	14	78 (75.25 - 80.5)
2/3	29	170.5
3/4	57	435 (415.25 - 455.25)
4/5	71	515.25
5/5e	123	660.5
5e/6	130	678 (675.25-680.5)

Table 5.2.1 overview of LRO4 stack age, and corresponding depths in core GS15-198-38CC. Chronostratigraphic marine isotope stages (MIS) follows the timescale defined in Lisiecki and Raymo (2005).

The age model was constructed by the use of software ANALYSERIES. Carbon dates retrieved was considered as an initial age control, while tie points were composed on the basis of similar characteristics in the oxygen isotope record of core 38CC (Figure 5.2.1). For additional verification of the tie point and transitions, carbon isotopes were considered, see table 5.2.1. This consideration was based on highly pronounced characteristic in the $\delta^{13}C$ record, where especially marked events of strong depletion of carbon were emphasized. To establish a coherent age- depth relation, linear interpolation has been applied between the tie points. The age scale is set to start at age 0, representing the present. In most cases this assumption is incorrect, but it is generally difficult to determine exact age of the core top without a radiocarbon date. It is therefore exclusively for simplifying reasons the beginning of the age scale is set to zero.

In general, there are some limiting factors related to the use of carbon isotopes in planktonic foraminifera as a correlation tool, mainly concerning species to species variation. During the life cycle the microorganism inhabit different depths of the water column, which in turn lead to secretion of carbonate in either ^{13}C depleted or ^{13}C enriched surface waters (Jansen 1989). Other factors, such as variations in primary production where the light isotope ^{12}C preferably is incorporated in biological processes, and therefore extracted from the ocean, will affect the isotope ratio of carbon (Jansen 1989).

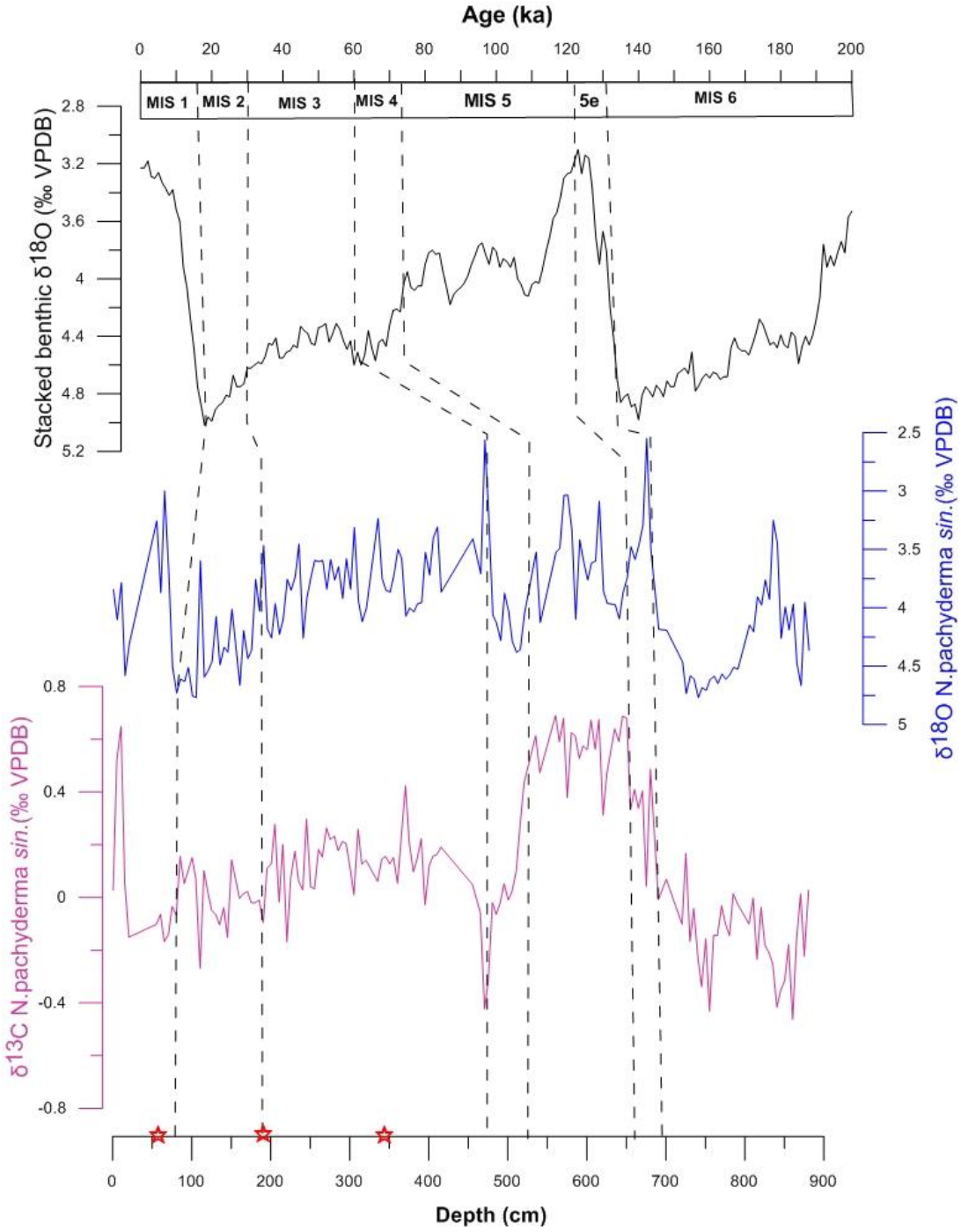

Figure 5.2.1 Correlation between LRO4 benthic stack and parameters in core 38CC. $\delta^{18}O$ (blue) and $\delta^{13}C$ (orange). MIS taxonomy from SPECMAP, Ruddiman et al (1989) in Lisiecki and Raymo (2005). Red stars indicate location of radiocarbon dates in the core. Dashed lines separate the different marine isotope stages indicated in capital letter above the curves.

Information about sedimentation rates was extracted from ANALYSERIES on the basis of the age model. The rates presented in figure 5.2.2 represent average values between two points in the model, for exact values (points) see appendix C. From the figure the lowest sedimentation rates occur during most part of MIS 5, with values ranging between 2 - 3 cm/1000 yr. On the contrary, the highest rates of ~12 cm/1000 yr can be observed at the start of interglacial MIS 3. The exceptionally high rates persist for approximately 15 kyr (60-45 ka BP), before a subsequent small decrease to ~ 8 cm/1000 yr. In general, moderate sedimentation rates appear during MIS 6 and 5e, before a prominent decrease in sediment influx dominates MIS 4 and 5. A remarkable increase to high sed. rates occurs during MIS 3, transitioning into moderate sedimentation again during MIS 2 and 1.

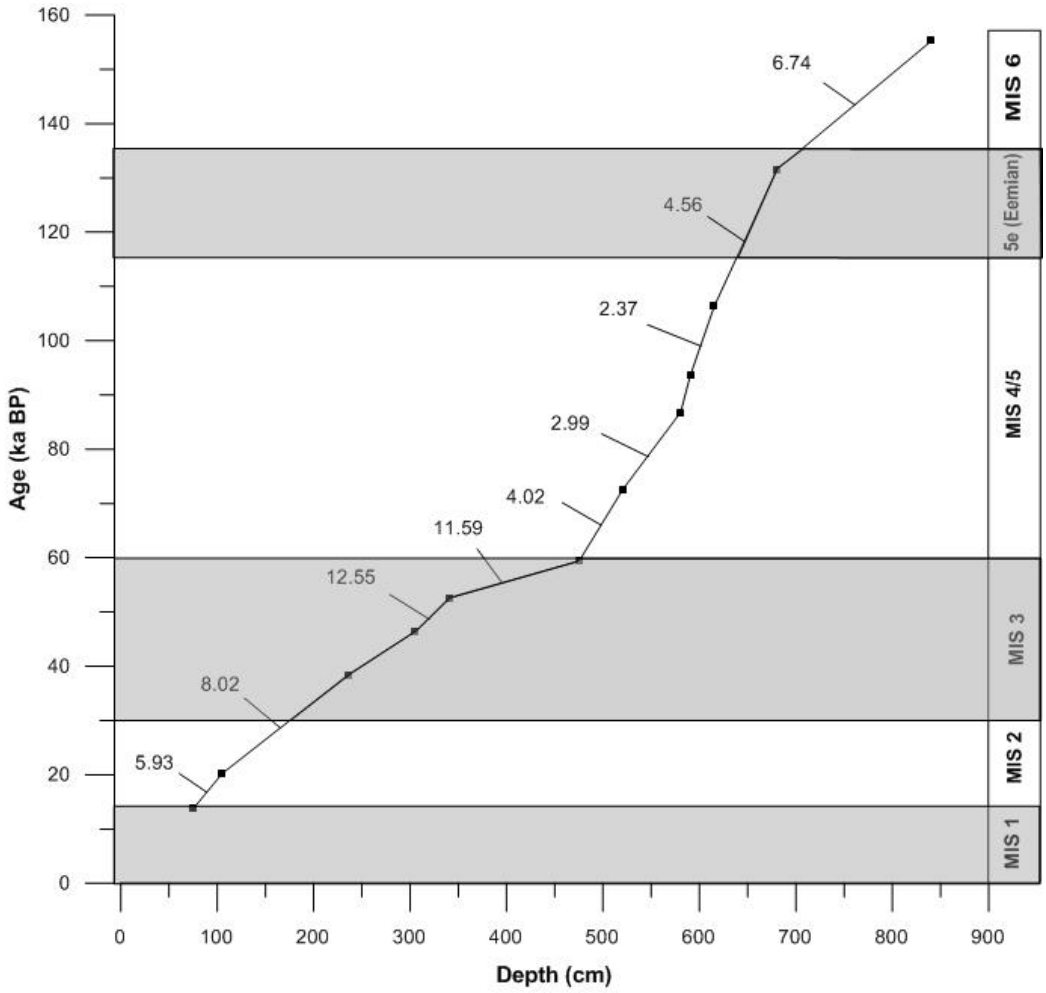

Figure 5.2.2. Average sedimentation rates (cm/1000yr) for core 38CC plotted against depth (cm). Grey shaded bars indicate interglacial conditions. MIS taxonomy is marked as capital letters to the right in the figure.

6. Results

Numerous proxies can be applied to better understanding the paleoceanographic parameters of a marine sediment core. I here have selected the results from the core analyses that are used for in the discussion concerning abrupt climatic events and paleoceanographic interpretations. Presented below are therefore results from stable isotopic measurements of $\delta^{18}O$ and $\delta^{13}C$ as well as x-ray fluorescence element analysis with emphasis on Ca, Fe and Ti. Assemblage counts of the planktonic foraminifer species *N. pachyderma sin* (NPS) and ice rafted detritus (IRD) are also presented.

6.1 Non intrusive core analyses

6.1.1 Magnetic Susceptibility

Results from the magnetic susceptibility (MS) measurements are plotted against depth (cm) in figure 6-2.1. Unites are given in SI. The general trend in the 900-725cm depth interval is decreasing values of MS with peaks at 870, 840, and 800 cm. The interval 725 – 375 cm displays smaller alternations ranging from 0,005 – 0,00125 SI. The lowest value appears at around 400 cm, with a subsequent rapid increase in values. There are four prominent peaks in the interval 400-225 cm, with the highest value of 0.0025 SI at 320 cm depth. The uppermost 250 cm of the core display smaller alternations with lowest recorded values at 230cm, 190cm, 120cm, 60cm and 20cm.

The most prominent characters of the MS-data are high magnetic values observed in the core during interval 400-225 cm. The first peak in values at 400 cm is interpreted as the initiation of a deglaciation, marking the MIS 4/3 transition. Higher content and larger fluctuations between the peaks might be linked to a period of stronger deep-water currents and transport. The depth interval 250-0 cm resemble some the same stable low value characteristics as observed in MIS 4 and MIS 5. The low point at 120 cm, is interpreted as the last glacial maximum, and the transition MIS 2/1.
The older part of the core, the interval 900-725cm is interpreted as glacial MIS 6, culminating in a low at 725 cm marking the transition MIS 6/5. The decreasing trend in values consequently comprises less magnetic faction in the terrigenous material transported to the site during glacial MIS 6. More stable conditions of the interval 725-375 cm display

generally lower values of magnetic susceptibility, indicating less variation in the transport of magnetic minerals to the site.

6.1.2 X-ray fluorescence elements (XRF)

Results from XRF-element analysis are plotted in figure 6.1.2a. The datasets for Ca, Fe and Ti are processed, and obvious outliers have been manually removed. The units are presented in counts per second (cps) and the measurements are plotted against depth (cm) in the core.

The interval 900-450 cm of the calcium data set are dominated by rapidly alternating values while the upper part, 450-50 cm are generally more stable and exhibit higher values. Four remarkable drops in calcium values occur at 730-690 cm, 460-430 cm, 50 -20 cm and around 100 cm. The lightness graph is used as an additional parameter for validation of sediment composition. From figure 6.1.1a, the general trend of the lightness curve follows the calcium, though with a considerable more moderate amplitude in fluctuations.

The Fe curve displays a gradual decrease in values in the interval 900 – 700 cm. There is a subsequent short-lived peak at around 700 cm with values of 140 000 cps. The following section features relatively stable values, before a clear drop appears at 450 cm depth. A new period of increasing Fe culminates in a second peak at approx. 350 cm. From this point a decreasing trend is observed until 150 cm, where the lowest value of 65 000 cps is recorded. The top 150 cm of the graph displays a new moderate increase in values.
From the Ti record, a smother curve with less alternations can be observed. Four peaks are prominent, all within the depth intervals of 410-250 cm. There is an additional peak at around 880 cm of values of 2750 cps. The following section up until 410 cm is dominated by stable Ti values. The two first peaks appear quite closely from approx. 425-400cm, the third peak, with the highest amplitude is seen at 375 cm. The fourth incident of high values ranges from 300-275 cm. The following interval display moderate decrease in values until around 125 cm, where a shift occurs and an increase trend applies for the top 125 cm.

The purpose of this xrf-element analysis is to distinguish between the marine and terrestrial signal. The four “peaks” of negative calcium values are all an indication of lower biogenic contribution. These low points presumably occur under cold conditions, and may indicate the presence of ice-cover. The low values at approx. 730-690 cm is interpreted to represent the MIS 6/5 transition, 460-430 cm the MIS 4/3 transition and the 100 cm one as the onset of the

last deglaciation marking the MIS 2/1 transition. The Fe data mirrors the calcium to some extent. The most prominent low values of calcium, as presented below, are seen as peaks in the iron graph, this is especially prominent at the two depth intervals 700 cm, and 400 cm. This indicates that during the glacial-interglacial transition, as the calcium content is building up as a result of warmer climate and less ice-cover, the terrestrial input is reduced due to less IRD transport to the site. The Ti curve has some of the same features as Fe in the MIS 3 interval; beside from this it has closest resemblance to the magnetic susceptibility curve, displaying almost the same characteristics. More generally, periods of apparently stable and low signals of the Ti and Fe, indicate that less input of detrital material occurred at that time. Consequently, reflecting a stable ice sheet, lending concurrent changes in the $\delta^{18}O$ record to different causes.

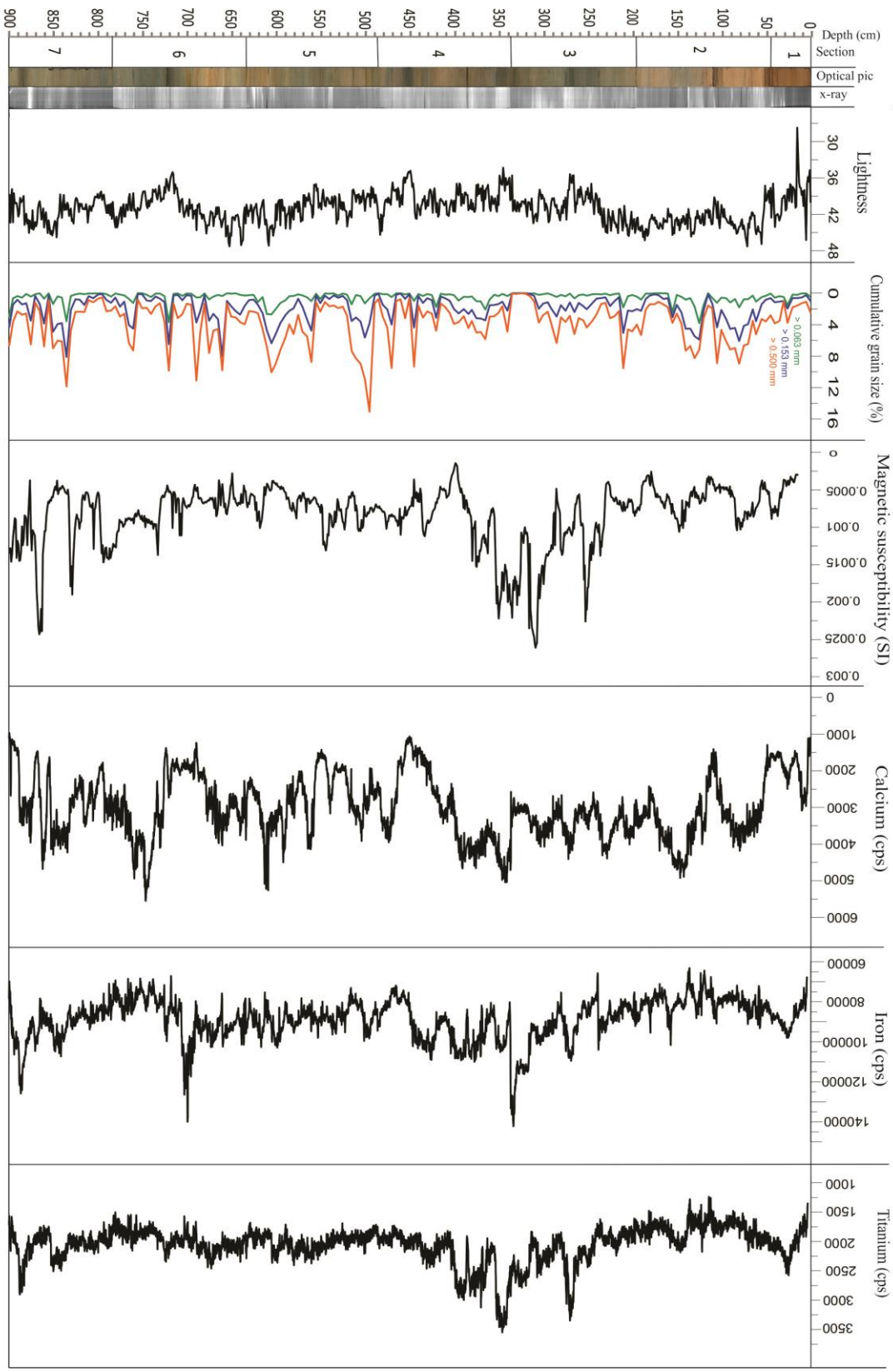

Figure 6.1.1a. An overview of XRF elements Ca, Fe and Ti are plotted on a depth (cm) scale. Included in the figure is also magnetic susceptibility and cumulative grain sizes, as well as optical and x-ray pictures.

The Ca/Fe ratio functions as an environmental indicator. Peaking higher values of calcium relate to open waters, with favorable conditions for productivity implying generally warmer climates. Especially high values can be seen observed at ages 100 ka, 80 ka, 55 ka, 25 ka (Figure 6.1.2b). More open waters are further an indication of a stronger influence of North Atlantic water masses flowing into the site from the southeast Norwegian Sea, and suppression of the East Greenland current. Oppositely, higher rates of Fe are related to glacial input in terms of transport of terrigenous material to the site through ice rafting. More sea ice is a result of colder climate, and a weaker influence of warm, salty North Atlantic water masses, and a broader extent of the Greenland Current (Fig. 6.1.2b)

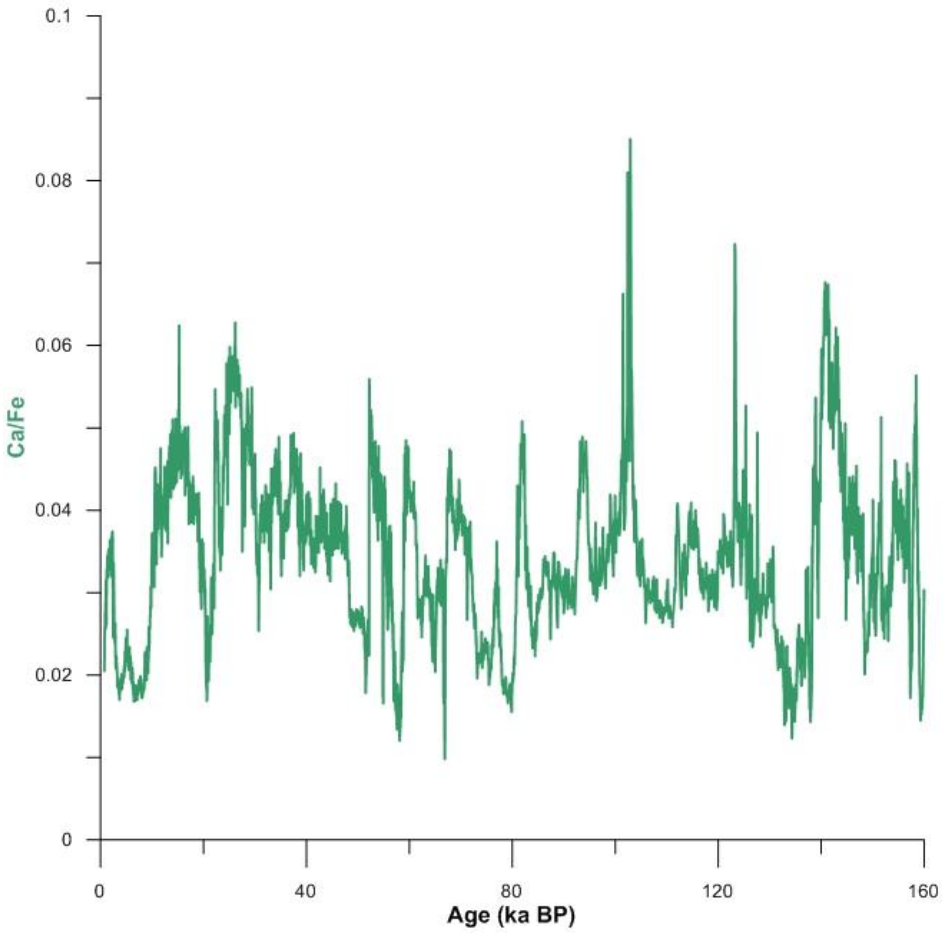

Figure 6.1.2b. Curve displaying the Ca/Fe ratio.

6.2 Discrete sample analyses

6.2.1 Oxygen isotopes

Results from oxygen isotope measurements are plotted in figure 6.2.1. The dataset is correlated to the age model obtained from the benthic stack LRO4 (chapter 5.2) and plotted on an age scale. The older part of the age model (130-160 ka) exhibits great uncertainties in terms of reliability. Mostly resulting from difficulties in correlating with the stack LRO4, due to lack of corresponding distinctive characters in both datasets. Because of these limiting factors, it will not be emphasized or commented on any further in this thesis.

In general, the $\delta^{18}O$ record of core 38CC displays largely fluctuating values. From figure 6.2.1a, three peaks of increase in lighter values are prominent. These occur at the ages 135 ka, 60 ka, and 15 ka with a decrease in values of 2.25, 1.75 and 1.75 ‰, respectively. The largest offset in values of the entire $\delta^{18}O$ dataset occurred 135 ka.
Two intervals dominated by generally lighter d18O values and separated by a significant drop in lightness, occur in the age intervals 130-65 ka and 60-15 ka. The two intervals display very different characteristics. The former show four distinct gradually occurring peaks at 105 ka, 95 ka, 85 ka and 75 ka. The frequency of peaks is generally higher during the age interval 60-15 ka with a large number of shifts in $\delta^{18}O$ values. The latter consists of the most rapidly occurring oscillations observed in the oxygen isotope dataset. A general trend of enrichment of heavy isotopes can also be observed in the 60-15 ka interval.
The overall heaviest values of $\delta^{18}O$ are found at 130 ka and 15 ka, with subsequently sharp increase into lighter $\delta^{18}O$ ratios.

An increase in lighter $d^{18}O$ values indicates a transition to warmer conditions. Sharp transitions from abundance in heavy isotopes to an increase in lighter ones are hence interpreted to represent shifts from glacial to interglacial conditions. The three most prominent peaks are interpreted to mark the oxygen isotope transitions 6/5 (135 ka), 4/3 (60 ka) and 2/1 (15 ka), all defining a shift from cold glacial conditions to a warmer interglacial state, also known as deglaciation. The four peaks in the interval 130-65 ka have been interpreted to represent the warm stages of MIS 5, terminating at the last high point to mark the transition into cold glacial conditions of MIS 4. Increasing values at the age 60 ka denotes

the transition to the warmer interglacial MIS 3. MIS 4/5 display fewer and longer peaks, in contrast to MIS 3, which is dominated by rapid oscillations. Indicating that climatic changes occurred at a faster pace during MIS 3 than MIS 5/4.

6.2.2 Carbon isotopes

Results from carbon isotope measurements are plotted against age in comparison with $\delta^{18}O$ values in figure 6.2.2. In general, the carbon measurements display a slightly smoother curve in comparison to the oxygen isotopes, especially in the age interval of 130-60 ka. There are two distinct peaks of negative values of approximately -0.4 at the ages 140 ka and 60 ka. A gradual increase to positive values of 0.7 appears from 140-120 ka, whilst the transition to positive values of maximum 0.4 in the interval 60-55 ka occurs more rapidly. Another important observation is that $\delta^{13}C$ values are significantly lower during ages 120-70 ka than 60-15 ka with an average of 0.4. The latter interval displays the same trend of decreasing values as seen in the $\delta^{18}O$ data, culminating in values of -0.2. In the age interval 120 – 75 ka the values are fairly stable of positive 0.7 – 0.4 ‰. At the interval 75-60 ka a sharp decrease in values are prominent. In general, the trends of the carbon isotopes appear to be in phase with the fluctuations observed in the oxygen isotope record.

Negative values of $\delta^{13}C$ at 140 ka and 60 ka most likely represent meltwater pulses and the initiation of a deglaciation, at the MIS 6/5 and 4/3 transitions respectively. The low values may also refer to suppressed ventilation conditions in the ocean during glacial times. As the influence of melt water is reduced, and ventilation processes is restored, the values increase to an interglacial max as seen at ages 80 ka and 5 ka in the figure. From the $\delta^{13}C$ record it is evident that the MIS 6/5 transition occurred more gradually than the MIS 4/3 transition, indicating a slower regain of ventilation in the water masses 130 ka. This may be due to a longer sustained freshwater flux compared to 60 ka. Generally higher $\delta^{13}C$ values during MIS 5 compared to MIS 3 can be related to more open waters and changes in the global carbon isotope budget (Jansen, 1989). Sharp decrease in values observed at 75 ka is interpreted to represent the MIS 5/4 transition, reflecting limitation to the carbon ventilation in the ocean, as a result of colder conditions and growth of sea-ice.

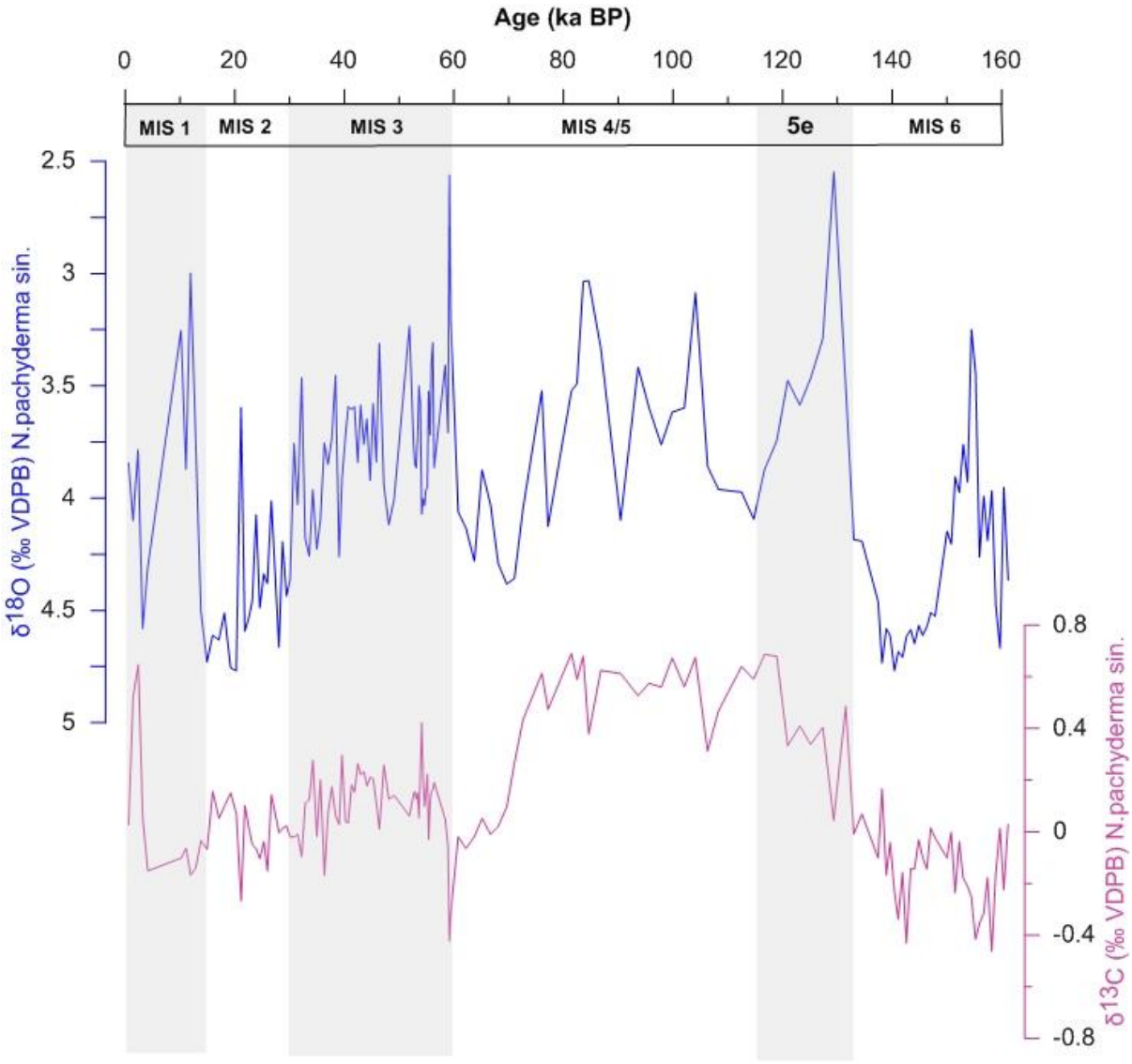

Figure 6.2.2. The graph displays oxygen and carbon isotopes from core GS15-198-38CC plotted on a constructed age scale. Darker shaded bars represent interglacials

6.2.3 *N. pachyderma sin.* assemblages and Ice Rafted Detritus (IRD)

The planktonic foraminifera species dominating the surface waters is the region is the left coiling *N. pachyderma*. The relative abundance NPS (%) in core GS15-198-38CC are generally high, ranging between 97-100%.

The first decrease in relative abundance NPS (%) can be seen just after 60 ka BP. This peak is short-lived, and quickly stabilizes into higher percentages. The following age interval 55-30 ka consists of rapid oscillations ranging in values from 97.5-100%. Intervals of 100% NPS can be observed at the approximate ages 55-50 ka and 27-25 ka ago. The observed

fluctuations are so small that it is questionable if they represent significant environmental changes.

Looking into the absolute abundance (ind/g) NPS the highest peak of approximately 3000 ind/g occur at 65-60 ka, see figure 6.2.3. Just below 60 ka the NPS abundance decrease to a low off 0 ind/g. In the interval 60-20 ka the abundance fluctuates sporadically with the highest value being 1300 ind/g. At 25 ka it is observed a second low of 0 ind/g before a rapid increase, peaking at 1500 ind/g and spanning from approximately 25-15 ka.

Three short-lived peaks in IRD are prominent in the data set. The first peak can be observed at 60 ka with a value of about 1400 grains/g. A subsequent decrease in IRD is seen in the 60-30 intervals. The second prominent peak appear at approximately 35 ka, culminating in a new absolute abundance low of 0 ind/g at 30 ka ago. The last 30 kyr, are dominated by fluctuating IRD, generally higher in values than previously observed in the data set, with the third clear peak at 20 ka. A subsequent drop in values appears at 15 ka.

The generally high percentages of NPS are an indication of prevailing cold waters at the site, furthermore short peaks of lower percentages may testify of periodically slightly higher temperatures (Knudsen et al., 2004). As the general relative abundance ranges between 97-100%, there is little change in ocean temperatures, and overall cold conditions. However, the variations in the abundance NPS may also reflect the extent of sea ice cover and open water conditions at the site. Less sea ice and more open waters provide preferable conditions for a higher productivity of photosynthesizing phytoplankton in surface waters and hence food source for the planktonic foraminifers. Introducing access food for microorganisms, such as NPS. This trend is also reflected in the NPS (%) as decreasing percentages correlates with peaks in abundances at ages 55,50,42,32,20 ka. This indicates less cold-water masses (warmer climate) and an environmental change into a habitat more suitable for other planktonic species as well.
The highest values of absolute abundance recorded in the data set are found at age 65 ka, see figure 6.2.3. These values indicate a higher ratio of foraminifera and less contribution of ice-rafted detritus, and is therefore interpreted to mark the transition from cold glacial MIS 4 to warmer interstadial conditions of MIS 3.
Coherent values are observed in both relative and absolute abundances at approx. ages of 20-25 ka represent a shift to colder conditions. As the relative abundance NPS show 100%, the

surface waters are dominated by this species, reflecting increasing amount of sea ice. At the same time absolute abundances are at their lowest indicating low foraminifer productivity, and a higher contribution and transport of terrigenous material to the site. This trend is also obvious in the absolute abundance IRD-graph as it peaks the ages 20-25 ka as well, see figure 6.2.3. Two additional peaks of high abundance ice-rafted detritus appear at 35kyr and 60 ka, both appear as short-lived and display rapid shifts to lower values. These characteristics are linked to changes in ice cover. As continental ice masses retreat, supply and deposition of ice-rafted detritus at the site decreases, marking the transition from cold glacial MIS 4 to warmer interstadial conditions of MIS 3.

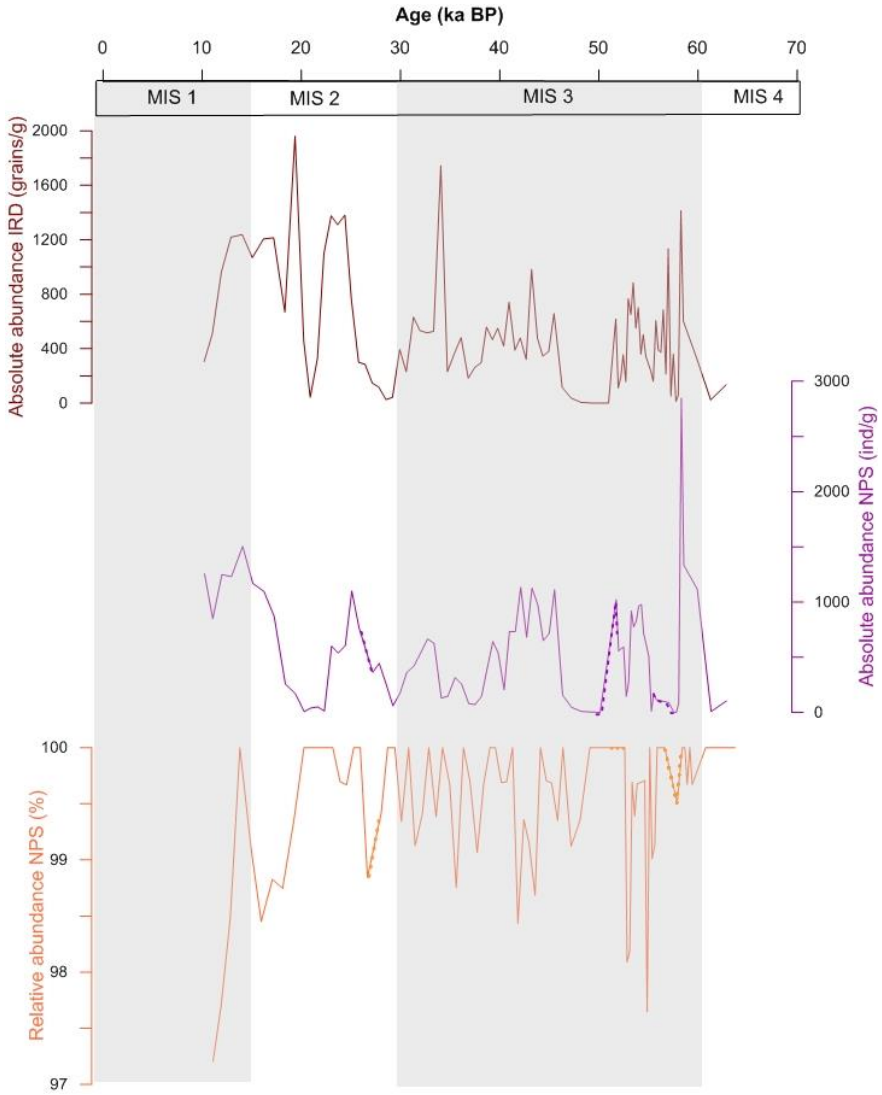

Figure 6.2.3. Assemblage counts from core GS15-198-38CC, plotted on a age scale correlated to LRO4 age model. Graphs are displaying absolute abundance IRD (grains/g), absolute abundance NPS (ind/g) and relative abundance NPS (%) from top to bottom respectively. Dotted areas represent uncertainties in the data.

7. Discussion

The mechanisms driving the earth`s climate system to enter and terminate ice ages are attributed to the changes in earth's orbital configuration commonly referred to as Milankovitch forcing (Oppo, 1997). However, observations of climatic fluctuations within glacials/interglacials, from Greenland ice cores (Dansgaard et al., 1993), occur with a higher frequently than the orbitally paced Milankovitch cycles, suggesting that other internal or external mechanisms constitute a major role in climatic alternations on millennial timescale.

Due to the proximity of the core site to the Greenland ice sheet (GrIS), modifications of the GrIS and associated sea ice fluxes into the Greenland basin can be documented in marine sediments through time. The core studied here is also situated close to the Iceland Sea gyre (Johannessen et al., 1994), thus potentially recording aspects of the thermohaline circulation of the Nordic seas and associated current transport of material in the area. On the basis of the known correlation between the Greenland ice core records and the oceanic records of the North Atlantic and Norwegian Sea (e.g. Dokken et al., 2013, Fronval et al.1995), it is natural to proceed matching events of abrupt climatic changes reflected in the Greenland ice core (NGRIP) to the marine sediment core GS15-198-38CC in the following discussion. Presented below in figure 7.1 is an overview of the all proxy data that was reviewed in the results, plotted on the same age scale.

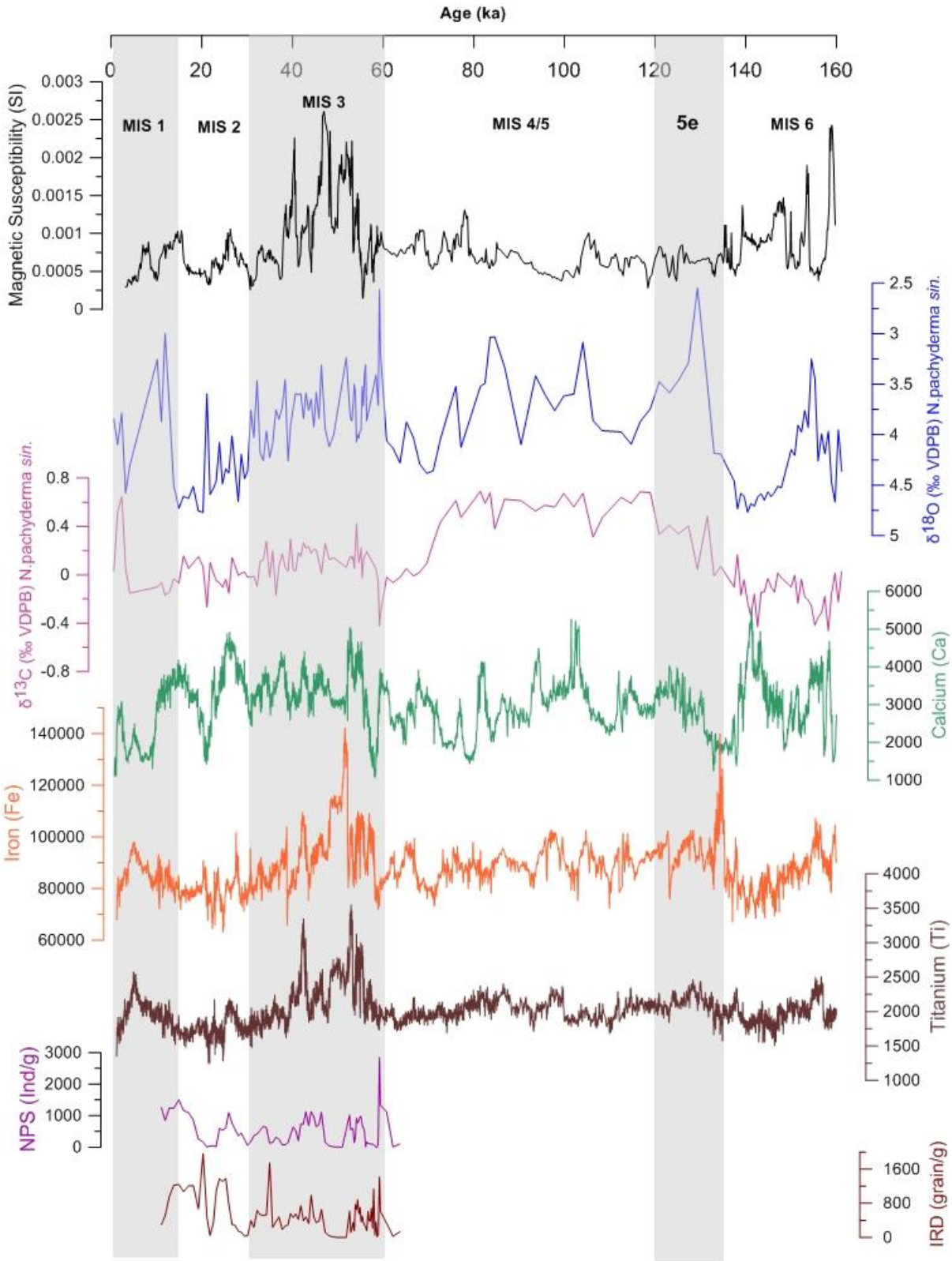

Figure 7.1. An overview of the proxy data evaluated in the study derived from core 38CC. From top to bottom: Magnetic Susceptibility (black), $\delta^{18}O$ (blue), $\delta^{13}C$ (orange), Calcium (green), Iron (purple), Titanium (brown), absolute abundance *N. pachyderma* (sin) (pink), absolute abundance ice rafted detritus (black). Marine Isotope Stages 1-6 are indicated by Lisiecki and Raymo (2005). Grey shaded bars represent interstadials.

7.1 Millennial scale climate variability during Marine Isotope Stage 3

7.1.1 Are abrupt climate change events recorded in the sediment record off East Greenland?

In order to investigate the degree of climatic coherency between the western Nordic Seas and the Greenland ice sheet (GrIS), different proxy records need to be considered. Oxygen isotopes constitute an important indicator of past climatic conditions, and planktonic foraminifera $\delta^{18}O$ serves as a proxy for variability in sea surface water physical properties. The oxygen isotopic composition of the foraminifera is highly dependent on the temperature and salinity of the surrounding water masses. The salinity of the surface waters varies according to the local evaporation processes and variability in freshwater inputs. The fluxes of freshwater to the studied area originate generally from two sources: precipitation and/or melting of adjacent glaciers and sea ice (Rohling, 2013). During evaporation, the lighter oxygen isotopes (^{16}O) more readily enter the vapor phase. The atmospheric wind system transports water vapor towards higher latitudes, where the lighter isotopes are incorporated into glaciers through precipitation processes. During warmer periods (interglacials), melting of glacial ice will increase input of ^{16}O rich water, resulting in lighter isotopic values.

The oxygen isotope record obtained from core 38CC displays a fluctuating pattern in high agreement with the NGRIP $\delta^{18}O$ data (Figure 7.1.1). The gradual increase in towards higher $\delta^{18}O$ values, denoted by the long-term trend between 58 to 25 ka BP, represents the buildup of continental ice-sheets. The abrupt decreases in isotopic values that repeatedly interrupt this long-term trend reflect the return of isotopically light waters from melting ice into the oceans and/or increases in near surface water temperature where the foraminifera are calcifying. It is important to note that core 38CC has lower temporal resolution than NGRIP. Thus, variations in the record are not recorded with the same detail. In general, the changes in oxygen isotopes of core 38CC fluctuate rapidly on timescales of 2-5 kyr. From the NGRIP ice core, similar rapidly occurring oscillations in the oxygen isotopes are categorized as Dansgaard-Oeschger cycles (D-O cycles). Despite lower resolution, the asymmetric shape of similar D-O cycles is prominent throughout the oxygen isotope record of MIS 3 in core 38CC (Figure 7.1.1). This indicates the presence of similar cycles imprinted in the Nordic Seas/Greenland Sea, reflecting a close interaction between water mass properties of the Greenland Sea and changes in air temperatures above the Greenland ice sheet.

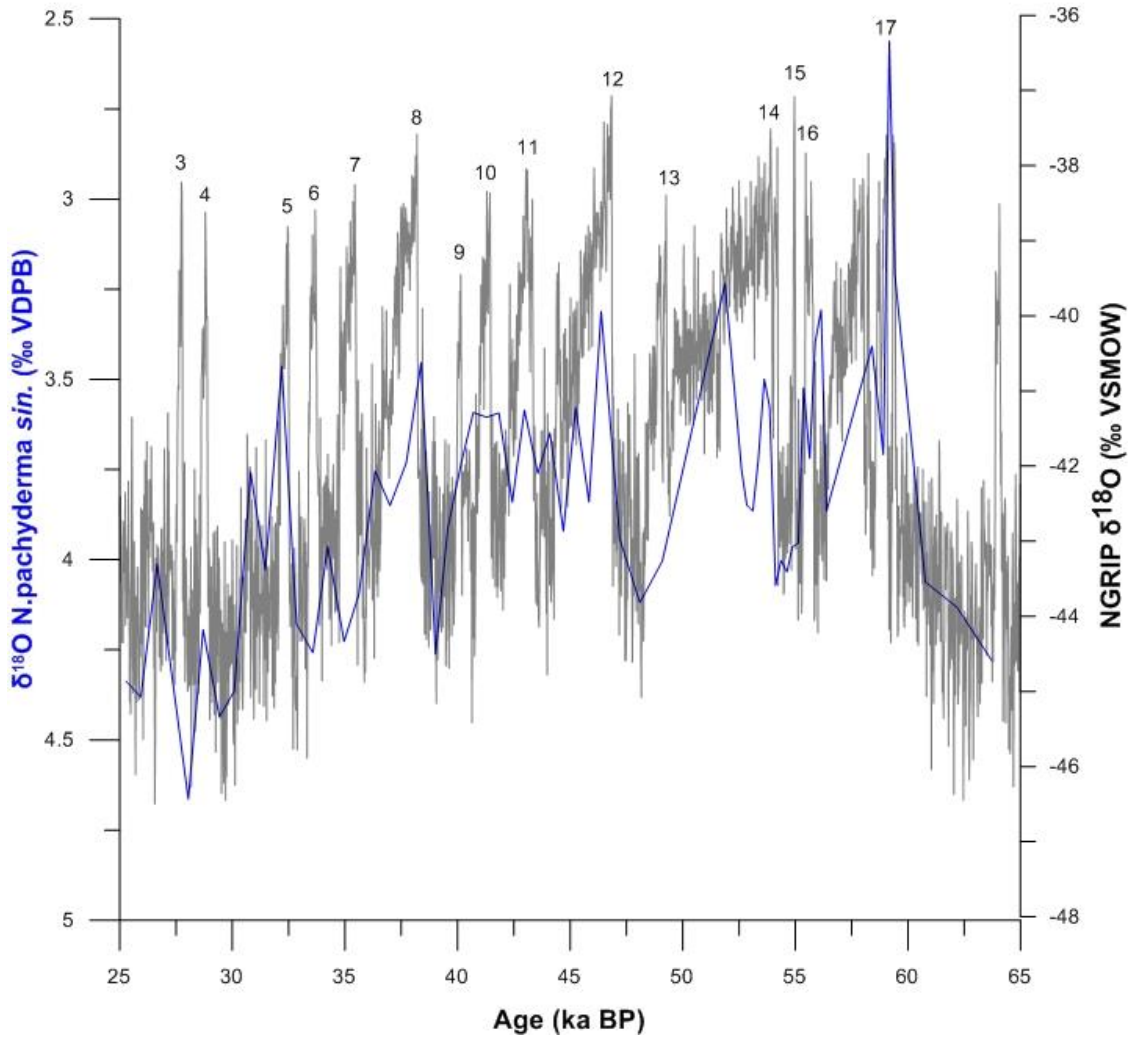

Figure 7.1.1. Comparison between North Grip (NGRIP) oxygen isotopes (grey curve; Anklin et al., 1993) and $\delta^{18}O$ from core 38CC (blue curve; this study). Numbers 3-17 in the figure indicates D-O interstadial numbers according to Rasmussen et al. (2016).

Another similar feature of both the NGRIP and 38CC $\delta^{18}O$ record is the saw-tooth shaped form of the events with longer periods of increase in high $\delta^{18}O$ values, culminating in a rapid decrease toward lower isotopic values. As stated above, this isotopic trend is associated with continental ice sheet growth, and is referred to as "cooling cycles" in figure 7.1.2. The apparently increasing ice growth during this interval is further supported by fluctuating patterns of ice-rafted detritus (IRD), indicating more sea ice available to transport terrigenous

material to the site. These cooling cycles occur on intervals of 10-15 kyr, spanning multiple D-O cycles. The latter part of the cycle is characterized by an abrupt decrease in abundance foraminifera, enrichment in ^{16}O (low $\delta^{18}O$) and high IRD input. From these records it seems that during most cooling cycles, there is an increase in IRD. But only a few of these features terminate simultaneously with decreased $\delta^{18}O$ values (indicating warmer conditions). Bond et al. (1993) recognized a similar pattern of fluctuating ice rafted detritus of 7-10 kyr cycles in the North Atlantic. The cold phase of these were later verified as iceberg discharges and known as Heinrich events (H-events). It is important to note that oxygen isotopes from Greenland ice cores primarily reflect changes in temperatures (Dansgaard et al., 1993). However, ice-rafting events observed in core 38CC, appear to coincide with the termination of the coldest periods of the ice core. This appears to be similar in the Nordic Seas as in the North Atlantic H-events, although the IRD in the H-layers primarily are sourced from the Laurentide ice sheet, whereas the IRD in core 38CC is most likely derived from ice sheets calving into the Nordic Seas.

The timing of Heinrich events as cited by Bond (1993), are plotted against the ice-rafted detritus records of core 38CC in fig. 7.1.2. From this comparison a strong relation between peaking IRD values and most Heinrich events are indicated. Heinrich events H3 (26 ka BP) and H4 (35 ka BP) both coincide with the highest values of IRD. Heinrich event H5 (49 ka BP) occur simultaneously with IRD and NPS (Figure 7.1.3) abundance minima, and is less prominent in the record of core 38CC. This indicates that locally colder conditions deprived calving of glaciers and melting at this age interval. However, this mismatch may also be due to uncertainties in the age model of the core. It appears that by conducting only minor adjustments to the age model, an event with the same characteristics can be detected at age 47 ka BP (see dotted line in Figure 7.1.2 and 7.1.3). This may imply that local conditions led to delayed imprint of the ice rafting event at the site, or a H5 correlative is not detected in the record of core 38CC due to low resolution of the data or that the age scale needs modifications.

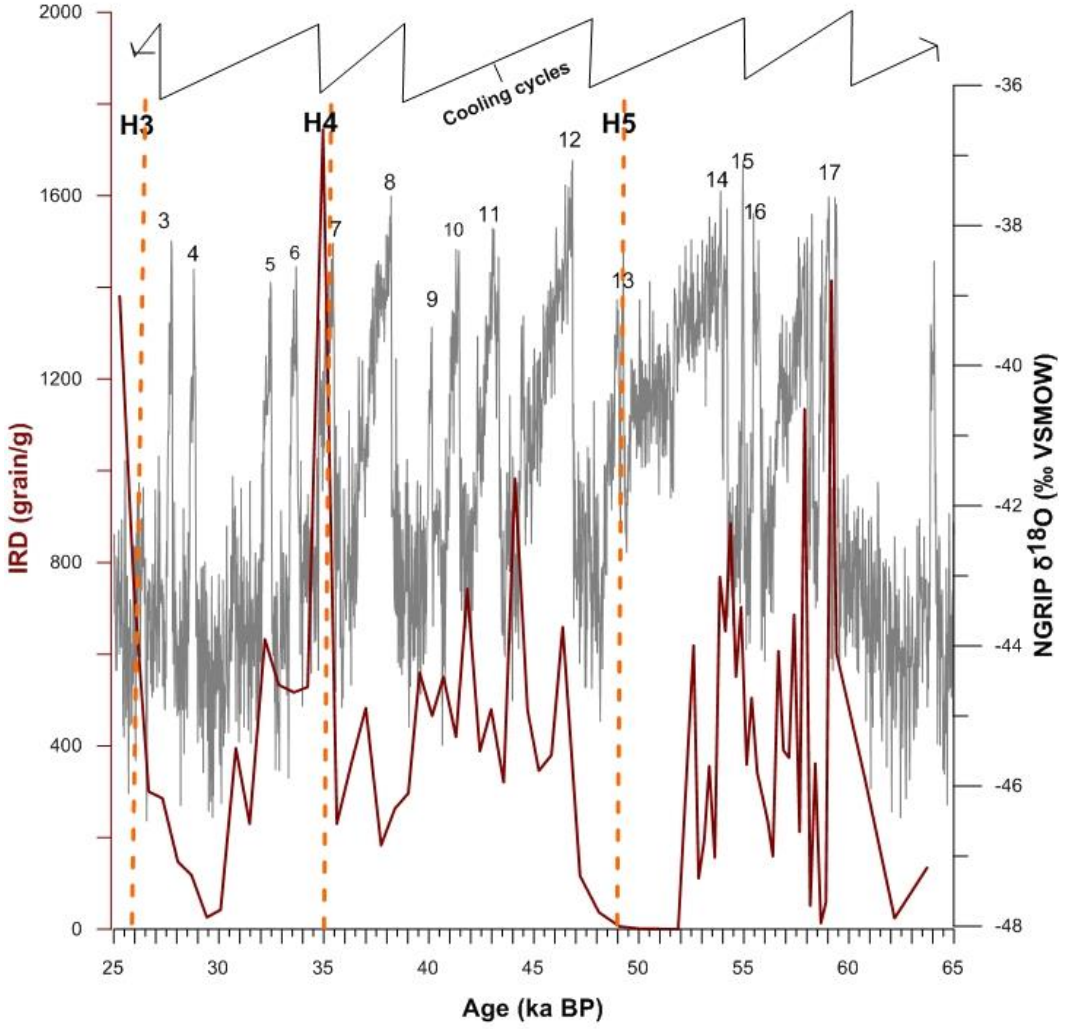

Fig. 7.1.2. Comparison of NGRIP $\delta^{18}O$ values (grey) and ice-rafted detritus (red) from core 38CC. Heinrich events displayed as orange dotted lines are identified by Bond (1993). Numbers 3-17 in the figure indicates D-O interstadial numbers according to Rasmussen et al. (2016). Cooling cycles in the figure are based on the 38CC oxygen isotope record.

Millennial scale climate variability, such as D-O cycles and Heinrich events display a close relationship. Heinrich events precede D-O warming, occurring at the initiation of the "D-O event", during the coldest part. The systematically coincident timing of the H-events within the D-O cycles suggests that Heinrich events are superimposed on the rhythm of the D-O cycles (Bond et al., 1995). A highly debated triggering mechanism is changes in the thermohaline circulation (e.g Bond et al., 1997, Broecker, 1997, Kreveld et al., 2000). An in-phase relationship between D-O cooling and coherent small scale ice rafting and melt water

input (lighter $\delta^{18}O$) from East Greenland glaciers, may have induced sea level rise inflicting instability to the Laurentide ice sheet. These combined factors may explain the consistency with major Heinrich ice rafting events in the North Atlantic (Kreveld et al., 2000). Bond et al (1999) also argued that a southward repositioning of the polar front is expressed as the cold periods of the D-O events, resulting in higher rates of iceberg input into the North Atlantic.

Information about the character of the climatic events can also be detected in the $\delta^{13}C$ record. The carbon isotopic signature incorporated in carbonate shells of foraminifera may reflect ventilation of the water masses, and hence the state of ocean-atmosphere interactions (Dokken et al., 2013). Input of freshwater and the presence of a sea ice cover both acts as inhibiting factors reducing deep-water formation and ventilation. The stadial/interstadial transitions associated with D-O cycles appear in a certain pattern. From the $\delta^{13}C$ record of core 38CC (Figure 7.1), a general increase of carbon isotopic values occurs during the end of the cycle, corresponding with the warmest (interstadial) portion of the D-O event. This is consistent with findings of Dokken et al (2013). During the interstadials the Nordic Seas was well ventilated, and ice free, promoting optimal conditions for CO_2 exchange with the atmosphere. Subsequently a decrease in $\delta^{13}C$ values is observed leading into the latter part of the interstadial. This trend can be explained as increasing amounts of sea ice and reestablishment of a stratification of the water masses, reducing ventilation (Dokken et al., 2013), and potentially drive the planktonic foraminifera to calcify deeper in the water column in more nutrient enriched (lower $\delta^{13}C$) waters.

The absolute abundance of Neogloboquadrina pachyderma (sin) serves as an additional sea surface temperature and salinity proxy. High abundances of the polar planktonic species is an indicator of open water conditions (Johannessen et al., 1994). From the comparison of NPS to the NGRIP $\delta^{18}O$ record, as previously discussed, long term "cooling cycles" can be observed coinciding with low foraminifera abundance at the onset of each ice-rafting event (Figure 7.1.3). This observation is consistent with ocean surface cooling and less open waters during these periods. Higher abundance peaks in the NPS record persist approximately for 5 kyr, and are generally consistent with higher temperatures in Greenland. However, during the interval 46-51 ka BP and 56-58 ka BP particularly low values of planktonic foraminifer occur. At 58 ka BP and 53 ka BP a short-lived prominent drop in NPS abundance occur during a stage of warm conditions in Greenland, thus, indicating lowering of the sea surface temperature and salinity during these periods. This is consistent with reduced ventilation as

indicated by a decrease in the 38CC $\delta^{13}C$ record. When discussing planktonic abundances, it is important not to exclude the possibility of certain Heinrich and D-O events not being as apparent due to lower resolution.

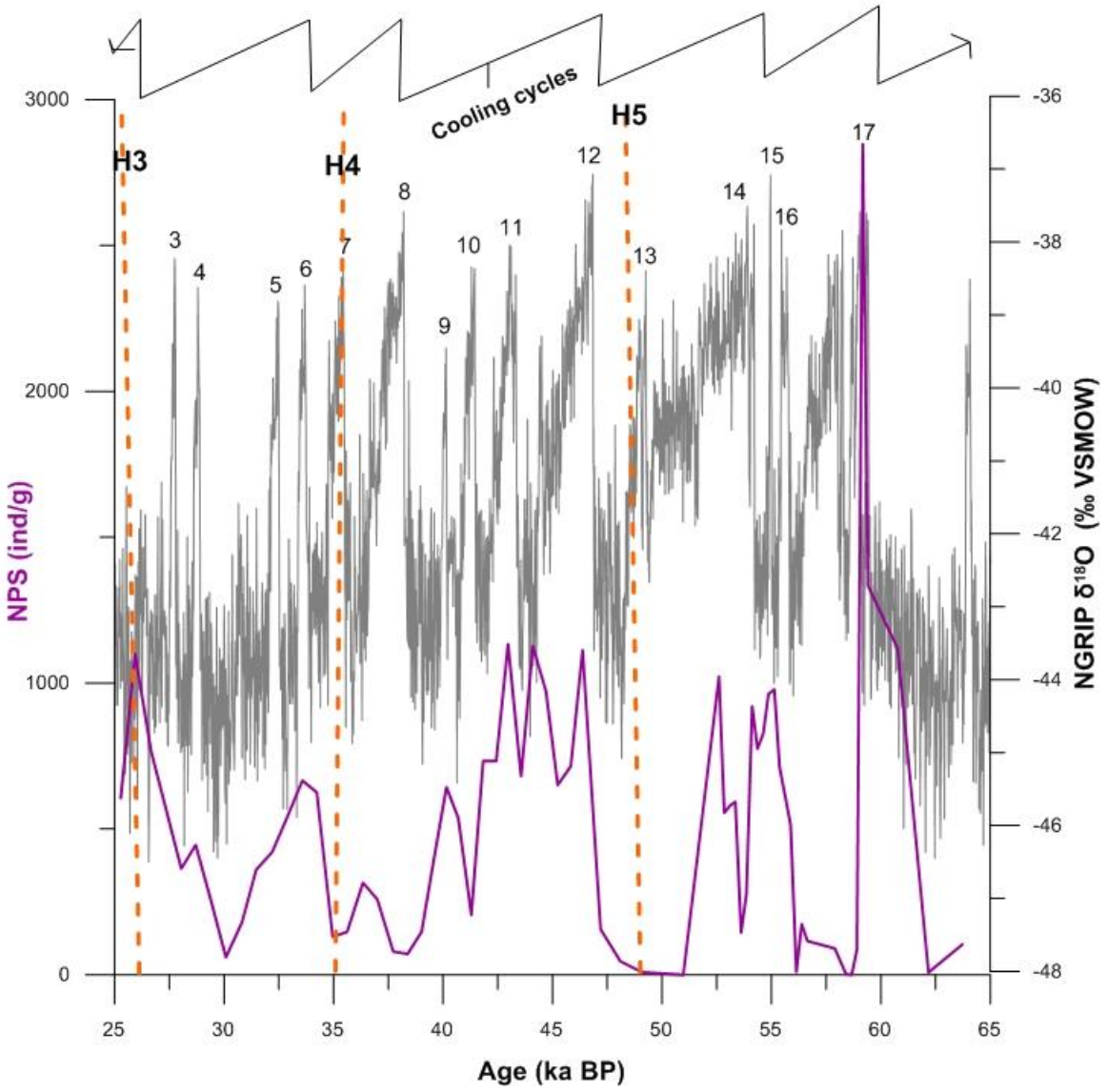

Fig. 7.1.3. Comparison of NGRIP $\delta^{18}O$ values (grey) and *N. pachyderma sin.* (purple) from core 38CC. Heinrich events displayed as orange dotted lines are identified by Bond (1993). Numbers 3-17 in the figure indicates D-O interstadial numbers according to Rasmussen et al. (2016). Cooling cycles in the figure are based on the 38CC oxygen isotope record.

To further evaluate the millennial scale climatic variability of MIS 3, the MS of core 38CC is compared to the NGRIP ice core data. In general, similar trends in the records can be observed, however with an apparent phase lag between the two parameters (Fig. 7.1.4). There are four prominent events of increasing MS values, each lasting no longer than 3-5 kyr. On the basis of their millennial scale oscillating nature and their consistency with the NGRIP oxygen isotopes, these four features are interpreted to resemble D-O cycles. Kissel et al (1999) attribute similar short-term fluctuations in sedimentary magnetic susceptibility to changes in deep ocean circulation, suggesting a reduction during stadials, and reestablishment during interstadials.

The lag observed in the record at ages 48-50 ka BP and 55-60 ka BP, can be explained as follows: Lower oxygen isotopes values reflect decreasing ice volume, and generally warmer sea surface temperatures. Inducing preferable conditions for biological productivity in the upper ocean. This productivity acts to dilute the magnetic minerals present, resulting in a decrease of MS values. Due to this mechanism, during abrupt warming (D-O event) on would expect a decrease in susceptibility. As the warming decline into colder conditions, a higher concentration of magnetic minerals is represented in the sediment, consequently leading to higher MS values

An additional comparison of MS and IRD is performed to detect any coherent relationship between events of ice transported terrigenous material to the site and the concentration of magnetic minerals. The records display peaks in MS, more or less associated with peaks in IRD content. However, no general relation between the amplitude of both parameters can be detected by visual inspection of the records.
The similarity between MS from core 38CC and NGRIP $\delta^{18}O$ during MIS 3 (Fig. 7.1.4) suggest that the same climatic forcing that acted on the Greenland temperatures is reflected in the east Greenland continental margin, confirming that MS variations (to some extent) are coupled to abrupt climatic oscillations. The abrupt increase in IRD mostly coincide with beginning of the stadials (Fig. 7.1.4), which stated by Rasmussen et al. (2016) indicate rapid growth in sea ice cover, and enhanced ice berg melting.

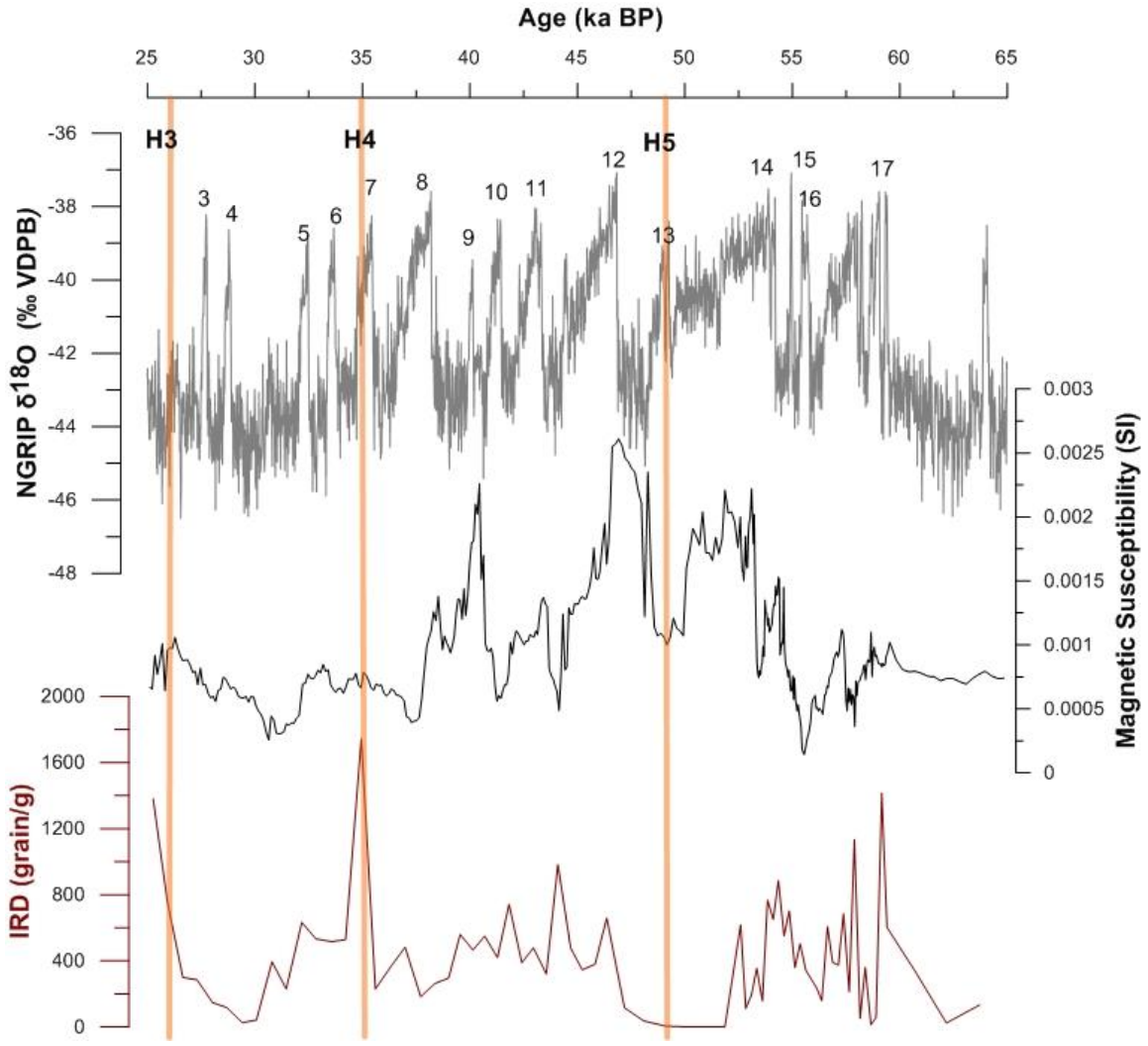

Fig. 7.1.4. Comparison of oxygen isotopes from NGRIP (grey), to Magnetic Susceptibility (black) and IRD (red) from core 38CC. Heinrich events displayed as orange lines are identified by Bond (1993). Numbers 3-17 in the figure indicates D-O interstadial numbers according to Rasmussen et al. (2016).

7.1.2 Links between surface ocean properties and millennial scale climate variability

Comparisons of a variety of proxy data, reflecting ice sheet variability in addition to sea surface properties, indicate millennial scale variability in the western Nordic Seas during Marine Isotope Stage 3 (MIS 3). High frequency fluctuations of stadial and interstadial conditions (D-O cycles), as well as long term cooling cycles culminating in Heinrich like ice-rafting events appear in the record of core 38 CC. However, the number of oscillating cycles is not as distinct in the marine record as in NGRIP, likely due to lower resolution of the marine records. The oceanographic changes in the Nordic Seas associated with lower atmospheric temperatures observed in Greenland ice cores are colder (high $\delta^{18}O$), icier (high IRD), and lower salinity (low foraminifera abundance) surface conditions. All of these changes could be due to increased freshwater input. A possible link between SST´s and discharge of icebergs, as stated by Moros et al (2002), is an enhanced northward flux of subsurface heat triggering ice sheet instability and consequently increasing calving and subsequent ice-rafting frequency. Such millennial scale events mark the transition from cold stadial to interstadial conditions. Within the precision of the age model, rapidly warmer temperatures offshore eastern Greenland are associated with warmer, higher in salinity waters, richer in planktonic foraminifera as well as ice-rafted detritus.

As discussed in the previous chapter, millennial scale variability coincides to a high degree with the NGRIP atmospheric signal. However, inconsistent features observed in interval 50-60 ka BP are recorded in several different proxy records. From the XRF-based Ca-record, two episodes of low values spanning 50-53 ka BP and 57-59 ka BP appear coincident with low rates of IRD and MS during warmer temperatures in Greenland. This indicates that even though one would expect Nordic seas temperatures to rise in line with Greenland warming, as generally indicated from the remaining record, the opposite apparently occurred during these intervals. The presence of colder surface waters is further supported by low absolute abundance of NPS. Preceding these intervals, episodes of high ice rafted detritus occur, potentially contributing to an enhanced fresh water input. This input may plausibly reduce the ocean-atmosphere interactions, and deep-water convection. Changes related to the surface water ventilation are simultaneously reflected as low values in the $\delta^{13}C$ record indicating stratification of the surface waters, calcification depths within the nutricline, and reductions of ventilation to the atmosphere (Figure 7.1.2).

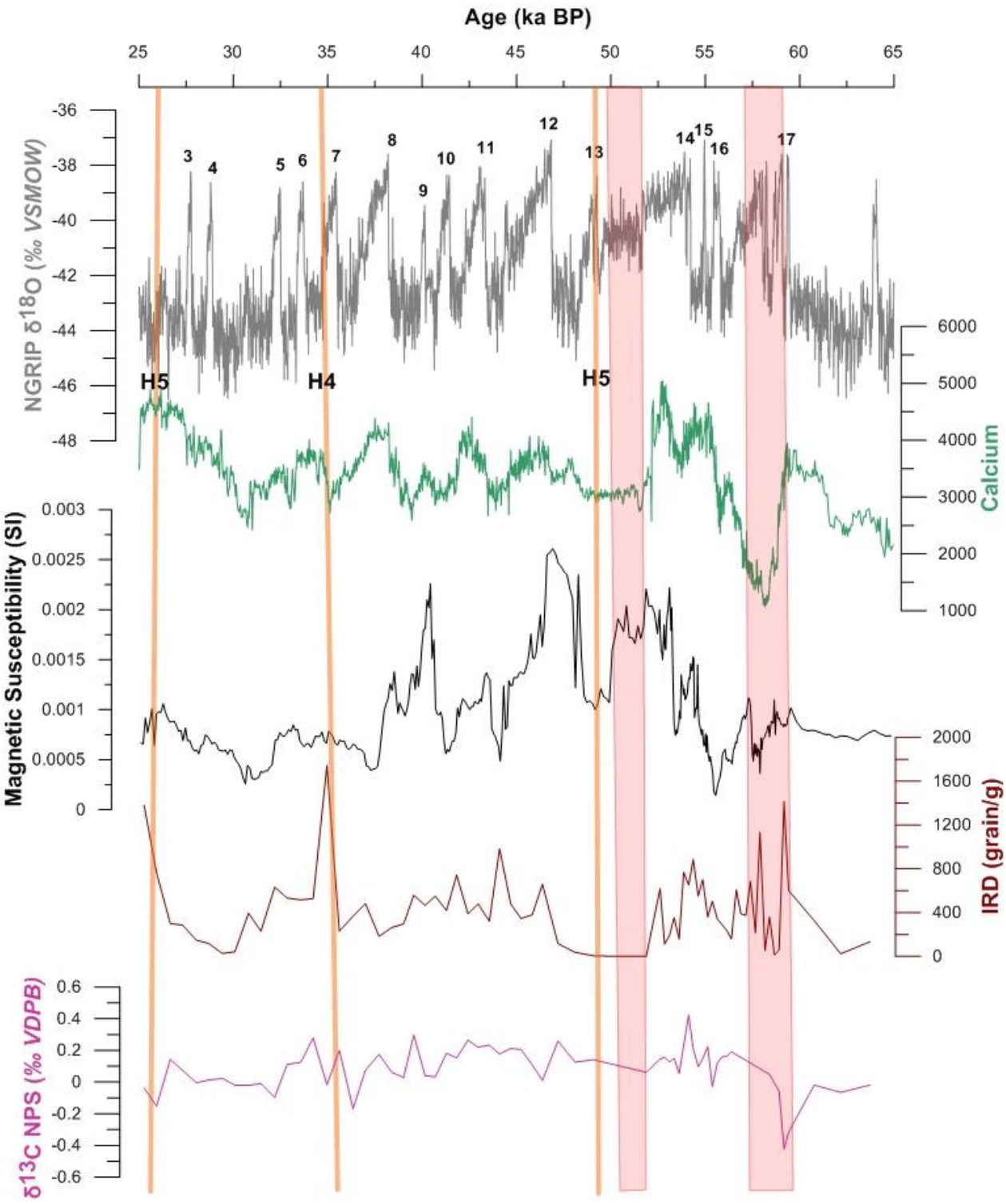

Figure 7.1.2. Comparison of oxygen isotopes from NGRIP (grey), Calcium (green), Magnetic Susceptibility (black), IRD (red) and $\delta^{13}C$, from core 38CC. Heinrich events H3-H5 displayed as orange lines are identified by Bond (1993). Numbers 3-17 in the figure indicates D-O interstadial numbers according to Rasmussen et al. (2016). Red shaded bars indicate intervals of low Ca and IRD.

7.2 Orbital and Millennial scale climate variability during Marine Isotope Stage 5

Having demonstrated that millennial scale climatic variation are indicated by surface ocean proxies during MIS 3, further emphasis on investigating whether the same fluctuations can be observed in the preceding interglacial, Marine Isotope Stage 5 (MIS 5). The degree of coherency between the two periods will be elaborated upon and related to variations in sea ice and oceanic conditions.

7.2.1 Orbital Millennial scale variability in surface ocean proxies

Comparison between oxygen isotope records of interstadial MIS 3 and interglacial MIS 5 reveals their contrasting characters, in regard to frequency and amplitudes. Marine Isotope sub-Stages 5e-5a consist of much lower frequency of climatic variations (Figure 7.2.1). This pattern is also apparent in the NGRIP $\delta^{18}O$ records. In general, long term cooling cycles observed in both records fluctuate over timescales of approximately 20 kyr. This indicates the influence of Milankovitch forcing, and precession cycles. However, the low resolution of the $\delta^{18}O$ signal in core 38CC makes it difficult to identify D-O cyclicity in this parameter during MIS 5.

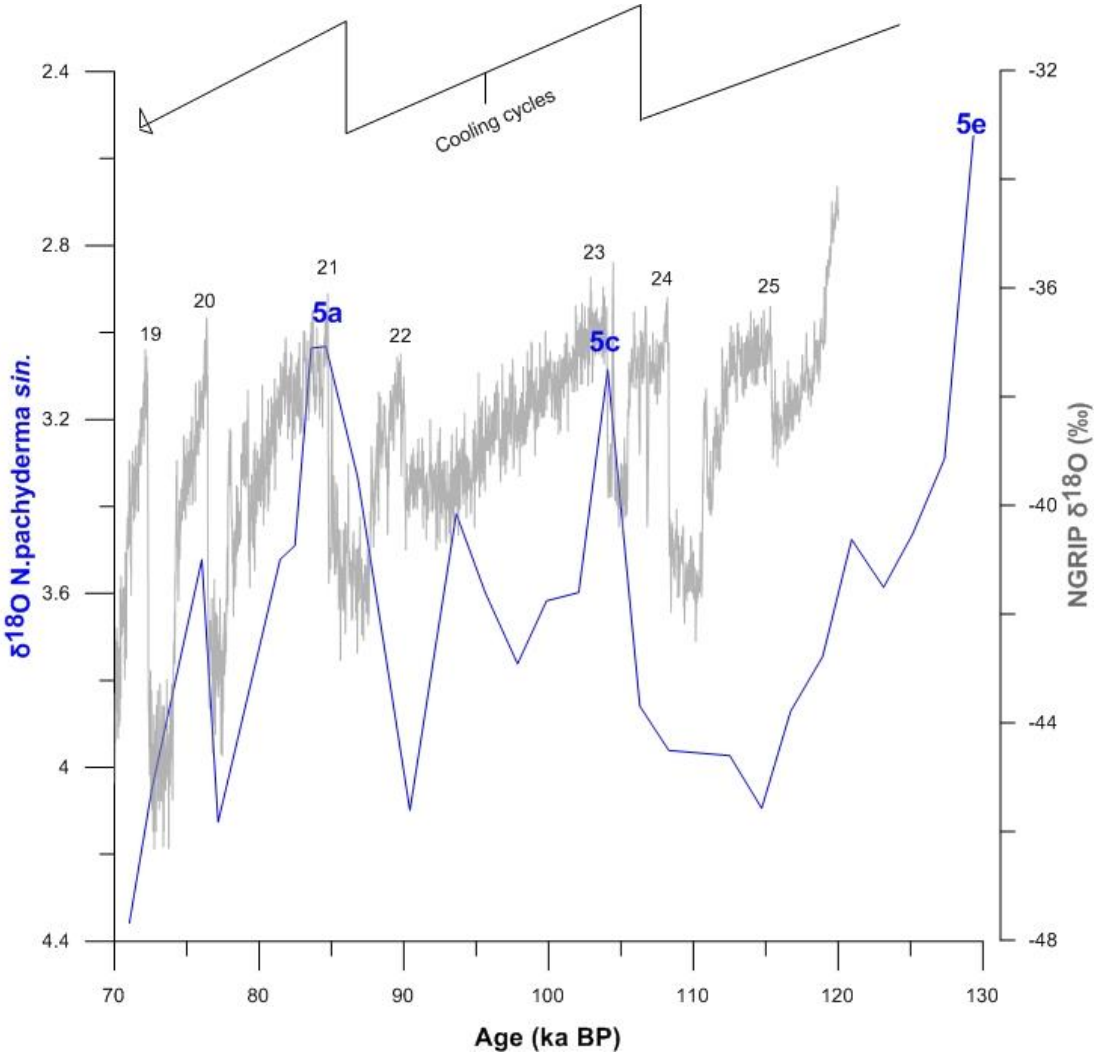

Figure 7.2.1. Comparisons of NGRIP $\delta^{18}O$ record (grey) and $\delta^{18}O$ values from core 38CC (blue). Labels 5e, 5c, 5a denote interstadials during MIS 5.
Numbers 19-25 in the figure indicates D-O interstadial numbers according to Rasmussen et al. (2016).

For further evaluation of the presence of millennial scale variations, the higher resolution Ca-record is considered. In chapter 6.2.2, arguments suggest that the calcium content in the sediments obtained from XRF scanning can be interpreted as measure of a marine signal (productivity of calcareous organisms). Here, a comparison between the calcium and the absolute abundance of the planktonic foraminifer species *N. pachyderma* (sin) is made (Figure 7.2.2, small box top left). The purpose of this comparison is to extend the absolute abundance signal into MIS 5 for evaluation of the sea surface water properties. From this a high degree of resemblance between the parameters is apparent, indicating that the abundance of the planktonic species *N. pachyderma* (sin) fluctuates in tandem with the marine $CaCO_3$ signal. As the XRF scan collect data on a higher resolution (every 0.5cm),

relative to counts (every 5 cm) any discrepancy may be a consequence of this inconsistency. However, the two parameters display a sufficient agreement to support the use of the high-resolution calcium content curve as an indicator of *N. pachyderma* (sin) abundance counts (Figure 7.2.2).

From the calcium records, longer cooling cycles of approximately 20 kyr, recognized as decreasing calcium values, are prominent. Comparisons between the NGRIP $\delta^{18}O$ record and calcium from core 38CC display similarities with low values of oxygen isotopes coinciding with high values of calcium (Figure 7.2.2). These parameters depict warmer temperatures in Greenland and warmer surface waters in the Nordic seas respectively. Conversely, increased $\delta^{18}O$ and lower Ca occur in conjunction with Heinrich events H7 and H8, at ages 85 ka BP and 105 ka BP (Figure 7.2.2), indicating cooler Greenland and Nordic Seas temperatures (respectively) at these times.
Within the cooling cycles, which resemble gradual buildup of continental ice sheet and lower biological productivity in the surface ocean, a few small-scale abrupt changes transitioning into interstadial conditions occur.

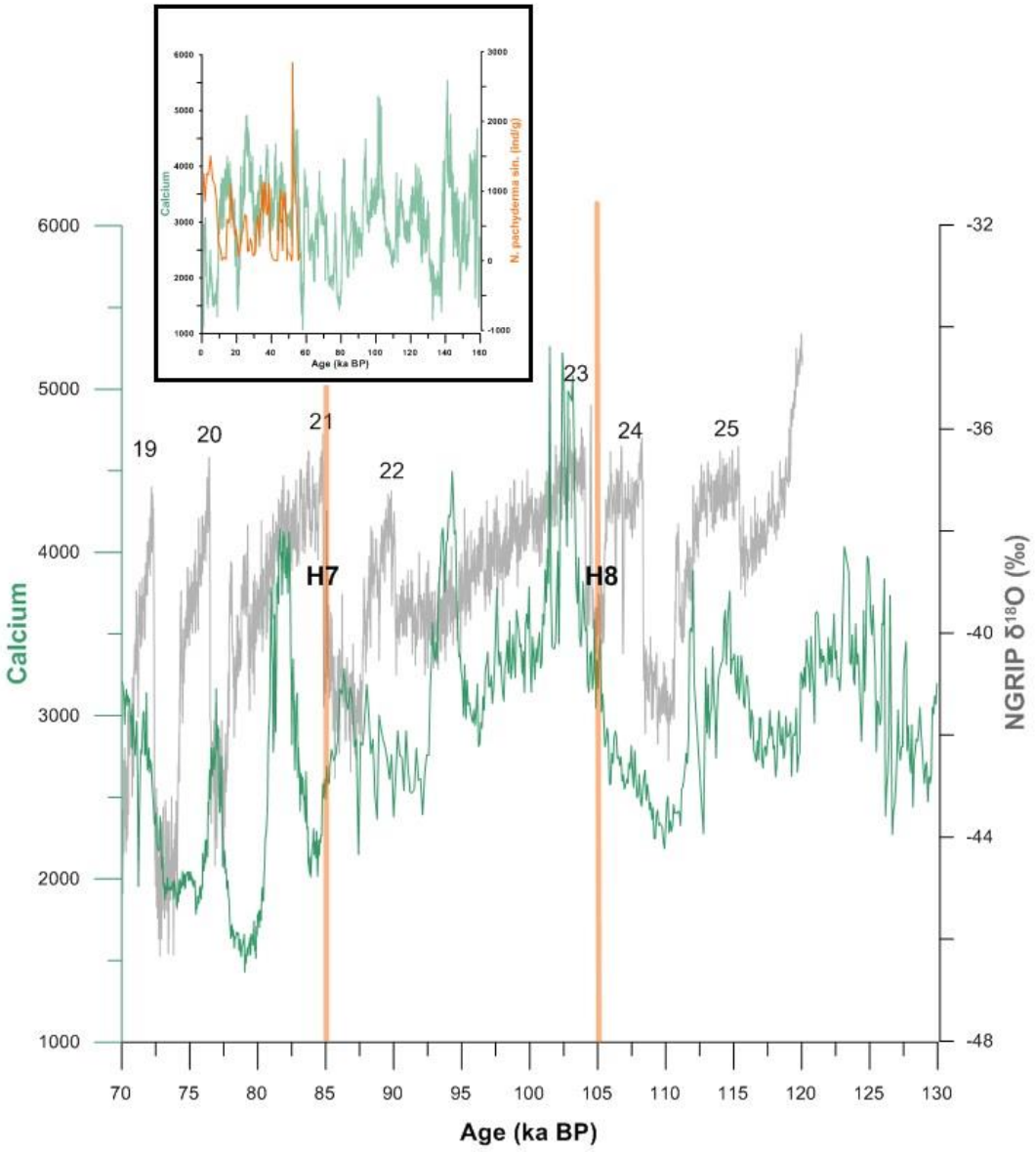

Figure 7.2.2. Small box, top left: Comparison of NGRIP δ18O values (grey) and Calcium (green). Main figure: Comparison of NGRIP (grey) and calcium (green) measurements from core 38CC. Numbers 19-25 in the figure indicates D-O cycles (Rasmussen et al., 2016).

.

Oxygen and carbon isotopes in combination with planktonic foraminifera content reflect the surface current systems and depict the varying characteristics of water masses in the Nordic Seas back in time (Johannessen et al, 1994). From the results presented in this study, proxy data show modifications in the oceanographic regime during the different interstadials and interglacials. In general, MIS 5 consists of higher values of $\delta^{13}C$ implying less frequent episodes of reduction in ventilation, and hence also more open waters. This implies more stable climatic conditions and less input of freshwater from melting sea ice, supported by the low magnetic susceptibility values. (High values of $\delta^{18}O$ recorded in MIS 5 may be linked to influence of arctic water masses, referring to conditions of generally colder surface waters and less biological productivity (Figure 7.1).

During MIS 3, carbon isotope values are generally lower and rapidly fluctuating, indicating less ventilation of the ocean potentially due to more frequently disturbances in the circulation. Rasmussen et al. (2016) argued that during the cold stadial of D-O cycles, convection was reduced, and hence the northward flow of warm North Atlantic waters was deprived, which may have led to cooling in the Nordic Seas. This is consistent with the $\delta^{18}O$ records from core 38CC during MIS 3, which show millennial scale variability in phase with lower temperature and salinities, possibly caused by higher extent of sea ice and fresh water input.

Renewal of convection during the beginning of D-O cycles, would restore the heat transport to the north, and initiate a rapid warming event (Rasmussen et al., 2016).
This is supported by Moros et al. (2002) stating that millennial scale variabilities such as Heinrich events were due to "warming events" initiated by enhanced northward heat transport. This would also explain the sudden increase in temperatures over Greenland following the stadial phases of the D-O cycles.
Mechanisms triggering the abrupt warming has been attributed to melting of icebergs (Rasmussen et al., 1996), producing a highly stratified water column characterized by a layer of cold, low salinity water masses, inhibiting the heat transfer to the atmosphere. Consequently, intermediate waters gradually warm the surface fresh water layer, until it reaches a threshold upon which abrupt warming and a restored convection occur (e.g Rasmussen et al., 2004, Dokken et al., 2013)

Summary of conclusions

On the basis of stable isotope measurements of planktic foraminifera, XRF-element analysis and assemblage counts from core GS15-198-38CC, it has established that natural climate variability occur in the Nordic Seas on millennial and sub-millennial time scales. This is in line with variabilities observed in the NGRIP $\delta^{18}O$ records obtained from the Greenland ice sheet. The main conclusions of the study are summarized as followed:

- Low-resolution planktic $\delta^{18}O$ records indicate sea surface physical properties from the past ~160.000 yr. with varying climatic character. From this record it is apparent that Marine Isotope Stage 3 (MIS 3) display a much higher frequency of abrupt events compared to Marine Isotope Stage 5 (MIS 5).

- Episodes of significant ice rafting, so called Heinrich events (5-10 yr) have been identified in the record according to well-established characteristics: high concentration of IRD, low abundance *N. pachyderma sin* and increasing values of $\delta^{18}O$. During MIS 3, a strong relation to Heinrich events H3-H5 is observed. Some uncertainties are related to the H5 event, but presumably resulting from uncertainties within the age model. Heinrich events H7 and H8, during MIS 5, have been recognized on the basis of higher oxygen isotopes ($\delta^{18}O$) and low Ca values. In general, our data suggest that substantial calving of ice into the Nordic Seas may have triggered these events of ice rafting.

- Observations of rapid oscillations (1-2 kyr), known as Dansgaard-Oeschger (D-O) cycles resembles a prominent feature in core 38CC during MIS 3. In general, these oscillations are in good agreement with similar fluctuations of the NGRIP $\delta^{18}O$. However, due to lower frequency of abrupt events during MIS 5 and generally low $\delta^{18}O$ of core 38CC, any specific determination of cycles during this interval is problematic.

- Proxy records from both MIS 3 and MIS 5 exhibit “saw-tooth” resembling trends of increasingly higher $\delta^{18}O$ values, culminating in a rapid decrease toward lower isotopic values and high IRD input. These trends are referred to as cooling cycles and

may reflect the buildup of ice sheets. The cooling cycles span multiple D-O cycles and culminate in Heinrich events.

- The primary cause of climatic instability in the Nordic seas is highly attributed to changes in ocean convection, and hence a reduction in the strength of the Atlantic Meridional Overturning Circulation (AMOC). This moderation is argued to be caused by enhanced heat transport to the north, which would induce iceberg melting and a stratification of the surface waters. Buildup of subsurface heat would eventually be released and appear as a rapid warming event in the proxy data.

References

Aagaard, K., Swift, J.H., Carmack, E.C. (1985). Thermohaline circulation in the Arctic Mediterranean Seas. *Jorunal of Geophysical Research, 90*(C3), s. 4833-4846.

Anklin, M., Barnola, J. M., Beer, J., Blunier, T., Chappellaz, J., Clausen, H.B., Dahl-Jensen, D., Dansgaard, W., Angelis, M.De., Delmas, R. J, Duval, P., Fratta, M., Fuchs, A., Fuhrer, K., Gundestrup, N., Hammer, C., Iversen, P., Johnsen, S., Jouzel, J., Kipfstuhl, J., Legrand, M., Lorius, C., Maggi, V., Miller, H., Moore, J. C., Oeschger, H., Orombelli, G., Peel, D.A., Raisbeck, G., Raynaud, D., Schøtt-Hvidberg, C., Schwander, J., Shoji, H., Souchez, R., Stauffer, B., Steffensen, J.P., Stievenard, M., Sveinbjørnsdottir, A., Thorsteinsson, T., Wolff, E. (1993). Climate instability during the last interglacial period recorded in the GRIP ice core. *Nature*, *364*, s. 203-207.

Arz, H. W., Gerhardt, S., Patzold, J., Rohl, U. (2001 a). Millennial-scale changes of surface- and deep-water flow in the western tropical Atlantic linked to Northern Hemisphere high-latitude climate during the Holocene. *Geology, 29*(3), s. 239-242.

Arz, H. W., Patzold, Muller, J.P., Moammar, M.O. (2003). Influence of Northern Hemisphere climate and global sea level rise on the restricted Red Sea marine environment during termination I. *Paleoceanography, 18*(2).

Barun, K. (1999). *Modern Foraminifera*: Kluwer Academic Publishers.

Bé, A. W. H., Hutson, W .H. (1977). Ecology of planktonic foraminifera and biogeographic patterns of life and fossil assemblages in the Indean Ocean. *Micropaleontology, 23*(4), s. 369-414.

Berger, A. (1988). Milankovitch theory and climate. *Reviews of geophysics, 26*(4), s. 624-657.

Bjerknes, J. (1964). Atlantic air-sea interaction. *Advances in geophysics, 10*.

Bond, G. C., Showers, W., Elliot, M., Evans, M., Lotti, R., Hajdas, I., ... & Johnson, S. (1999). The North Atlantic's 1-2 Kyr Climate Rhythm: Relation to Heinrich Events, Dansgaard/Oeschger Cycles and the Little Ice Age. *Mechanisms of global climate change at millennial time scales*, 35-58.

Bond, G. C., Heinrich, H., Broecker, W., Labeyrie, L., McManus, J., Andrews, J., Huon, S., Jantschik, R., Clasen, S., Simet, C., Tedesco, K., Klas, M., Bonani, G., Ivy, S. (1992). Evidence of massive discharges of icebergs into the North Atlantic ocean during the last glacial period. *Letters to nature, 360*, s. 245-249.

Bond, G., Broecker, W., Johnsen S., McManus, J., Labeyrie, L., Jouzel, J., Bonani, G. (1993). Correlations between climate records from North Atlantic sediments and Greenland ice. *Letters to nature, 365*, s. 143-147.

Bond, G., Showers, W., Cheseby, M., Lotti, R., Almasi, P., Priore, P., ... & Bonani, G. (1997). A pervasive millennial-scale cycle in North Atlantic Holocene and glacial climates. *science*, *278*(5341), 1257-1266.

Bond, G. C., Lotti, R. (1995). Iceberg discharges into the North Atlantic on millennial time scales during the last glaciation. *Science, 267*, s. 1005-1010.

Bradley, R. S. (2014). *Paleoclimatology: reconstructing climates of the Quaternary* (Third ed. Vol. 68): Academic Press.

Broecker, W., Bond, G.C., Klas, M. (1990). A salt oscillator in the glacial atlantic? *Paleoceanography, 5*(4), s. 469-477.

Broecker, W. S. (1997). Thermohaline circulation, the Achilles heel of our climate system: Will man-made CO2 upset the current balance? *Science, 278*(5343), s. 1582-1588.

Broecker, W. S. (1998). Paleocean circulation during the last deglaciation: a bipolar seesaw? *Paleoceanography, 13*(2), s. 119-121.

Carmack, E., Aagaard, K. (1973). On the deep water of the Greenland Sea. *Deep Sea Research and Oceanographic Abstracts, 20*(8), s. 687-715.

Cermeño, P., Dutkiewicz, S., Harris, R. P., Follows, M., Schofield, O., & Falkowski, P. G. (2008). The role of nutricline depth in regulating the ocean carbon cycle. *Proceedings of the National Academy of Sciences*, *105*(51), 20344-20349

Chapman, M. R., Shackleton, N.J. (1998). Millennial-scale fluctuations in North Atlantic heat flux during the last 150,000 years. *Earth and Planetary Science Letters, 159*(1), s. 57-70.

Coachman, L. K., Aagaard, K. (1988). Transports through Bering Strait: annual and interannual variability. *Journal of geophysical research, 93*(C12), s. 15525-15539.

Croudace, I. W., Rindby, A., Rothwell, R.G. (2006). ITRAX: description and evaluation of a new multi-function X-ray core scanner. *Geological Society London, Special Publications, 267*(1), s. 51-63.

Dansgaard, W., Johnsen, S.J., Clausen, H.B., Dahl-Jensen, D., Gundestrup, N.S., Hammer, C.U., Hvidberg, C.S., Steffensen, J.P., Sveinbjørnsdottir, A.E., Jouzel, J., Bond, G. (1993). Evidence for general instability of past climate from a 250-kyr ice-core record. *Letters to nature, 364*, s. 218-220

Dearing, J. (1994). *Environmental magnetic susceptibility." Using the Bartington MS2 system* (Vol. 8): Kenilworth, Chi Publ

Deser, C. (2000). On the teleconnectivity of the Arctic Oscillation. *Geophysics Research Letters, 27*(6), s. 779-782.

Dokken, T. M., Nisancioglu, K.H., Li, C., Battisti, D.S, Kissel, C. (2013). Dansgaard-Oeschger cycles: Interactions between ocean and sea ice intrinsic to the Nordic seas. *Paleoceanography, 28*, s. 491-502.

Dowdeswell, J. A., Villinger, H., Whittington, R.J., Marienfeld, P. (1993). Iceberg scouring in Scoresby Sund and on the East Greenland continental shelf. *Marine Geology, 111*(1-2), s. 37-53.

Dowsett, H. J. (2007). Planktonic foraminifera. *Encyclopedia of Quarternary Science*, s. 1678-1682.

Duplessy, J. C., Shackleton, N. J., Matthews, R. K., Prell, W., Ruddiman, W. F., Caralp, M., & Hendy, C. H. (1984). 13 C record of benthic foraminifera in the last interglacial ocean: implications for the carbon cycle and the global deep water circulation. *Quaternary Research*, *21*(2), s. 225-243

Enfield, D. B., Mestas-Nunez, A.M., Trimble., P.J. (2001). The Atlantic multidecadal oscillation and its relation to rainfall and river flows in the continental U.S. *Geophysical Research Letters, 28*(10), s. 2077-2080.

Fronval, T., Jansen, E. (1996). Rapid changes in ocean circulation and heat flux in the Nordic seas during the last interglacial period. *Letters to nature, 383*, s. 806-810.

Fronval, T., Jansen, E., Bloemendal, J., Johnsen, S. (1995). Oceanic evidence for coherent fluctuations in Fennoscandian and Laurentide ice sheet on millennium timescales. *Letters to nature, 374*(6521), s. 443-446.

Grossmann, I., Klotzbach, P. J. (2009). A review of North Atlantic modes of natural variability and their driving mechanisms. *Journal of geophysical research, 114*(D24).

Hepp, D. A., Morz, T., Grutzner, J. (2006). Pliocene glacial cyclicity in a deep-sea sediment drift (Antarctic Peninsula Pacific Margin). *Paleoceanography, 231*(1), s. 181-198.

Hopkins, T. S. (1991). The GIN Sea - A synthesis of its physical oceanography and literature review 1972-1985. *Earth-Science Reviews, 30*(3), s. 175-318.

Imbrie, J., Mix, A.C., Martinson, D.G. (1993). Milankovitch theory viewed from Devils Hole. *363*, s. 531-533.

Jansen, E. (1989). The use of stable oxygen and carbon isotope stratigraphy as a dating tool. *Quaternary International, 1*, s. 151-166.

Johannessen, T., Jansen, E., Flatøy, A., Ravelo, A.C. (1994). The relationship between surface water masses, oceanographic fronts and paleoclimatic proxies in surface sediments of the Greenland, Iceland and Norwegian Seas. *Carbon cycling in the glacial ocean: constraints on the ocean's role in global change*, s. 61- 85.

Jull, A. J. T. (2007). Radiocarbon dating- AMS Method. *Encyclopedia of Quarternary Science*, s. 2911-2918.

Kissel, C., Laj, C., Labeyrie, L., Dokken, T., Voelker A., Blamart, D. (1999). Rapid climatic variations during marine isotopic stage 3: magnetic analysis of sediments from Nordic Seas and North Atlantic. *Earth and Planetary Science Letters, 171*(3), s. 489-502.

Knudsen, K. L., Eiriksson, J., Jansen, E., Jiang, H., Rytter, F., Gudmundsdóttir, E.G. (2004). Palaeoceanographic changes off North Iceland through the last 1200 years: foraminifera, stable isotopes, diatoms and ice rafted debris. *Quaternary Science Reviews, 23*(20), s. 2231-2246.

Knudsen, M. F., Seidenkrantz, M-S., Jacobsen, B.H., Kuijpers, A. (2011). Tracking the Atlantic Multidecadal Oscillation through the last 8,000 years. *Nature communications, 2*, s. 178. doi:10.1038/ncomms1186

Kreveld, S. V., Sarnthein, M., Erlenkeuser, H., Grootes, P., Jung, S., Nadaeu, M.J., Pflaumann, U., Voelker, A. (2000). Potential links between surging ice sheets, circulation changes, and the Dansgaard-Oeschger Cycles in the Irminger Sea, 60-18 kyr. *Paleoceanography, 15*(4), s. 425-442.

Lebreiro, S. M., Voelker, A.H.L., Vizcaino, A., Abrantes, F.G., Alt-Epping, U., Jung, S., Thouveny, N., Gracia, E. (2009). Sediment instability on the Portuguese continental margin under abrupt glacial climate changes (last 60kyr). *Quaternary Science Reviews, 28*(27), s. 3211-3223.

Lisiecki, L. E., Raymo, M.E. (2005). A Pliocene-Pleistocene stack of 57 globally distributed benthic δ18O records. *Paleoceanography, 20*(1).

Lowe, J. J., Walker, M J.C. (1997). *Reconstructing quaternary environments* (Vol. 2): Londres: Longman.

MacAyeal, D. R. (1993). Binge/Purge oscillations of the Laurentide ice sheet as a cause of the North Atlantic`s Heinrich events. *Paleoceanography, 8*(6), s. 775-784.

Marshall, J., Kushnir, Y., Battisti, D., Chang, P., Czaja, A., Dickson, R., Hurrel, J., McCartney, M., Saravanan, R., Visbeck, M. (2001). North Atlantic Climate Variability: Phenomena, Impacts and Mechanisms. *International Journal of Climatology, 21*, s. 1863-1898.

Moros, M., Kuijpers, A., Snowball, I., Lassen, S., Backstrom, D., Gingele, F., McManus, J. (2002). Were glacial iceberg surges in the North Atlantic triggered by climatic warming? *Marine Geology, 192*(4), s. 393-417.

Mortyn, P. G., Martinez-Boti, M.A. (2007). Planktonic foraminifera and their proxies for the reconstruction of surface ocean climate parameters. *Contributions to science, 3*(3), s. 387-396.

Murphy, J. J. (1869). On the nature and cause of the glacial climate. *Quarterly Journal of the Geological Society*, *25*(1-2), 350-356.

Nakamura, N. (1996). Year-to-year and interdecadal variability in the activity of intraseasonal fluctuations in the NorthernHemisphere wintertime circulation. *Theoretical and Applied Climatology, 55*(1-4), s. 19-32.

Nam, S. I., Stein, R., Grobe, H., Hubberten, H. (1995). Late Quaternary glacial-interglacial changes in sediment composition at the East Greenland continental margin and their paleoceanographic implications. *Marine Geology, 122*(3), s. 243-262.

Oppo, D. (1997). Millennial Climate Oscilliations. *Paleoclimatology, 278*(5341), s. 1244.

Pirrung, M., Futterer, D., Grobe, H., Matthiessen, J. (2002). Magnetic susceptibility and ice-rafted debris in surface sediments of the Nordic Seas: implications for Isotope Stage 3 oscillations. *Geo-Marine Letters, 22*(1), s. 1-11.

Rahmstorf, S. (2000). Thermohaline ocean circulation: A system with dangerous thresholds? *Climatic Change, 46*(3), s. 247-256.

Rasmussen, T. L., Thomsen, E., Labeyrie, L., & van Weering, T. C. (1996). Circulation changes in the Faeroe-Shetland Channel correlating with cold events during the last glacial period (58–10 ka). *Geology*, *24*(10), s. 937-940.

Rasmussen, T. L., & Thomsen, E. (2004). The role of the North Atlantic Drift in the millennial timescale glacial climate fluctuations. *Palaeogeography, Palaeoclimatology, Palaeoecology*, *210*(1), s. 101-116

Rasmussen, T. L., Thomsen, E., Moros, M. (2016). North Atlantic warming during Dansgaard-Oeschger events synchronous with Antarctic warming and out-of-phase with Greenland climate. *Scientific reports, 6*.

Reimer, P. J., Reimer, R.W. (2007). *Radiocarbon dating: calibration*. Encyclopedia of Quaternary Science: Oxford: Elsevier.

Robinson, S. G. (1986). The late Pleistocene palaeoclimatic record of North Atlantic deep-sea sediments revealed by mineral-magnetic measurements. *Physics of the Earth and Planetary Interiors, 42*(1), s. 22-47.

Robinson, S. G., Maslin, M.A., McCave, I.N. (1995). Magnetic susceptibility variations in Upper Pleistocene deep-sea sediments of the NE Atlantic: Implications for ice rafting and paleocirculation at the last glacial maximum. *Paleoceanography, 10*(2), s. 221-250.

Rogers, J. C. (1985). Atmospheric circulation changes associated with the warming over the northern North Atlantic in the 1920s. *Journal of Climate and Applied Meteorology, 24*, s. 1303-1310.

Rogers, J. C. (1990). Patterns of low-frequency monthly sea level pressure variability (1899–1986) and associated wave cyclone frequencies. *Journal of climate, 3*(12), s. 1364–1379.

Rogers, J. C., & Van Loon, H. (1979). The seesaw in winter temperatures between Greenland and northern Europe. Part II: Some oceanic and atmospheric effects in middle and high latitudes. *Monthly Weather Review*, *107*(5), s. 509-519.

Rohling, E. J. (2013). *Paleocenography, physical and chemical proxies: Oxygen isotope composition of seawater* (Vol. 2): Encyclopedia of Quaternary Science

Rohling, E. J., Cooke, S. (1999). *Modern foraminifera: Stable oxygen and carbon isotopes in foraminiferal carbonate shells*: Springer Netherlands.

Rothwell, R. G. (2015). *Micro-XRF studies of sediment cores*: Springer Netherlands.

Rousse, S., Kissel, C., Laj, C., Eiriksson, J., Knudsen, K-L. (2006). Holocene centennial to millennial-scale climatic variability: Evidence from high-resolution magnetic analyses of the last 10 cal kyr off North Iceland (core MD99-2275). *Earth and Planetary Science Letters, 242*(3), s. 390-405.

Ruddiman, W. F., Raymo, M. E., Martinson, D. G., Clement, B. M., Backman J. (1989). Pleistocene evolution; Northern Hemisphere ice sheet and North Atlantic Ocean. *Paleoclimatology, 4*(4), s. 353-412.

Shackleton, N. J., Le, J., Mix, A., Hall, M. A. (1992). Carbon isotope records from Pacific surface waters and atmospheric carbon dioxide. *Quaternary Science Reviews, 11*(4), s. 387-400.

Skov, N. A. (1967). The ice cover of the Greenland Sea: an evaluation of oceanographic and meteorological causes for year-to-year variations.

Spero, H. J., Bijma, J., Lea, D. W., Bermis, B.E. (1997). Effect of seawater carbonate concentration on foraminiferal carbon and oxygen isotopes. *Nature, 390*(6659), s. 497-500.

Van Loon, H., Rogers, J.C. (1978). The seesaw in winter temperatures between Greenland and northern Europe. Part 1: General description. *Monthly Weather Review, 106*(3), s. 296-310.

Vidal, L., Bickert, T., Wefer, G., Rohl, U. (2002). Late Miocene stable isotope stratigraphy of SE Atlantic ODP Site 1085: relation to Messinian events. *Marine Geology, 180*(1), s. 71-85.

Wadhams, P. (1981). The ice cover in the Greenland and Norwegian Seas. *Reviews of geophysics, 19*(3), s. 345-393.

Walker, G. T. (1924). Correlations in seasonal variations of weather *Mem. Ind. Meteorol. Dept., 24*, s. 275 - 332.

Wallace, J. M., Gutzler, D.S. (1981). Teleconnections in the geopotential height field during the Northern Hemisphere winter. *Monthly Weather Reviews, 109*, s. 784-812.

Wefer, G., Berger, W. H., Bijma, J., Fisher, G. (1999). *Clues to ocean history: a brief overview of proxies*: Springer Berlin Heidelberg.

Zhang, X., Lohmann, G., Knorr, G., Purcell, C. (2014). Abrupt glacial climate shifts controlled by ice sheet changes. *Letters to nature, 512*, s. 290-294.

Online references:

Denoux, Eric (2010). SST: Les paléotempératures océaniques. S.E.M. images. Retrieved 17.03.2016, from http://acces.ens-lyon.fr/acces/terre/paleo/systemclim/gulf-stream/pages_gulfstream/dosstech/techpaleoclim/sst/sst

Ice2ice (2016) objective of the ice2ice project [Internett]. Retrieved 15.04.2016, from https://ice2ice.b.uib.no/overview/ice2ice-objectives/

Kleyfrance (2016) Products: Deep Sea corer [Internett]. Retrieved 20.05.2016, from http://www.kleyfrance.fr/product_06.htm

Open Source, Systems, Science, Solutions (2016) Project and resources: North Atlantic Oscilliation (NAO) [Internett]. Retrieved 24.04.2016, from http://ossfoundation.us/projects/environment/global-warming/north-atlantic-oscillation-nao

Appendix

Appendix A: Oxygen- and carbon isotope measurements from core GS15-198-38CC

Table A.1: Mean values of isotope measurements. *N. pachyderma* (*sin*).

Appendix B:

Table B.1: Assemblage counts from core GS15-198-38CC. *N. pachyderma* (*sin*).

Table B.2: Ice rafted detritus

Appendix C:

Table C.1: Sedimentation rates of core GS15-198-38CC. Display exact time and sedimentation rate of which the averaged values are based on.

Appendix D:

Table D.1: AMS ^{14}C dating. The results from radiocarbon dating as received from Beta Analytic Inc.

Appendix A

Oxygen- and carbon isotope measurements from core GS15-198-38CC

Table A.1. Mean values of isotope measurements.

Sample depth (cm)	Mean depth (cm)	$^{18}O/^{16}O$ Mean	$^{13}C/^{12}C$ Mean
0-1	0,5	3,84	0,03
5-5,5	5,25	4,10	0,52
10-10,5	10,5	3,79	0,65
15-15,5	15,25	4,58	0,05
20-21	20,5	4,31	-0,15
55-55,5	55,25	3,25	-0,10
60-61	60,5	3,87	-0,06
65-65,5	65,25	3,00	-0,17
70-71	70,5	3,71	-0,14
75-75,5	75,25	4,50	-0,03
80-81	80,5	4,73	-0,07
85-85,5	85,25	4,61	0,16
90-91	90,5	4,63	0,05
95-95,5	95,25	4,51	0,10
100-101	100,5	4,76	0,15
105-105,5	105,25	4,77	0,07
110-111	110,5	3,60	-0,27
115-115,5	115,5	4,59	0,10
120-121	120,5	4,54	0,02
125-125,5	125,25	4,46	-0,05
130-131	130,5	4,08	-0,07
135-135,5	135,25	4,49	-0,10
140-141	140,5	4,34	-0,04
145-145,5	145,25	4,38	-0,15
150-151	150,5	4,01	0,14
160-161	160,5	4,66	0,00
165-165,5	165,25	4,19	0,01
170-171	170,5	4,44	0,02
175-175,5	175,25	4,36	-0,02
180-181	180,5	3,76	-0,02
185-185,5	185,25	4,03	-0,01
190-191	190,5	3,46	-0,10
195-195,5	195,25	4,18	0,11
200-201	200,5	4,26	0,13
205-205,5	205,25	3,96	0,28
210-210	210,5	4,23	-0,02

215-215,5	215,25	4,10	0,20
220-221	220,5	3,75	-0,17
225-225,5	225,25	3,85	0,08
230-231	230,5	3,73	0,18
235-235,5	235,25	3,45	0,06
240-241	240,5	4,26	0,03
245-245,5	245,25	3,91	0,30
250-251	250,5	3,73	0,04
255-255,5	255,25	3,59	0,03
260-261	260,5	3,61	0,18
265-265,5	265,25	3,59	0,15
270-271	270,5	3,84	0,26
275-275,5	275,25	3,59	0,22
280-281	280,5	3,76	0,23
285-285,5	285,25	3,65	0,18
290-291	290,5	3,92	0,21
295-295,5	295,25	3,58	0,21
300-301	300,5	3,84	0,11
305-305,5	305,25	3,31	0,01
310-311	310,5	3,94	0,26
315-315,5	315,25	4,12	0,13
320-321	320,5	4,00	0,14
335-335,5	335,25	3,23	0,06
340-341	340,5	3,75	0,15
345-345,5	345,25	3,85	0,16
350-351	350,5	3,87	0,13
355-355,5	355,25	3,72	0,15
360-361	360,5	3,50	0,05
365-365,5	365,25	3,58	0,23
370-371	370,5	4,07	0,42
375-375,5	375,25	4,00	0,21
380-381	380,5	4,03	0,10
385-385,5	385,25	3,97	0,15
390-391	390,5	3,95	0,22
395-395,5	395,25	3,52	-0,03
400-401	400,5	3,72	0,12
404-405,5	405,25	3,40	0,16
410-411	410,5	3,31	0,16
415-415,5	415,25	3,87	0,19
455-455,5	455,25	3,41	0,05
465-465,5	465,25	3,71	-0,06
470-471	470,5	2,56	-0,42
475-475,5	475,25	3,20	-0,32
480-481	480,5	4,06	-0,02
485-485,5	485,25	4,13	-0,07
490-491	490,5	4,28	-0,02

495-495,5	495,25	3,88	0,05
500-501	500,5	4,03	-0,01
505-505,5	505,25	4,29	0,02
510-511	510,5	4,38	0,10
515-515,5	515,25	4,36	0,27
520-521	520,5	4,05	0,43
535-535,5	535,25	3,52	0,61
540-541	540,5	4,13	0,47
560-561	560,5	3,52	0,69
565-565,5	565,25	3,49	0,59
570-571	570,5	3,04	0,68
575-575,5	575,25	3,03	0,38
580-581	580,5	3,33	0,63
585-585,5	585,25	4,10	0,61
590-591	590,5	3,42	0,53
595-595,5	595,25	3,60	0,58
600-601	600,5	3,76	0,56
605-605,5	605,25	3,62	0,67
610-611	610,5	3,60	0,56
615-615,5	615,25	3,09	0,68
620-621	620,5	3,86	0,31
625-625,5	625,25	3,96	0,47
635-635,5	635,25	3,97	0,64
640-641	640,5	4,09	0,59
645-645,5	645,25	3,87	0,69
650-651	650,5	3,75	0,68
655-655,5	655,25	3,48	0,33
660-661	660,5	3,59	0,41
665-665,5	665,25	3,46	0,34
670-671	670,5	3,29	0,40
675-675,5	675,25	2,55	0,04
680-681	680,5	3,50	0,49
690-691	690,5	4,18	-0,01
700-701	700,5	4,19	0,07
720-721	720,5	4,46	-0,10
725-725,5	725,25	4,74	0,17
730-731	730,5	4,58	-0,17
735-735,5	735,25	4,61	-0,04
740-741	740,5	4,77	-0,23
745-745,5	745,25	4,68	-0,34
750-751	750,5	4,71	-0,16
755-755,5	755,25	4,62	-0,43
760-761	760,5	4,59	-0,14
765-765,5	765,25	4,65	-0,15
770-771	770,5	4,57	-0,03
775-775,5	775,25	4,61	-0,10

780-781	780,5	4,57	-0,15
785-785,5	785,25	4,51	0,02
790-791	790,5	4,53	-0,02
805-805,5	805,25	4,15	-0,10
810-811	810,5	4,21	0,00
815-815,5	815,25	3,91	-0,24
820-821	820,5	3,98	-0,04
825-825,5	825,25	3,76	-0,18
830-831	830,5	3,93	-0,21
835-835,5	835,25	3,25	-0,25
840-841	840,5	3,45	-0,42
845-845,5	845,25	4,26	-0,35
850-851	850,5	3,99	-0,32
855-855,5	855,25	4,19	-0,18
860-861	860,5	3,97	-0,46
865-865,5	865,25	4,48	-0,17
870-871	870,5	4,67	0,01
875-875,5	875,25	3,95	-0,22
880-881	880,5	4,37	0,03

Appendix B

Assemblage counts from core GS15-198-38CC.

Table B.1. Neogloboquadrina pachyderma senestre.

	Neogloboquadrina pachyderma senestre (NPS) counts						
Depth (cm)	**Amount NPS**	**Amount other planktonic species**	**Total number of planktonic species**	**Toltal amount sqaures**	**Number of counted squares**	**Number of splits**	**Split factor**
60.5	313	9	322	50	7	2	4
65.25	341	8	349	50	7	1	2
70.5	325	5	330	50	7	3	8
75.25	325	0	325	50	8	2	4
80.5	330	3	333	50	5	3	8
85.25	318	5	323	50	8	2	4
90.5	337	4	341	50	7	3	8
95.25	315	4	319	50	11	2	4
100.5	303	2	305	50	7	1	2
105.25	308	0	308	50	27	1	2
110.5	130	0	130	50	100	1	2
115.25	317	0	317	50	50	0	1
120.5	308	0	308	50	32	1	2
125.25	179	0	179	50	100	0	1
130.5	329	1	330	50	10	3	8
135.25	300	1	301	50	13	2	4
140.5	319	0	319	50	12	3	8
145.25	362	0	362	50	7	2	4
150.5	342	4	346	50	5	2	4
155.25	0	0	0	50	0	0	1
160.5	341	2	343	50	5	1	2
165.25	341	0	341	50	5	0	1
170.5	309	0	309	50	3	0	1
175.25	302	2	304	50	29	0	1
180.5	328	0	328	50	13	0	1
185.25	340	3	343	50	5	0	1
190.5	336	2	338	50	8	2	4
195.25	340	0	340	50	8	1	2
200.5	323	2	325	50	11	3	8
205.25	347	0	347	50	6	1	2
210.5	303	1	304	50	50	3	8
215.25	316	4	320	50	11	0	1

220.5	309	0	309	50	6	1	2
225.25	331	1	332	50	11	1	2
230.5	318	3	321	50	12	0	1
230.25	309	1	310	50	20	0	1
240.5	326	0	326	50	13	1	2
245.25	315	0	315	50	9	1	2
250.5	321	1	322	50	6	2	4
255.25	327	1	328	50	7	1	2
260.5	340	0	340	50	10	1	2
265.25	314	5	319	50	10	2	4
270.5	310	2	312	50	6	2	4
275.25	348	3	351	50	8	2	4
280.5	300	4	304	50	6	2	4
285.25	351	0	351	50	7	2	4
290.5	338	1	339	50	5	2	4
295.25	316	1	317	50	6	1	2
300.5	306	2	308	50	6	2	4
305.25	327	0	327	50	7	2	4
310.5	338	3	341	50	6	0	1
315.25	307	2	309	50	31	0	1
320.5	140	0	140	50	50	0	1
325.15	0	0	0	50	0	0	1
330.5	2	0	2	50	50	0	1
335.25	0	0	0	50	0	0	1
340.5	306	0	306	50	8	3	8
345.25	308	6	314	50	4	0	1
350.5	325	6	331	50	5	1	2
355.25	326	1	327	50	6	1	2
360.5	325	2	327	50	12	1	2
365.25	309	1	310	50	13	1	2
370.5	320	1	321	50	8	3	8
375.25	325	1	326	50	10	2	4
380.5	343	1	344	50	6	2	4
385.25	332	8	340	50	8	2	4
390.5	352	0	352	50	5	2	4
395.25	300	3	303	50	5	1	2
400.5	342	3	345	50	7	2	4
405.25	347	0	347	50	7	1	2
410.5	168	0	168	50	50	0	1
415.25	329	0	329	50	10	0	1
420.5	311	0	311	50	17	1	2
425.25	0	0	0	50	0	0	1
430.5	0	0	0	50	0	0	1
435.25	0	0	0	50	0	0	1
440.5	0	0	0	50	0	0	1

445.25	201	1	202	50	50	2	4
450.5	0	0	0	50	0	0	1
455.25	27	0	27	50	50	0	1
460.5	1	0	1	50	50	0	1
465.25	304	1	305	50	21	0	1
470.5	316	0	316	50	5	4	16
475.25	303	1	304	50	5	2	4
480.5	344	0	344	50	6	3	8
485.25	79	0	79	50	50	0	1
490.5	318	0	318	50	8	0	1

Table B.2. Ice rafted detritus (IRD).

Ice rafted detritus (IRD)				
Depth (cm)	**Amount mineral grains**	**Number of counted squares**	**Number of splits**	**Split factor**
60.5	325	15	1	2
65.25	321	11	1	2
70.5	323	9	3	8
75.25	322	8	2	4
80.5	326	6	3	8
85.25	327	9	2	4
90.5	318	6	3	8
95.25	320	8	2	4
100.5	337	3	1	2
105.25	398	3	1	2
110.5	358	4	1	2
115.25	309	45	0	1
120.5	315	5	1	2
125.25	309	4	1	2
130.5	301	4	3	8
135.25	337	6	2	4
140.5	303	5	3	8
145.25	323	9	2	4
150.5	321	12	2	4
155.25	328	7	0	1
160.5	304	11	1	2
165.25	307	17	0	1
170.5	304	28	0	1
175.25	302	41	0	1
180.5	335	6	0	1

185.25	304	7	0	1
190.5	316	5	2	4
195.25	339	8	1	2
200.5	319	14	3	8
205.25	342	7	1	2
210.5	324	4	3	8
215.25	315	7	0	1
220.5	360	6	1	2
225.25	337	6	1	2
230.5	304	5	0	1
230.25	341	6	0	1
240.5	303	6	1	2
245.25	304	6	1	2
250.5	310	8	2	4
255.25	335	7	1	2
260.5	348	5	1	2
265.25	318	10	2	4
270.5	329	12	2	4
275.25	313	17	2	4
280.5	306	13	2	4
285.25	350	8	2	4
290.5	332	10	2	4
295.25	308	11	1	2
300.5	325	12	2	4
305.25	332	12	2	4
310.5	337	8	0	1
315.25	300	38	0	1
320.5	87	45	0	1
325.15	13	45	0	1
330.5	10	45	0	1
335.25	3	45	0	1
340.5	301	13	3	8
345.25	309	20	0	1
350.5	304	14	1	2
355.25	326	10	1	2
360.5	322	11	1	2
365.25	330	5	1	2
370.5	311	11	3	8
375.25	334	9	2	4
380.5	343	9	2	4
385.25	303	10	2	4
390.5	310	12	2	4
395.25	340	8	1	2
400.5	329	12	2	4
405.25	311	11	1	2

410.5	308	4	0	1
415.25	302	10	0	1
420.5	384	4	1	2
425.25	328	5	0	1
430.5	363	3	0	1
435.25	354	3	0	1
440.5	350	5	0	1
445.25	354	7	2	4
450.5	312	20	0	1
455.25	347	5	0	1
460.5	241	50	0	1
465.25	310	32	0	1
470.5	314	10	4	16
475.25	301	11	2	4
480.5	302	18	3	8
485.25	238	50	0	1
490.5	307	6	0	1

Appendix C

Sedimentation rates of core GS15-198-38CC

Table C.1. Display exact time and sedimentation rate of which the averaged values are based on.

Time (ka BP)	Sed. Rate (cm/1000 yr)
13,08	4,64
20,67	7,23
38,63	8,81
46,63	5,30
52,51	19,80
59,45	3,39
73,66	4,67
85,32	1,31
92,63	2,37
105,53	2,38
131,50	6,74
155,47	6,74

Appendix D

AMS ^{14}C dating

Table D.1. The results from radiocarbon dating as received from Beta Analytic Inc.

BETA ANALYTIC INC.
DR. M.A. TAMERS and MR. D.G. HOOD
4985 S.W. 74 COURT
MIAMI, FLORIDA, USA 33155
PH: 305-667-5167 FAX:305-663-0964
beta@radiocarbon.com

REPORT OF RADIOCARBON DATING ANALYSES

Sample Data	Measured Radiocarbon Age	d13C	Conventional Radiocarbon Age(*)
Beta - 419048	14760 +/- 50 BP	0.0 o/oo d18O= +4.0 o/oo	15170 +/- 50 BP
SAMPLE : GS15-198-38 60cm ANALYSIS : AMS-Standard delivery MATERIAL/PRETREATMENT : (foraminifera): none 2 SIGMA CALIBRATION : Cal BC 16100 to 15925 (Cal BP 18050 to 17875)			
Beta - 419049	22380 +/- 110 BP	-4.1 o/oo	22720 +/- 110 BP
SAMPLE : GS15-198-38 180cm ANALYSIS : AMS-Standard delivery MATERIAL/PRETREATMENT : (foraminifera): none 2 SIGMA CALIBRATION : Cal BC 24970 to 24310 (Cal BP 26920 to 26260)			
Beta - 419050	41730 +/- 560 BP	+0.4 o/oo d18O= +4.1 o/oo	42150 +/- 560 BP
SAMPLE : GS15-198-38 345cm ANALYSIS : AMS-Standard delivery MATERIAL/PRETREATMENT : (foraminifera): sonicated in alkali 2 SIGMA CALIBRATION : Cal BC 44070 to 42275 (Cal BP 46020 to 44225)			